UC Berkeley
UC Berkeley Electronic Theses and Dissertations

Title
The changing interhemispheric temperature difference: mechanisms and impacts

Permalink
https://escholarship.org/uc/item/8hr876rn

Author
Friedman, Andrew Ronald

Publication Date
2014

Peer reviewed|Thesis/dissertation

eScholarship.org Powered by the California Digital Library
University of California

The changing interhemispheric temperature difference: mechanisms and impacts

By

Andrew Ronald Friedman

A dissertation submitted in partial satisfaction of the requirements for the degree of

Doctor of Philosophy

in

Geography

in the

Graduate Division

of the

University of California, Berkeley

Committee in charge:

Professor John C. H. Chiang, Chair
Professor Nathan Sayre
Professor Inez Fung
Professor William D. Collins
Professor Shih-Yu Lee

Spring 2014

Abstract

The changing interhemispheric temperature difference: mechanisms and impacts

by

Andrew Ronald Friedman

Doctor of Philosophy in Geography

University of California, Berkeley

Professor John C. H. Chiang, Chair

The surface temperature difference between the northern and southern hemispheres is the simplest climate change indicator following global mean temperature, and reveals unique information about the state of the global climate, in particular regarding tropical atmospheric circulation and rainfall. This dissertation examines the historical behavior, future projections, and tropical hydrologic impacts of this interhemispheric (north–south) temperature difference.

Historically, most of the variability in the interhemispheric temperature difference is from the northern hemisphere. Investigation of specific-forcing simulations shows that globally uniform radiative forcing from well-mixed greenhouse gases causes asymmetric northern warming due to the hemispheric land-ocean contrast and Arctic amplification. However, sulfate aerosols, which were disproportionately emitted in the northern hemisphere, caused cooling that masked the northern warming until the mid 1970s. Air pollution regulations in North America and Europe combined with sustained emissions of greenhouse gases have resulted in a positive trend in the interhemispheric temperature difference in the past few decades.

Future simulations of phases 3 and 5 of the Coupled Model Intercomparison Project (CMIP3 and CMIP5) project that this recent asymmetric northern hemispheric warming will continue in the 21st century. The projected increase is well outside the range of historical variability in both moderate and business-as-usual scenarios. There is also a projected multimodel mean northward shift in the Hadley circulation and tropical rainfall, though the multimodel spread is much larger than for temperature.

A prominent feature in the interhemispheric temperature record is an abrupt decrease around 1970, which was most pronounced in sea surface temperature (SST). Examination of the shift using surface and subsurface ocean datasets reveals that there were pronounced cooling and freshening at depth in the subpolar North Atlantic north of 50°N, which coincided with opposing warming and salting in the western mid-latitude North Atlantic between 35° and 45°N. These combined features cannot be completely accounted for by atmospheric forcing alone. Rather, they point to a discrete subpolar North Atlantic freshening known as the Great Salinity Anomaly and the corresponding weakening of the North Atlantic thermohaline circulation as causes of the 1970 interhemispheric shift.

Spatially, the strongest surface temperature correlations with the interhemispheric SST difference are found in the extratropical North Atlantic and southern hemisphere oceans, which are key regions for the shift around 1970. Additionally, the correlations with

low-latitude rainfall and the flow of major rivers are examined. Positive rainfall correlations are found in tropical North Africa, South and Southeast Asia; and negative correlations are found in Australia, southern and eastern South America, and northern Mexico. Among the rivers examined, the Niger, which flows through the Sahel, is most strongly correlated with the interhemispheric SST difference. The Indus is also significantly positively correlated, while the Mississippi and Parana are significantly negatively correlated. Based on this assessment, these regions are likely to experience impacts in response to future variations in the interhemispheric temperature difference from the extratropical Atlantic and southern hemisphere oceans, such as from the meridional overturning circulation or aerosol forcing.

Table of Contents

Acknowledgments

Many people have helped in the process of writing this dissertation over the past several years, and I am happy to acknowledge them here. Additional acknowledgements are also listed for specific chapters. I apologize to anyone I have thoughtlessly omitted.

This dissertation is the culmination of research into hemispheric asymmetry that began as an undergraduate working with John Chiang, and followed under his guidance as my graduate advisor. John has patiently nurtured my growth as a climatologist, offering candid and always constructive feedback, and continuing to believe in my scientific potential. Without him, this work would not have been possible.

I owe a great deal of thanks to my other committee members. Inez Fung's probing questions pushed me to a higher level of scientific inquiry and practice. I especially appreciate her critical feedback on constructing scientific narrative. Shih-Yu Lee was an engaged advisor during the exhilarating months I spent as a visitor at Academia Sinica, and also remotely when I was in Berkeley. Her encouragement, astute suggestions, and oceanographic perspective made a really positive impact. Nathan Sayre provided the intellectual guidance for my collaborative work on Mexico, offering many valuable recommendations for the interdisciplinary project. Bill Collins offered useful suggestions and particularly guided me in radiative forcing and climate feedbacks.

Different chapters of this dissertation are from of fruitful collaborations with other researchers. Working with Yen-Ting Hwang on interhemispheric temperature asymmetry was incredibly rewarding; I learned a great deal from her research approach and candid advice. Dargan Frierson has also been extremely helpful and supportive throughout the project. Discussions with Paul Rogé several years ago about integrating climate science with his work in agroecology grew into a highly rewarding collaboration. The resulting interaction between very different fields and methodologies has been intellectually challenging and fulfilling. I also appreciate our other collaborators Marta Astier and Miguel Altieri.

I have received valuable assistance from several other professors. Instruction from Zhaohua Wu on climate time series data analysis was especially illuminating. Discussions with Eric Guilyardi were helpful in thinking about the Great Salinity Anomaly. Robert Rhew, Laurel Larson, David Romps, and Kurt Cuffey also offered helpful feedback.

I appreciate the professionalism, kindness, and personal engagement of the Geography Department staff. Carol Page advised me with discretion and humor. Marjorie Ensor also was an extremely helpful and patient academic advisor. Darin Jensen helped with many maps and figures, printed countless posters, and was a trusted counselor. Mike Jones instructed me in how to interact with computers and in implementing an organizational system for this dissertation and my life. Natalia Vonnegut and Delores Dillard handled countless administrative and logistical matters. Dan Plumlee ensured a safe workspace, and solved technical issues that calmed many frantic moments. Elsewhere in McCone Hall, Charlie Paffenbarger in EPS also solved many computing issues with calm and ease. Zachariah Veley and the staff in the Earth Sciences & Map Library were of great assistance.

I feel very grateful to the Climate Dynamics lab members. Yuwei Liu has been a generous scientific collaborator and keen proofreader; my graduate career has been greatly enriched by his straightforward input, sharp wit, and philosophical perspective. Yugarshi Mondal's curious questions, energy, and scientific insights have been a great boon to my research. Wenwen Kong's encouragement and suggestions this past year are much appreciated.

Previous lab members have also played a big role. Ivana Cvijanovic has been a wonderful guide and a source of laugher; her specific help with atmospheric energy budgets is especially appreciated. Mai Nguyen also gave valuable feedback throughout this process; she has been a terrific coach and problem-solver. Miren Vizcaino helped me grow in the lab; I specifically appreciate that she introduced me to shell scripting. Ching-Yee Chang offered thoughtful reflections and assistance with software. Hugo Lambert and Ben Lintner were also very helpful. I also appreciate help from Alyssa Atwood, Christina Patricola, Mollie Van Gordon, Jin Jian, and Juli Rubin during their tenure in room 531. Finally, thanks to Lan Ma for her group involvement and infectious scientific curiosity.

The other Berkeley Geography students helped make graduate school rewarding. A few deserve particular mention. Mary Whelan answered many incessant questions about the atmosphere, calmly guided me through dissertation challenges, and always made me laugh. Conversations with Tripti Bhattacharya about statistics, paleoclimate, and Mexican climate dynamics were highly clarifying. I deeply appreciate Naomi Schultz for being such an ardent supporter and wonderful ally. Thanks to Andy Bliss for his consistent help and scripting assistance.

I thank the present and past members of the Fung, Collins, and Romps groups for helpful feedback in my research development. Alexander Stine has been a mentor and role model of an engaged climate scientist since I was an undergraduate, and contributed much in the development of my ideas. Abby Swann also provided supportive guidance and technical assistance. In addition, I specifically appreciate help from Nadir Jevanjee, Ju-Mee Ryoo, Percy Link, Dan Feldman, Daniele Rosa, Aparna Bamzai, Charlie Koven, and Jung-Eun Lee.

I've received wonderful input and support from many others in the research and writing process. Gautam Agarwal assisted with scripting and spatial data analysis, suggested innovative interpretations, and shared his sense of wonder. Tom Pessah joined in many study sessions, offered insights into investigation and the daunting writing process, and was deeply supportive. Matt Tucker-Simmons helped me with math and computer questions. Elliot Block shared strategies on project management and workflow. A partial list of others who contributed includes John Anderson, Angel Ryono, Kevin Chan, Dominic Yu, Tim Ruckle, Yong-Ha Jeong, Megan Williams, and Nakul Sathaye. Linda Boukhris, thank you for exhorting me to express my own voice, and for the lives before us.

I especially appreciate funding from the UC Berkeley Geography Department Restricted Award. I was also fortunate to participate in the National Science Foundation (NSF) East Asia and Pacific Institute in Taiwan, with financial support from the NSF and the National Science Council of Taiwan. Thanks to the staff and researchers at the Academia

Sinica Research Center for Environmental Changes for being so welcoming and accommodating during my two visits.

This dissertation was produced with the help of several freely available climate data analysis and visualization software programs. I especially thank Jennifer Adams and other developers of the Grid Analysis and Display System (GrADS), and Charlie Zender and the other developers of the netCDF Operators (NCO). I also thank Bin Guan, Chihiro Kodama, Todd Mitchell, and Teddy Allen for sharing helpful scripts; the developers of the Climate Data Operators (CDO); and Rich Pawlowicz for developing the m_map mapping package.

My family has been wonderfully supportive throughout this entire process. From purchasing me the companion guide to *Sim Earth* where I learned about climate feedbacks as a child, to sneaking into AGU fall meetings to catch my presentations, my dad has nurtured and encouraged my scientific endeavors my entire life. My mom has also been incredibly involved and engaged in my work, sending me articles on climate change in addition to all of the recipes and baked goods. Lisa is a fantastic sister, and her reviewing of my writing and presentations has been no exception. Her careful feedback went far beyond the grammar that I had asked for, and encouraged me to clarify my arguments and thinking. Much appreciation to Nana and Russell for all of the food, music, and love; and thanks to the Norman and Friedman families for all their support. I specifically acknowledge Mark Friedman for excellent writing advice and for keeping me on track.

My grandfather, David Norman, was an observer of the natural world. I remember when I was a child how he used to explain the propagation of thunder in the air above Lake Tahoe, and how the salt marshes at Palo Alto's Baylands Nature Preserve had resulted from human management. I wish that I had gotten to share this research with him - he would have been very interested in the all of the different connections.

1. Introduction

Though it is often described in terms of a single variable, global climate change is not spatially uniform across the earth's surface. This dissertation examines one of the most important spatial divisions: the temperature difference between the northern and southern hemispheres.

1.1 Motivation and focus

There are two major reasons to focus on the interhemispheric temperature difference: its importance for tropical atmospheric circulation and rainfall, and its use as an indicator of for determining forcings and the transient climate response.

a. Tropical circulation and rainfall

The idea that tropical atmospheric overturning circulation is driven by the pole-equator temperature difference goes back to 18th century scientist George Hadley (Webster 2005). However, as far as we are aware, the climatologist Hermann Flohn in the 1960s and 1970s was the first to explicitly suggest the importance of the temperature contrast between the hemispheres — or hemispheric asymmetry — for determining the position of the 'meteorological equator' and the Intertropical Convergence Zone (ITCZ) (Flohn 1981).

Observational studies since the 1980s have found linkages between the interhemispheric temperature difference and tropical rainfall on multidecadal timescales. Notably, Folland et al. (1986) first identified a global interhemispheric sea surface temperature (SST) dipole pattern associated with the pronounced Sahel drought of the 1970s. Subsequent studies have connected the interhemispheric temperature (or SST) difference and zonal mean tropical rainfall over land (C. Chung and Ramanathan 2007; Sun et al. 2013). Paleoclimate evidence has revealed connections between the interhemispheric temperature difference and the location of the ITCZ and strength of the monsoons in glacial-interglacial transitions (Toggweiler and Lea 2010) and during the Holocene (Marcott et al. 2013).

Several theoretical and modeling studies in the past decade have advanced an energy flux framework for meridional shifts of tropical rainfall from the interhemispheric temperature difference. According to this mechanism, the ascending branch of the Hadley cell shifts meridionally into the anomalously warmer hemisphere to flux energy across the equator and maintain energy balance in each hemisphere; this shifts the latitude of the ITCZ and affects the strength of the monsoons. (Yoshimori and Broccoli 2008; S. M. Kang 2009; Frierson and Hwang 2012). This energetic framework has been used to attribute the global southward shift in tropical rainfall in the second half of the 20th century (Hwang, Frierson, and Kang 2013).

b. Use as indicator of forcings and transient sensitivity

Since the 1980s, modeling studies have explored the sensitivity of the interhemispheric temperature difference to both greenhouse gas and aerosol forcing.

Simulations from the 1980s have found that the northern hemisphere has a larger temperature response to uniform CO_2 due to its larger land fraction (Stouffer, Manabe, and Bryan 1989). Conversely, it has been shown that sulfate aerosols have preferentially cooled the northern hemisphere due to their industrial sources and short atmospheric lifetimes (Kiehl and Briegleb 1993; Rotstayn and Lohmann 2002).

Based on these established relationships, changes in the observed interhemispheric temperature difference have been used to infer the magnitude of aerosol radiative forcing (Kaufmann and Stern 1997; Shindell and Faluvegi 2009). While these studies have been promising, it has also been recognized that more accurate estimates of the contribution of internal variability is required to constrain these parameters (Isaac Held 2012).

c. Focus

The overall goal of this dissertation is to explain the historical behavior of the interhemispheric temperature difference, and thus contribute to the motivating questions of tropical rainfall impacts and radiative forcing attribution. Rainfall impacts are examined directly in **Chapter 2** and **Chapter 4**, but the main emphasis is on the temperature record itself.

As the focus is on observations, the time period considered is from the late 19th century to the present when gridded temperature data are available. The analysis of gridded subsurface ocean data in **Chapter 3** and land surface rainfall and river flow in **Chapter 4** are further limited from the second half of the 20th century to the present.

1.2 Structure

The broad structure of this dissertation is as follows. **Chapter 2** provides an overview of the interhemispheric temperature difference, discussing the overall historical behavior, attribution to forcings, and impacts on tropical rainfall. The next two chapters are more specific. **Chapter 3** focuses on the mechanisms behind the abrupt shift around 1970, which is a key feature in the interhemispheric temperature difference time series. **Chapter 4** examines the impacts on low-latitude rainfall and river flow in observations from the second half of the 20th and early 21st centuries.

Chapter 2 investigates the interhemispheric temperature difference in historical observations and Coupled Model Intercomparison Project phases 3 and 5 (CMIP3 and CMIP5) simulations. Observations of the interhemispheric temperature difference feature a significant positive trend since around 1980. This increase is attributed to greenhouse gas forcing, which causes hemispheric asymmetry due to amplified warming in the Arctic and northern landmasses. CMIP5 specific-forcing simulations indicate that, before 1980, the greenhouse-forced interhemispheric difference trend was primarily countered by anthropogenic sulfate aerosols that caused northern hemisphere cooling. The implementation of air pollution regulations in North America and Europe combined with increased global emissions of greenhouse gases have resulted in the subsequent positive trend.

Chapter 2 also examines 21st century climate simulations in CMIP3 and CMIP5. In both ensembles, both moderate and business-as-usual scenarios project a continued increase in the ITA, reaching well outside its 20th century range. This is mainly due to continued greenhouse gas emissions, which accumulate in the atmosphere. Examination of 21st century business-as-usual CMIP5 simulations shows significant weakening of the atmospheric meridional overturning circulation in the northern hemisphere, and a small strengthening in the southern hemisphere; this Hadley cell asymmetry is in accordance with the interhemispheric temperature asymmetry. Additionally, there is a projected northward shift of tropical (combined land+ocean) rainfall in the multimodel ensemble mean. However, the multimodel spread is large, and it is difficult to fully attribute this shift to the north–south temperature difference considering the complexities of the rainfall response to global warming.

The penultimate section of **Chapter 2** discusses a rapid decrease in the interhemispheric temperature difference from around 1968–1972, which projects most strongly over the extratropical oceans and is not well-simulated by the CMIP historical ensemble means. **Chapter 3** focuses on this abrupt shift in the interhemispheric SST difference timeseries, investigating both its timing and spatial pattern. Applying an objective regime shift detection algorithm to the observational interhemispheric SST timeseries from 1900–2013 finds that the shift was the most pronounced in the record. The spatial SST regression map corresponding to the shift has largest amplitude in the subpolar North Atlantic. Upper-ocean temperature, heat content, and salinity are also examined. The regression maps reveal a coherent spatial dipole pattern of freshening and cooling in the North Atlantic north of 50°N, and warming and salting in the western mid-latitude North Atlantic offshore the U.S. east coast between 35° and 45°N. These features suggest that the shift was associated with the late-1960s subpolar North Atlantic known as the Great Salinity Anomaly, which disrupted northward Atlantic heat and salt transport.

Chapter 4 first compares two forms of the interhemispheric temperature difference: the combined land+SST difference, and the SST-only difference. Both timeseries are dominated by the abrupt drop around 1970 discussed in **Chapter 3**; as such, they are most significantly correlated with surface temperatures over the extratropical North Atlantic and southern hemisphere oceans. The main difference is that the combined land+SST difference has increased much more rapidly since the end of the shift in the early 1970s.

Next, **Chapter 4** focuses on the low-latitude hydrologic impacts of the interhemispheric temperature difference indices. Correlations are examined for low-latitude rainfall over land from 1948–2013, and river discharge of the largest rivers by flow, from 1948–2004. Positive rainfall correlations are found in tropical North Africa, South and Southeast Asia; while negative correlations are found in Australia, southern and eastern South America, and northern Mexico. The Niger river, which flows through the Sahel, has the largest correlation with the interhemispheric SST difference of any river examined; the Indus is also significantly positively correlated. The Mississippi and the Parana rivers are most significantly negatively correlated with the interhemispheric SST difference. **Chapter 4** concludes with a brief discussion of additional observational

questions, and likely future hydrologic impacts from variability of the interhemispheric temperature difference.

Finally, **Chapter 5** is an interdisciplinary collaborative study that examines how maize farmers in the Mixteca Alta region of Oaxaca, Mexico, perceive and adapt to climate changes. Farmers were interviewed about their cropping systems, their perceptions of climate changes, and how they adapt to climate variability. They reported that their cropping systems were changing for both climate-related and non-climate reasons: more drought, later rainfall onset, decreased rural labor, and introduced labor-saving technologies. Examination of climate data found that farmers' climate narratives were largely consistent with the observational record. In the last few decades there have been increases in temperature and rainfall intensity, and an increase in rainfall seasonality that may be perceived as later rainfall onset. From this analysis, farmers proposed strategies to improve the ability of their agroecosystems to cope with climatic variability. While not explicitly about the interhemispheric temperature difference, it illustrates a methodology for how the impacts of climate change on agriculture can be studied at the community scale.

1.3 Cross-chapter comparison

Different terminology is used for the interhemispheric temperature difference. **Chapter 2** uses *Interhemispheric Temperature Asymmetry,* which emphasizes the increased northern hemisphere warming. This is the same as the *combined land+SST difference* in **Chapter 4**. **Chapter 3** only discusses the interhemispheric difference in SST.

There are some differences between the chapters in terms of the base period for anomalies and months used for annual means. Anomalies in **Chapter 2** are calculated relative to 1891–1920; **Chapter 3** and **Chapter 4** use 1961–1990 as a base period. Annual means are calculated from January–December in **Chapter 2** and **Chapter 3**; **Chapter 4** uses the October–September annual mean, which is better suited to the hydrologic cycle.

2. Interhemispheric Temperature Asymmetry over the Twentieth Century and in Future Projections

The majority of this chapter is from the following:

Friedman, Andrew R., Yen-Ting Hwang, John C. H. Chiang, Dargan M. W. Frierson, 2013: "Interhemispheric temperature asymmetry over the twentieth century and in future projections." *Journal of Climate*, **26**, 5419–5433.
http://dx.doi.org/10.1175/JCLI-D-12-00525.1
©American Meteorological Society. Used with permission.

2.1. Introduction

The thermal contrast between the Northern and Southern Hemispheres is an emerging index of climate change. In paleoclimate, hemispheric cooling events may have played important roles in abrupt climate changes during the last glacial period (Chiang 2009) and glacial–interglacial cycles (Toggweiler and Lea 2010). In the twentieth century, hemispheric differences in sea surface temperature (SST) have been shown to be important for tropical rainfall and the Hadley circulation and have been implicated in regional climate changes such as the onset of the Sahel drought in the late 1960s (Folland, Palmer, and Parker 1986) and the decrease in the South Asian monsoon in recent decades (C. E. Chung and Ramanathan 2006; Bollasina, Ming, and Ramaswamy 2011). A review can be found in Chiang and Friedman (2012).

Observational and modeling studies over the past few decades have found different temperature responses to climatic forcings between the Northern Hemisphere (NH) and Southern Hemisphere (SH). Early modeling experiments showed that greenhouse gas (GHG) forcing resulted in greater NH warming because of the hemispheric asymmetry in land distribution and Southern Ocean vertical mixing (Stouffer, Manabe, and Bryan 1989; Manabe et al. 1991). On the other hand, sulfate aerosols are unevenly distributed in the NH, causing greater NH cooling (Kiehl and Briegleb 1993; Santer et al. 1996; Kaufmann and Stern 1997). Recently, Karoly and others studied simple indices, including the interhemispheric temperature contrast, for detecting and attributing global climate changes (Karoly and Braganza 2001; Braganza et al. 2004; Drost, Karoly, and Braganza 2012; Drost and Karoly 2012). These studies do not find robust significant trends in the twentieth century (unlike their other indices), which they suggest is because of compensating effects of GHGs and aerosols. However, they do find a significant increase in future projections from a subset of phases 3 and 5 of the Coupled Model Intercomparison Project (CMIP3 and CMIP5).

Our main purpose in this study is to explore the interhemispheric temperature asymmetry (ITA) as an indicator of climate change. We continue from previous studies and report on the behavior of the ITA in updated observational datasets and multimodel simulations from CMIP3 and CMIP5. We investigate the causes of ITA changes by examining CMIP5 simulations of specific natural and anthropogenic forcings and by exploring the spatial pattern associated with the pronounced increasing ITA trend since the

1980s, which is projected to continue through the twenty-first century. Additionally, we return to the motivating climate impacts, discussing some of the ways that the ITA may explain historical and future responses of tropical circulation and precipitation. Finally, we briefly address the abrupt ITA shift in the late 1960s.

2.2. Indices and datasets

a. ITA index

We define the ITA index as the difference between the hemispheric-mean surface air temperatures, NH minus SH. The net hemispheric surface air temperature contrast has the benefit of consistency, as observational estimates can be constructed extending back to the late nineteenth century. Dynamically, there is a basis for comparing net hemispheric temperatures (as opposed to only SSTs) in that both extratropical land and ocean temperatures have been shown to influence tropical circulation and rainfall (Chiang and Bitz 2005). We compute anomalies (ΔITA) relative to 1891–1920, similar to Drost et al. (2012).

b. Datasets

We analyze hemispheric-average temperature anomalies from the Goddard Institute for Space Studies (GISS) Surface Temperature Analysis (GISTEMP; Hansen et al. 2010), which we also compare with those from the National Climatic Data Center (NCDC; Smith et al. 2008), and the Hadley Centre/Climatic Research Unit, version 4 (HadCRUT4; Morice et al. 2012). The datasets combine land surface air temperature with SST measurements to represent surface air temperature anomalies. The SST anomalies are used as they have been shown to closely approximate surface air temperature anomalies over large (ice free) areas, and there are more consistent SST measurements than of marine air temperature (Rayner et al. 2003). We also investigate hemispheric-average SST anomalies from the National Oceanic and Atmospheric Administration (NOAA) extended reconstructed sea surface temperature dataset, version 3b (ERSST.v3b; Smith and Reynolds 2004).

We investigate available multimodel near-surface air temperature *tas* output from CMIP3 (Meehl et al. 2007) and CMIP5 (Taylor, Stouffer, and Meehl 2012). For the CMIP3, we use the twentieth-century climate simulation (20c3m) and the Special Report on Emissions Scenarios (SRES) A2 and B1; for the CMIP5, we use the historical simulation and representative concentration pathway (RCP) scenarios 4.5 and 8.5. The B1 and A2 are comparable in terms of net radiative forcing to the RCP4.5 and RCP8.5 scenarios, respectively (van Vuuren et al. 2011). We additionally examine CMIP5 historical simulations forced by specific agents: natural forcing, land-use change, well-mixed GHGs, and anthropogenic aerosols. **Table 2.1** summarizes the CMIP3 models and **Table 2.2** summarizes the CMIP5 models used. We show the ITA time series for CMIP3 and CMIP5 but focus most of our analysis on CMIP5. We do not apply any additional masking of model regions that are missing in the datasets, which we find has very little effect on the ITA index.

In **Section 2.5**, we investigate precipitation *pr* and mean meridional mass streamfunction from most of the CMIP5 historical and RCP8.5 simulations, which are also

shown in **Table 2.2**. The mean meridional mass streamfunction is calculated from meridional wind v [e.g., Eq. (6.9) in Hartmann (1994)]. Streamfunction is shown in Sverdrups (1 Sv $\equiv 10^6$ m^3 s^{-1}); we use Sverdrups as a unit of mass transport (instead of the typical water volume transport). All calculations use January–December annual-mean values unless noted otherwise. For trend analysis, we use ordinary least squares regression and Student's two-tailed t test for significance (Wilks 2006).

2.3. Results

a. Historical period: Observations and models

The GISTEMP hemispheric temperature anomalies are shown in **Fig. 2.1a**. **Figure 2.1b** plots ΔITA for GISTEMP along with the other observational indices, which are almost identical. The GISTEMP ΔITA ranges between −0.39°C in 1972 and 0.41°C in 2010. We find no meaningful linear trend over the entire record. There is a noticeable drop in the late 1960s (0.25°C difference between 1950–67 and 1971–80), followed by a positive trend from 1981 to 2011 (0.17°C decade^{-1}; $p < 0.01$). There are also significant positive trends for each season: December–February, March–May, June–August, and September–November ($p < 0.01$).

The CMIP3 and CMIP5 ensemble mean and standard deviation of ΔITA are shown in **Figs. 2.1c** and **2.1d**, respectively, along with the GISTEMP ΔITA from **Fig. 2.1b**. The CMIP5 ensemble mean captures more of the observed multidecadal variability, with a correlation of 0.56 with the 5-yr running-mean GISTEMP ΔITA (not shown) from 1880 to 1999, compared with 0.33 for CMIP3. Both the CMIP3 and CMIP5 ensemble means have positive trends since 1980; the CMIP5 trend is larger and more realistic [CMIP3: 0.08°C decade^{-1} from 1981 to 1999; CMIP5: 0.10°C (0.13°C) decade^{-1} from 1981 to 1999 (1981 to 2004); GISTEMP: 0.19°C decade^{-1} from 1981 to 1999 and from 1981 to 2004; $p < 0.01$ for all trends]; the CMIP5 trends are significant at all seasons ($p < 0.01$). Neither ensemble mean captures the drop in the late 1960s.

b. Future projections

Figure 2.2 shows the future projected ΔITA. The striking feature of all future scenarios is the pronounced ΔITA increase, exceeding well beyond the twentieth-century range. The future ΔITA is apparently a continuation of the upward trend since 1980 (which we discuss in **Section 2.4**). Within each CMIP, the scenario with the larger radiative forcing has the larger increase. For the CMIP3, the mean 2080–99 ΔITA ranges from 0.23° to 1.30°C (mean: 0.64°C) in the B1 scenario and from 0.61° to 1.87°C (mean: 1.15°C) in the A2 scenario. For the CMIP5, the 2080–99-mean ΔITA ranges from −0.87° (FIO-ESM is the only model with a decrease) to 1.98°C (mean: 0.93°C) in RCP4.5 and from 0.01° to 2.96°C (mean: 1.63°C) in RCP8.5. The RCP8.5 ensemble-mean ΔITA projection is highly linear: the trend of 0.17°C decade^{-1} explains 99.5% of the variance from 2006 to 2099.

2.4. Attribution of the ITA trend

Figure 2.3 shows the ensemble-mean ΔITA from the CMIP5 specific-forcing simulations compared with observations. Neither natural forcings (**Fig. 2.3a**) nor land-use

change (**Fig. 2.3b**) affect long-term ΔITA departures over the historical period. In **Fig. 2.3a**, we have marked major tropical volcanic eruptions following Fig. 9.5 in Hegerl et al. (2007), which are largely followed by short-lived ΔITA decreases from the large-scale effects of stratospheric sulfate aerosols. Anthropogenic aerosols (**Fig. 2.3c**) and GHGs (**Fig. 2.3d**) force opposing ΔITA trends: aerosols disproportionately cool the NH, and GHGs disproportionately warm it. The compensating effects of these forcings explain why ΔITA remained relatively stable over much of the twentieth century, until around 1980. This is similar to global temperature, in which anthropogenic aerosols are believed to have masked GHGs over the middle of the twentieth century, though the global warming trend resumed slightly earlier (Hegerl et al. 2007). The ΔITA from anthropogenic aerosols levels off around 1970, when clean air laws took effect in much of Europe and North America, similar to previous findings of tropical Atlantic interhemispheric SST asymmetry (Chang et al. 2011). In contrast, the GHG-only ΔITA continues to increase along with GHG accumulation in the atmosphere. Summing ΔITA from the anthropogenic aerosol and GHG-only simulations (**Fig. 2.3e**) results in a positive ΔITA trend starting around 1980, which is similar to the observational record.

A direct comparison between the global-mean temperature anomaly ΔT_{glob} and ΔITA further highlights the origins and emergence of the ΔITA trend after 1980. **Figure 2.4** shows ΔITA plotted against ΔT_{glob}, for GISTEMP observations (**Fig. 2.4a**) and CMIP5 historical and specific-forcing simulations (**Figs. 2.4b–f**). For the observations (**Fig. 2.4a**), the years before and after 1980 feature two modes of behavior. Until 1980, the relationship between ΔITA and ΔT_{glob} is relatively weak (r = 0.29); however, from 1981 to 2011, ΔITA and ΔT_{glob} both feature positive anomalies and are much more strongly correlated (r = 0.84). Though the CMIP5 historical ΔITA and ΔT_{glob} show much less overall scatter than the observations, most likely caused by ensemble averaging (Hegerl et al. 2007), they similarly feature positive anomalies and a much stronger correlation after 1980 (r = 0.46 vs. 0.96). Though ΔT_{glob} and ΔITA are positively correlated for the natural forcing (**Fig. 2.4c**) and anthropogenic aerosol (**Fig. 2.4f**) simulations, these forcings do not produce the strong positive anomalies of ΔITA and ΔT_{glob} after 1980. Of the specific-forcing simulations, only GHGs (**Fig. 2.4e**) simulate the combination of post-1980 positive anomalies and positive correlation of ΔITA and ΔT_{glob}. (The positive slopes in both **Figs. 2.4c** and **2.4e** likely reflect the disproportionate effects of global radiative forcing on the NH, which is discussed below.) This comparison of the different forcing simulations thus suggests that GHGs have been dominant for ΔITA since 1980. Beforehand, the weak relationship between ΔT_{glob} and ΔITA does not point to any specific forcing as the primary factor.

What spatial features account for the positive ΔITA trend in the last few decades along with global-mean temperature? We focus on the period 1981–2011 in the observations, with the trend line delineated in **Fig. 2.5a**. **Figure 2.5b** shows the regression onto the 1981–2011 ΔITA trend line from **Fig. 2.5a**. This pattern of pronounced warming over the continents and NH extratropics has been discussed in previous analyses of global temperature change (Hansen et al. 2006; Trenberth et al. 2007), with eastern Pacific Ocean cooling described as part of the interdecadal Pacific oscillation (Wang et al. 2012). **Figure 2.5c** delineates the 1981–2004 trend in the CMIP5 historical ensemble mean, and **Fig. 2.5d** shows the regression slopes onto the trend line. The spatial pattern is similar to that of the observations (minus the eastern Pacific Ocean cooling), with more distinct NH

extratropical and continental warming because of the ensemble averaging that filters out each model's natural variability (Hegerl et al. 2007). The observational and model slopes are strongly spatially correlated (r = 0.67). [The correlation with the 1981–2004 CMIP5 ensemble-mean trend is higher for the GISTEMP trend through 2011 than through 2004 (r = 0.55), which suggests that the observational trend signal has become more significant over the last decade.] The 1981–2011 GISTEMP regression slopes are also highly correlated with the spatial regression slopes of ΔITA in future simulations (r = 0.64 for the RCP8.5 2005–99 ensemble mean). The spatial regression map of the 2006–2099 multimodel mean CMIP5 8.5 surface temperature anomalies onto ΔITA is shown in **Figure 2.5e**.

The regression slopes of zonal-mean observational, CMIP5 historical, and RCP8.5 temperature anomalies, shown in **Fig. 2.6a**, have very similar latitudinal gradients, though the mean warming differs among them. This hemispherically asymmetric zonal-mean pattern, also similar to regressions onto global temperature trends (Xu and Ramanathan 2012), has long been studied as a robust feature of the transient climate change response (Stouffer, Manabe, and Bryan 1989; Manabe et al. 1991). The prominent Arctic amplification has been attributed to feedbacks from melting snow and sea ice, water vapor, increasing clouds, and lapse rate changes (Bekryaev, Polyakov, and Alexeev 2010; Serreze and Barry 2011; Hwang, Frierson, and Kay 2011). Outside the Arctic, the zonal-mean pattern has largely been attributed to hemispheric differences in land and ocean, resulting in less NH evaporation and heat uptake (Hegerl et al. 2007), as the land–ocean warming contrast has been shown to be a robust feature of the global warming response (Lambert and Chiang 2007). However, we find that there has also been an increase in interhemispheric SST asymmetry over the last few decades [0.09°C decade^{-1} (p < 0.01), 1981–2011; ERSST.v3b], which contributes to the ΔITA increase. The recent interhemispheric SST asymmetry increase may have more than one cause. First, land and ocean temperatures are correlated because of land–sea advection (Thompson et al. 2009). Additionally, the warming minimum around 60°S has been attributed to heat uptake in the Southern Ocean, which mixes heat downward (S. Xie et al. 2010). Ocean dynamical variability may also play a role, which we discuss (for a different time period) in **Section 2.6**.

Figure 2.6b shows the relative contribution of three latitude zones to the ΔITA trends. The ΔITA trend contribution is calculated as the interhemispheric temperature asymmetry of the specific latitude band, multiplied by its surface area fraction. These zones (0°–44°, 44°–64°, and 64°–90°) cover about 70%, 20%, and 10% of the globe, respectively. To first order, these three latitude bands with very different areas have similar contributions to the ΔITA trend, which illustrates that the high latitudes are proportionally more important. However, it also puts the large Arctic warming in **Fig. 2.6a** into perspective: with its limited area, the Arctic amplification alone does not explain the majority of the ΔITA increase.

2.5. Impacts on tropical circulation and precipitation

Previous studies have found that increasing ITA causes weakening of the NH Hadley cell, strengthening of the SH Hadley cell, and a northward shift of tropical precipitation

(Yoshimori and Broccoli 2008; S. Kang, Frierson, and Held 2009; Frierson and Hwang 2012). Our analysis of the CMIP5 ensemble-mean future projections largely agrees with these prior findings.

First, we consider the Hadley circulation changes. **Figures 2.7a** and **2.7b** show the time series of NH and SH maximum meridional overturning mass streamfunction in the historical and RCP8.5 simulations. Comparing these with **Fig. 2.2**, the increase of ΔITA in the twenty-first century is accompanied by a significant weakening of the NH Hadley cell and a small strengthening of the SH Hadley cell. Hemispheric differences can be explained by the combination of the increased ITA and the overall weakening of tropical circulation with global warming (M. Zhang and Song 2006; Vecchi and Soden 2007). In the NH, both the increasing ITA and global warming weaken the circulation after around 1980, whereas in the SH the increasing ITA compensates for global warming and results in a small strengthening trend during this period. **Figure 2.7c**, the SH minus the NH maximum streamfunction (**Fig. 2.7a** minus **Fig. 2.7b**), removes much of the tropical-mean signal and thus more strongly shows the influence of the ITA on the Hadley circulation asymmetry.

Recent studies have also suggested that strengthening of the SH Hadley cell and weakening of the NH Hadley cell should lead to a northward shift of the tropical rainbands in the twenty-first century (S. Kang, Frierson, and Held 2009; Frierson and Hwang 2012). However, this signal is difficult to separate from a precipitation intensification from global warming (IM Held and Soden 2006), which would disproportionately increase NH tropical rainfall since there is more tropical NH rainfall in the present-day climate (Chou, Tu, and Tan 2007). We remove part of this effect by normalizing the precipitation changes by the tropical-mean amount. We define the precipitation asymmetry index as precipitation from the equator to 20°N minus precipitation from the equator to 20°S, normalized by tropical-mean precipitation (20°S–20°N). Even with this normalization, however, defining a precipitation index to represent the northward shift is challenging, as different GCMs project different kinds of spatial patterns in precipitation changes that affect our tropical precipitation asymmetry index. For example, some GCMs project a uniform northward shift of the present-day precipitation pattern, whereas some project a tropical precipitation shift toward the north without shifting the location of maximum precipitation.

Figure 2.7d shows the change in this tropical precipitation asymmetry index. Qualitatively, it resembles the behavior of the historical and projected ΔITA in **Fig. 2.2**: a relative lack of trend over the first half of the twentieth century and a northward trend starting around 1980 and extending into the future. However, we note that the positive trend in the precipitation asymmetry after 1980 appears to be smaller than expected from increasing ΔITA alone. The northward shift does not become significant (compared with the twentieth-century ensemble standard deviation) until 2040, whereas ΔITA is anomalously positive from the beginning of the twenty-first century. We have also noticed that some GCMs with a smaller increase of ΔITA actually project a relative decrease in the SH minus NH Hadley circulation difference and a southward shift of tropical precipitation (which can be inferred from the wide ensemble standard deviation shading in **Figs. 2.7c and 2.7d**).

Though the association in the CMIP5 models is promising, there are additional caveats to directly linking the ITA with the shifts in tropical precipitation. First, the marine

ITCZ is more strictly dynamically tied to the tropical SST asymmetry (Lindzen and Nigam 1987), so latitudes closer to the equator may have a larger effect on tropical rainfall for a given change in ΔITA. Precipitation variability in CMIP5 models has recently been attributed to SST change disparities among models (Ma and Xie 2013). For example, SST warming at the equator (which may be caused by, e.g., a weaker Walker circulation) does not contribute to the ITA index; however, it is expected to cause a southward ITCZ shift (Vecchi et al. 2006; Seager and Naik 2012). Furthermore, from an energy flux perspective, an increasing ITA may not necessarily lead to southward cross-equatorial atmospheric heat transport and a northward ITCZ shift; the ITCZ can actually shift away from the warmed hemisphere when enhanced GHG warming leads to increased outgoing radiation (Frierson and Hwang 2012; Zelinka and Hartmann 2012). Thus, we caution against applying a simplistic association between future ITA changes and tropical rainfall asymmetry. Another hemispherically asymmetric process we have yet to consider for both circulation and rainfall is Antarctic stratospheric ozone depletion. Twenty-first-century ozone recovery is projected to strengthen the SH summer Hadley cell and contract the subtropical dry zones, opposing greenhouse forcing (Polvani, Previdi, and Deser 2011).

2.6. Late-1960s ITA shift

Finally, we consider the abrupt ITA shift in the late 1960s. The rapid time scale and the spatial pattern associated with the late-1960s ITA drop suggest different processes than those contributing to the ITA increase of the last few decades. **Figure 2.8a** shows the GISTEMP ΔITA, with a linear fit connecting the means of 1950–67 and 1971–80. **Figure 2.8b** shows the regression slopes of GISTEMP anomalies onto this linear fit of the drop. The slopes are characterized by extratropical SST cooling in the NH and warming in the SH, with the largest magnitude slopes corresponding to cooling in the North Atlantic. Additionally, there is warming in the southern Atlantic and Indian Oceans and also cooling in the North Pacific. Comparison with **Fig. 2.5b** shows that this spatial pattern is quite distinct from that of the increasing ITA trend since 1980, which is driven by hemispherically asymmetric warming in the Arctic and northern landmasses. **Figure 2.8c**, the zonal-mean regression slopes onto the linear fit of the drop, shows values of opposite sign and similar magnitude that are strongest in the mid latitudes of both hemispheres. This zonal-mean mid-latitude dipole can be contrasted with the zonal-mean trends in **Fig. 2.6a**, which are positive in both hemispheres and feature strong Arctic amplification.

What caused the abrupt shift? Baines and Folland (2007) speculate that either global ocean meridional overturning circulation (MOC) or an increase in anthropogenic sulfate aerosols was responsible. Investigating unsmoothed monthly data, Thompson et al. (2010) argue that the rapid time scale of the interhemispheric SST shift points to an abrupt change in ocean circulation centered in the dynamically active North Atlantic. They suggest that the source was a rapid freshening in the northern North Atlantic, previously identified as the "Great Salinity Anomaly" from the late 1960s through early 1970s (Dickson et al. 1988; R. Zhang and Vallis 2006). Dima and Lohmann (2010) describe an interhemispheric mode of SST variability with a large amplitude in the North Atlantic that underwent a shift around 1970. They ascribe this mode to the Atlantic MOC response to freshwater forcing, triggered by the great salinity anomaly. A recent attribution study of North Atlantic SSTs

also points to internal ocean variability as primarily responsible for the late-1960s cooling event that contributed to the interhemispheric SST difference (Terray 2012).

As shown in **Figs. 2.1c and 2.1d**, the CMIP historical ensemble means do not simulate the observational ITA shift in the late 1960s, suggesting that the observed drop is caused by internal variability. However, some individual CMIP5 realizations do produce a realistic ITA shift during this period (not shown), which leaves open some questions about the extent to which it was externally forced. The impacts of the late-1960s ITA shift on tropical circulation and precipitation also remain a topic of investigation. Concurrent changes have been identified in several atmospheric circulation indices in the late 1960s, correlated with the interhemispheric SST shift (Baines and Folland 2007; Mantsis and Clement 2009). There was also a coordinated weakening of the West African and Asian monsoons around this time, which has been linked the decrease in North Atlantic SST (Liu and Chiang 2012).

2.7. Conclusions

In this study, we have presented the interhemispheric temperature asymmetry as an index of climate change. In addition to being conceptually simple and available from observations prior to the satellite record, we argue that it can provide insight into climate change forcings and also point to changes in tropical circulation and precipitation.

Our major findings about the ITA are as follows: The observed ITA did not exhibit a significant trend over most of the twentieth century; however, it began a pronounced upward trend (north warming faster than south) around 1980, which the CMIP5 simulations reproduce more strongly. Our analysis of the CMIP5 specific-forcing simulations suggests that the effects of GHGs and aerosols on the ITA largely compensated for each other until around 1980, when steadily accumulating GHGs overtook aerosols that had leveled off from pollution regulations. The upward trend continues in the twenty-first-century projection simulations we examined. Spatial regressions show that the positive ITA trend of the last few decades is primarily driven by disproportionate warming in the Arctic and NH landmasses, which was previously shown to be a hemispherically asymmetric response pattern to global climate forcing.

The CMIP5 simulations indicate that the atmospheric circulation will respond to the increased ITA via a strengthening of the southern Hadley cell and a weakening of the northern Hadley cell, a result that is not predicted from the dynamical response to global warming alone. Our analysis suggests that this will be accompanied by a northward shift in tropical precipitation, though there are difficulties distinguishing this response from other components of the hydrological response to global warming. Another caveat is that tropical circulation and rainfall may also have hemispherically asymmetric responses to projected ozone recovery.

We ended with a short discussion of the late-1960s abrupt ITA decrease. Unlike the response to GHGs, which is characterized by hemispherically asymmetric warming with polar amplification, the late-1960s ITA shift is characterized by a mid-latitude SST dipole. We presented evidence that the abrupt decrease was driven by a sudden change in the ocean meridional overturning circulation centered in the North Atlantic; though intriguing,

the mechanisms remain to be worked out. Future steps in pursuing this problem include investigating the high-resolution ITA time series to follow the propagation of temperature anomalies and studying the behavior of individual models that do simulate a realistic ITA shift. The impacts of the late-1960s abrupt ITA shift on the Hadley cell and tropical rainfall will also be a focus of future studies.

2.8. Acknowledgments

GISTEMP hemispheric and zonal-mean averages are from data.giss.nasa.gov/gistemp/ and gridded data from www.esrl.noaa.gov/psd/data/gridded/data.gisstemp.html (1200-km smoothing). NCDC hemispheric averages are from www.ncdc.noaa.gov/cmb-faq/anomalies.php; HadCRUT4 hemispheric averages are from www.metoffice.gov.uk/hadobs/hadcrut4/ (median "best estimate" realization). CMIP3 and CMIP5 output are available from https://esg.llnl.gov:8443/index.jsp and http://pcmdi3.llnl.gov/esgcet/home.htm respectively.

We acknowledge the World Climate Research Program's Working Group on Coupled Modeling, which is responsible for CMIP. For CMIP, the U.S. Department of Energy's Program for Climate Model Diagnosis and Intercomparison provides coordinating support and led development of software infrastructure in partnership with the Global Organization for Earth System Science Portals. This work was funded by the Office of Science Biological and Environmental Research, U.S. Department of Energy (DE-FG02-08ER64588), and by NSF Grant AGS-1143329, AGS-0846641, and AGS-0936059.

We acknowledge the developers of the Grid Analysis and Display System (GrADS), the netCDF Operators (NCO), and the Climate Data Operators (CDO). We thank Paulo Ceppi for the CMIP5 streamfunction calculations; Darin Jensen for helpful feedback on figures; Lisa Friedman for careful editing; and Shang-Ping Xie, Tripti Bhattacharya, and Yuwei Liu for valuable discussions. We appreciate the constructive suggestions of three anonymous reviewers.

2.9. Tables and figures

Model		Scenario		
Institute	Expansion (acronym)	20c3m	SRES A2	SRES B1
Bjerknes Centre for Climate Research (BCCR)	BCCR Bergen Climate Model, version 2.0 (BCCR-BCM2.0)	X	X	X
National Center for Atmospheric Research (NCAR)	Community Climate System Model, version 3.0 (CCSM3.0)	X	X	X
Canadian Centre for Climate Modelling and Analysis (CCCma)	Coupled Global Climate Model, version 3.1 (T47) [CGCM3.1(T47)]	X	X	X
CCCma	Coupled Global Climate Model, version 3.1 (T63) [CGCM3.1(T63)]	X		X
Centre National de Recherches Météorologiques (CNRM)	CNRM Coupled Global Climate Model, version 3 (CNRM-CM3)	X	X	X
Commonwealth Scientific and Industrial Research Organisation (CSIRO)	CSIRO Mark, version 3.0 (CSIRO Mk3.0)	X	X	X
CSIRO	CSIRO Mark, version 3.5 (CSIRO Mk3.5)	X	X	X
Istituto Nazionale di Geofisica e Vulcanologia	ECHAM4 (ECHAM4)	X	X	
Max Planck Institute (MPI) for Meteorology	ECHAM5/MPI Ocean Model (ECHAM5/MPI-OM)	X	X	X
Meteorological Institute of the University of Bonn, Meteorological Research Institute of the Korean Meteorological Administration, and Model and Data Group	ECHAM and the global Hamburg Ocean Primitive Equation (ECHO-G)	X	X	X
NOAA Geophysical Fluid Dynamics Laboratory (GFDL)	GFDL Climate Model, version 2.0 (GFDL CM2.0)	X	X	X
NOAA GFDL	GFDL Climate Model, version 2.1 (GFDL CM2.1)	X	X	X
National Aeronautics and Space Administration (NASA) GISS	GISS, Atmosphere–Ocean Model (GISS-AOM)	X		X
NASA GISS	GISS Model E, coupled with the HYCOM ocean model (GISS-EH)	X		
NASA GISS	GISS Model E-R (GISS-ER)	X	X	X
Hadley Centre/Met Office	Hadley Centre Coupled Model, version 3 (HadCM3)	X	X	X
Hadley Centre/Met Office	Hadley Centre Global Environmental Model, version 1 (HadGEM1)	X	X	
Institute for Numerical Mathematics (INM)	INM Coupled Model, version 3.0 (INM-CM3.0)	X	X	X
L'Institut Pierre-Simon Laplace (IPSL)	IPSL Coupled Model, version 4 (IPSL-CM4)	X	X	X
Center for Climate System Research (The University of Tokyo), National Institute for Environmental Studies, and Frontier Research Center for Global Change	Model for Interdisciplinary Research on Climate, version 3.2 (high resolution) [MIROC3.2(hires)]	X		X
Center for Climate System Research (The University of Tokyo), National Institute for Environmental Studies, and Frontier Research Center for Global Change	Model for Interdisciplinary Research on Climate, version 3.2 (medium resolution) [MIROC3.2(medres)]	X	X	X
Meteorological Research Institute (MRI)	MRI Coupled Atmosphere–Ocean General Circulation Model, version 2.3.2 (MRI-CGCM2.3.2)	X	X	X
NCAR	Parallel Climate Model (PCM)	X	X	X

Table 2.1. List of CMIP3 models and respective scenarios used for the analysis. In this table, "X" denotes availability of the scenarios. One ensemble member from each scenario is used.

Model		tas							v + pr
Institute	Expansion (acronym)	H	RCP4.5	RCP8.5	Nat	GHG	AA	LU	H + RCP8.5
CSIRO and Bureau of Meteorology, Australia	Australian Community Climate and Earth-System Simulator, version 1.0 (ACCESS1.0)	1	1	1					1
CSIRO and Bureau of Meteorology, Australia	Australian Community Climate and Earth-System Simulator, version 1.3 (ACCESS1.3)	1	1	1					1
Beijing Climate Center (BCC), China Meteorological Administration	BCC, Climate System Model, version 1.1 (BCC-CSM1.1)	1	1	1					1
College of Global Change and Earth System Science, Beijing Normal University (BNU)	BNU—Earth System Model (BNU-ESM)	1	1	1					1
CCCma	Second Generation Canadian Earth System Model (CanESM2)	1	1	1	5	5	5	5	1
NCAR	Community Climate System Model, version 4.0 (CCSM4.0)	1		1					1
Community Earth System Model Contributors	Community Earth System Model, version 1.0–Biogeochemistry (CESM1-BGC)	1	1	1					1
Community Earth System Model Contributors	Community Earth System Model, version 1.0–Community Atmosphere Model, version 5.0 (CESM1-CAM5)	1	1	1					1
Community Earth System Model Contributors	Community Earth System Model, version 1.0–Community Atmosphere Model, version 5.1-Finite Volume 2° [CESM1-CAM5.1 (FV2)]	1							
Community Earth System Model Contributors	Community Earth System Model, version 1.0–Whole Atmosphere Community Climate Model (CESM1-WACCM)	1	1	1					
Euro-Mediterranean Centre on Climate Change (CMCC)	CMCC Climate Model (CMCC-CM)	1	1	1					
CNRM/Centre Européen de Recherche et de Formation Avancée en Calcul Scientifique	CNRM Coupled Global Climate Model, version 5 (CNRM-CM5)	1	1	1					1
CSIRO in collaboration with Queensland Climate Change Centre of Excellence	CSIRO Mark, version 3.6.0 (CSIRO Mk3.6.0)	1	1	1					1
EC-Earth Consortium	EC-EARTH	1	1	1					
State Key Laboratory of Numerical Modeling for Atmospheric Sciences and Geophysical Fluid Dynamics (LASG), Institute of Atmospheric Physics, Chinese Academy of Sciences and Center for Earth System Science, Tsinghua University	Flexible Global Ocean–Atmosphere–Land System Model gridpoint, version 2.0 (FGOALS-g2.0)	1		1					
LASG, Institute of Atmospheric Physics, Chinese Academy of Sciences	Flexible Global Ocean–Atmosphere–Land System Model gridpoint, second spectral version (FGOALS-s2)	1	1	1					1
The First Institute of Oceanography (FIO), State Oceanic Administration	FIO Earth System Model (FIO-ESM)	1	1	1					1
NOAA GFDL	GFDL Climate Model, version 3 (GFDL CM3)	1	1	1	3	3	3		1
NOAA GFDL	GFDL Earth System Model with GOLD ocean component (GFDL ESM2G)	1	1	1					1
NOAA GFDL	GFDL Earth System Model with MOM4 ocean component (GFDL ESM2M)	1	1	1	1	1	1	1	1
NASA GISS	GISS Model E, coupled with the HYCOM ocean model (GISS-E2H)	1	1	1					
NASA GISS	GISS Model E, coupled with the Russell ocean model (GISS-E2-R)	1	1	1					1
National Institute of Meteorological Research/Korea Meteorological Administration	Hadley Centre Global Environmental Model, version 2, Atmosphere and Ocean (HadGEM2-AO)	1	1	1					1
Hadley Centre/Met Office	Hadley Centre Coupled Model, version 3 (HadCM3)	1							
Hadley Centre/Met Office	Hadley Centre Global Environmental Model, version 2, Carbon Cycle (HadGEM2-CC)	1	1	1					1
Hadley Centre/Met Office	Hadley Centre Global Environmental Model, version 2, Earth System (HadGEM2-ES)	1	1	1					1
INM	INM Coupled Model, version 4.0 (INM-CM4)	1	1	1					1
IPSL	IPSL Coupled Model, version 5, coupled with NEMO, low resolution (IPSL-CM5A-LR)	1	1	1					1
IPSL	IPSL Coupled Model, version 5, coupled with NEMO, mid resolution (IPSL-CM5A-MR)	1	1	1					1
IPSL	IPSL Coupled Model, version 5(B), coupled with NEMO, low resolution (IPSL-CM5B-LR)	1	1	1					1
Japan Agency for Marine-Earth Science and Technology, Atmosphere and Ocean Research Institute (The University of Tokyo), and National Institute for Environmental Studies	Model for Interdisciplinary Research on Climate, version 5 (MIROC5)	1	1	1					1
Japan Agency for Marine-Earth Science and Technology, Atmosphere and Ocean Research Institute (The University of Tokyo), and National Institute for Environmental Studies	Model for Interdisciplinary Research on Climate, Earth System Model (MIROC-ESM)	1	1	1					1
Japan Agency for Marine-Earth Science and Technology, Atmosphere and Ocean Research Institute (The University of Tokyo), and National Institute for Environmental Studies	Model for Interdisciplinary Research on Climate, Earth System Model, Chemistry Coupled (MIROC-ESM-CHEM)	1	1	1					1
MPI for Meteorology	MPI Earth System Model, low resolution (MPI-ESM-LR)	1	1	1					1
MPI for Meteorology	MPI Earth System Model, medium resolution (MPI-ESM-MR)	1	1	1					1
MPI for Meteorology	MPI Earth System Model, paleo (MPI-ESM-P)	1							
MRI	MRI Coupled Atmosphere–Ocean General Circulation Model, version 3 (MRI-CGCM3)	1	1	1					1
Norwegian Climate Centre	Norwegian Earth System Model, version 1, medium resolution (NorESM1-M)	1	1	1	1	1	1		1

Table 2.2. List of CMIP5 models and respective scenarios used for the analysis. The number of realizations investigated for each scenario is indicated for each scenario: H = historical, Nat = natural, GHG = well-mixed greenhouse gases, AA = anthropogenic aerosols, and LU = land-use change. All but the last column refer to near-surface air temperature *tas*. The last column indicates the models used in our analysis of meridional wind *v* and precipitation *pr* in the historical and RCP8.5 scenarios.

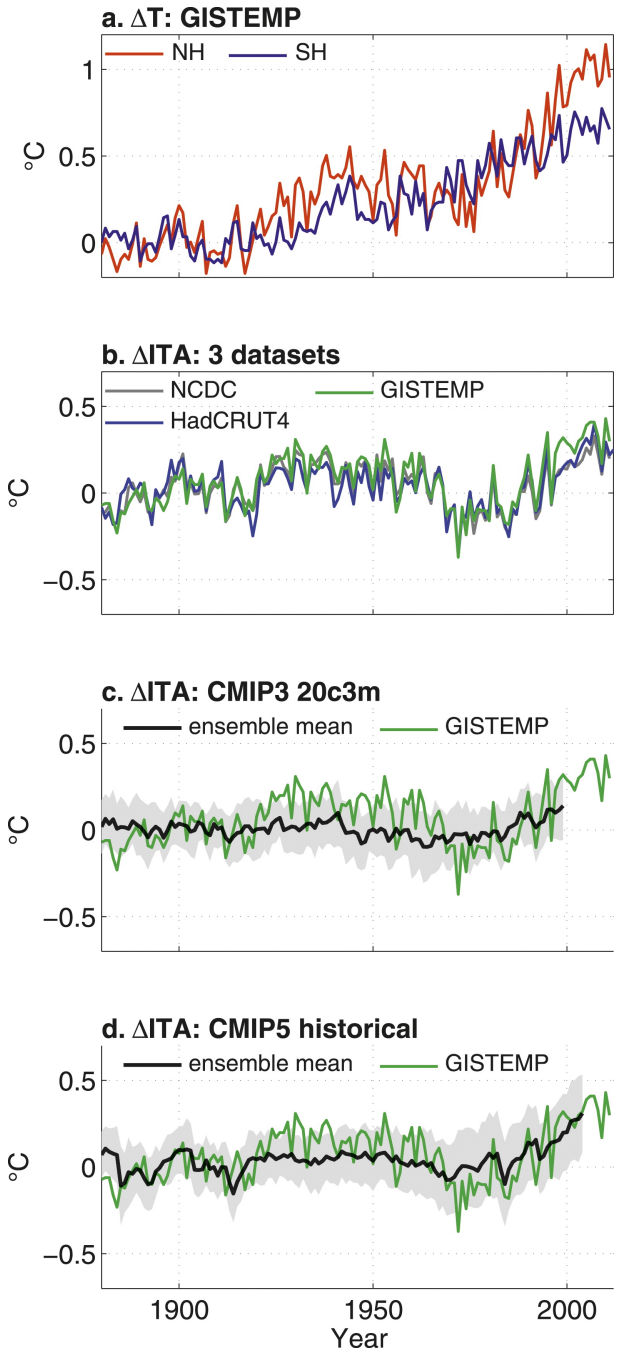

Figure 2.1. (a) GISTEMP temperature anomalies for NH (red) and SH (blue). (b) GISTEMP (green), NCDC (gray), and HadCRUT4 (blue) ΔITA. (c) CMIP3 20c3m ΔITA. (d) CMIP5 historical ΔITA. In (c),(d), the black solid line is the ensemble mean, the gray shading indicates ± one ensemble standard deviation, and the green line shows GISTEMP ΔITA from (b).

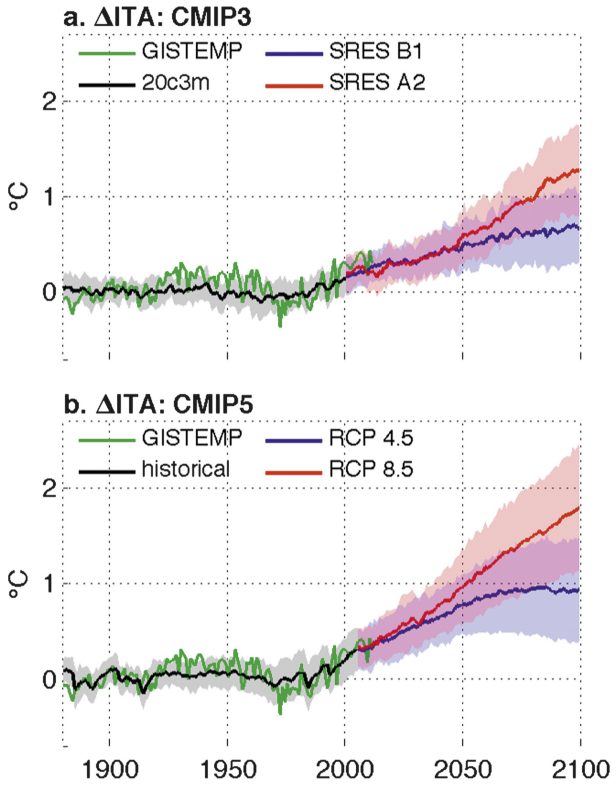

Figure 2.2. Twentieth- and twenty-first-century projected ΔITA. GISTEMP and twentieth-century scenarios are as in **Fig. 2.1**. (a) CMIP3 SRES B1 (blue) and SRES A2 (red). (b) CMIP5 RCP4.5 (blue) and RCP8.5 (red). Solid lines indicate the ensemble mean, and shading indicates ± one ensemble standard deviation.

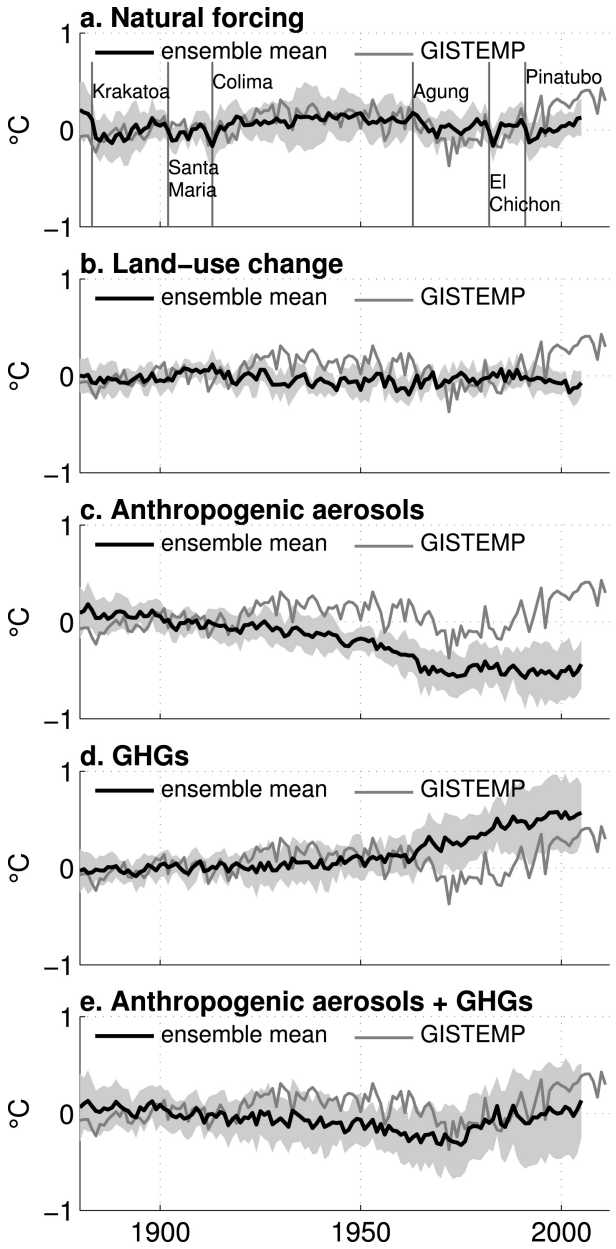

Figure 2.3. CMIP5 twentieth-century specific-forcing ΔITA. The black line shows the ensemble mean, and the gray line shows the observational ΔITA as in **Figs. 2.1** and **2.2**. Shading indicates ± one ensemble standard deviation of the models indicated in **Table 2.2**. (a) Natural forcing, with major volcanic eruptions indicated: Krakatoa (1883), Santa Maria (1902), Colima (1913), Agung (1963), El Chichón (1982), and Pinatubo (1991). (b) Land-use change. (c) Anthropogenic aerosols. (d) GHGs. (e) Sum of anthropogenic aerosols and GHGs. The ensemble standard deviation for (e) is constructed by summing the ensemble standard deviation of (c) and (d) in quadrature.

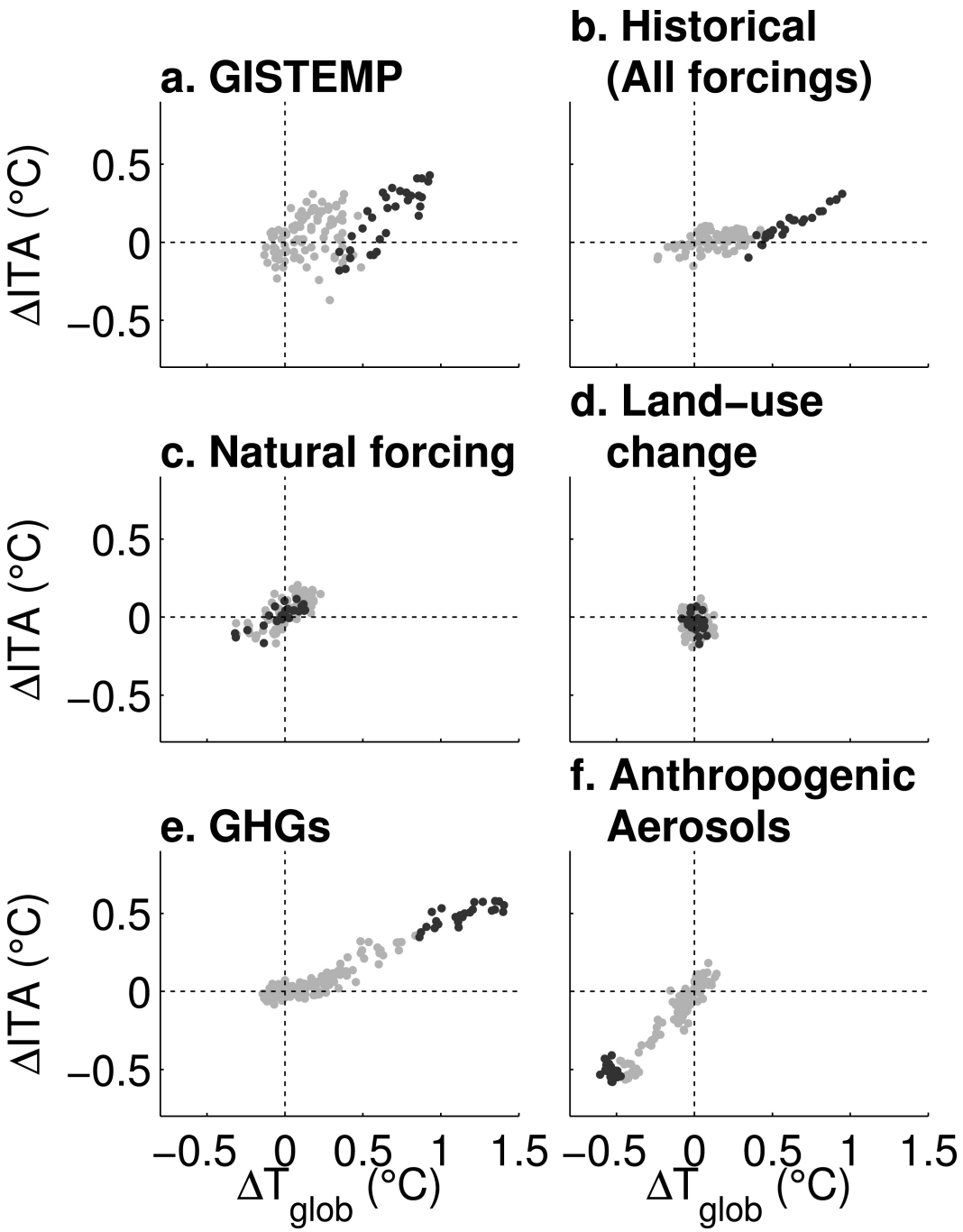

Figure 2.4. ΔITA vs. ΔT_{glob} for (a) observations and (b)–(f) CMIP5 ensemble means. Each point represents one year. (a) GISTEMP. (b) Historical (all forcings). (c) Natural forcing. (d) Land-use change. (e) GHGs. (f) Anthropogenic aerosols. Years before (since) 1981 are shaded light (dark) gray. GISTEMP is from 1880 to 2011, and CMIP5 is from 1880 to 2004.

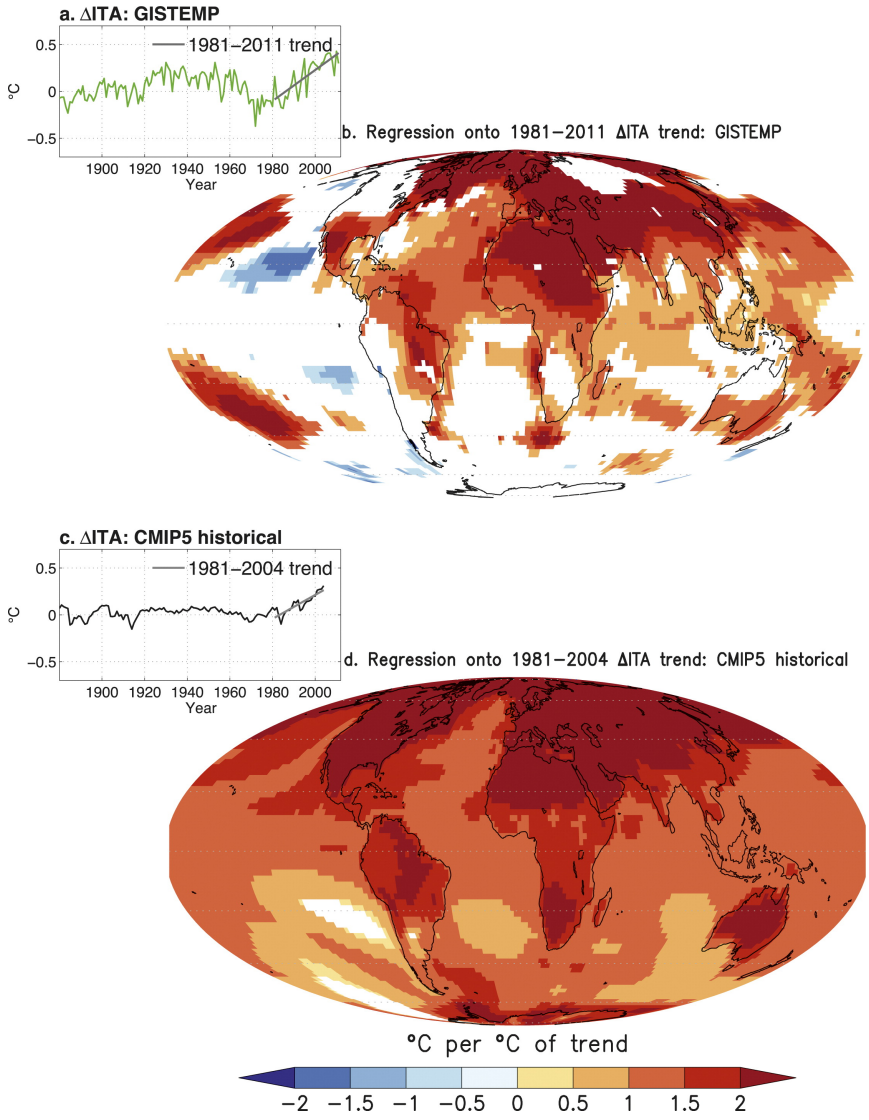
a. ΔITA: GISTEMP
1981–2011 trend
0.5
0
−0.5
°C
1900 1920 1940 1960 1980 2000
Year
b. Regression onto 1981–2011 ΔITA trend: GISTEMP
c. ΔITA: CMIP5 historical
1981–2004 trend
0.5
0
−0.5
°C
1900 1920 1940 1960 1980 2000
Year
d. Regression onto 1981–2004 ΔITA trend: CMIP5 historical
°C per °C of trend
−2 −1.5 −1 −0.5 0 0.5 1 1.5 2

(e)

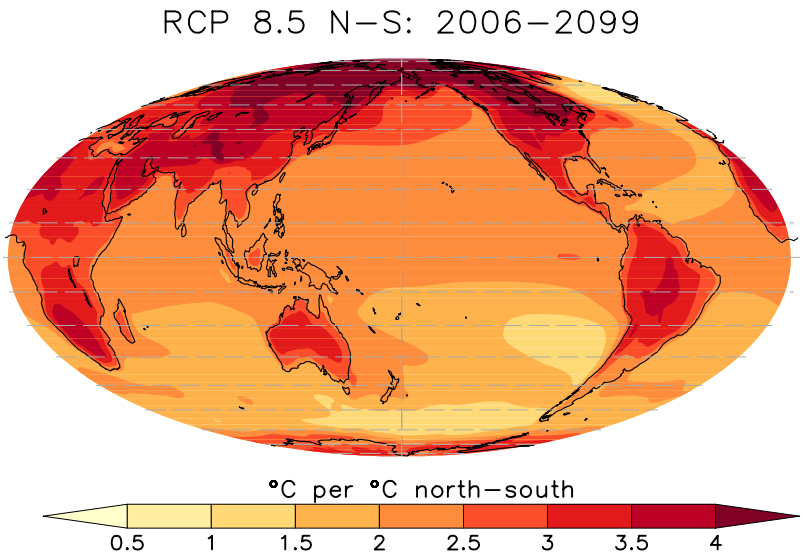

Figure 2.5. (a) GISTEMP ΔITA with 1981–2011 linear trend indicated. (b) Regression of GISTEMP temperatures onto the 1981–2011 ΔITA trend (°C °C^{-1} of ΔITA trend), plotted where $p < 0.05$. (c) CMIP5 historical ensemble-mean ΔITA with 1981–2004 linear trend indicated. (d) Regression of CMIP5 historical ensemble-mean surface temperatures onto the 1981–2004 ΔITA trend (°C °C^{-1} of ΔITA trend), plotted where $p < 0.05$. (e) Regression of CMIP5 RCP 8.5 ensemble-mean surface temperatures onto 2006–2099 ΔITA (°C °C^{-1} of ΔITA).

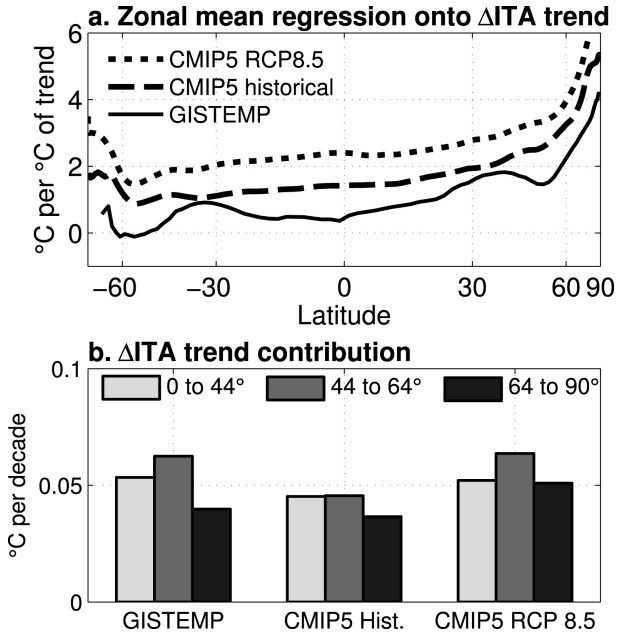

Figure 2.6. (a) Regression of zonal-mean temperatures onto the ΔITA linear trend (°C °C^{-1} of ΔITA trend) for GISTEMP (1981–2011), CMIP5 historical ensemble mean (1981–2004), and CMIP5 RCP8.5 ensemble mean (2006–99). The *x* axis is linear in sine of latitude so that spacing corresponds to surface area. Positive (negative) latitude values indicate degrees north (south). (b) Contribution to ΔITA trend by latitude zone (°C decade^{-1}) for GISTEMP (1981–2011), CMIP5 historical ensemble mean (1981–2004), and RCP8.5 ensemble mean (2006–09).

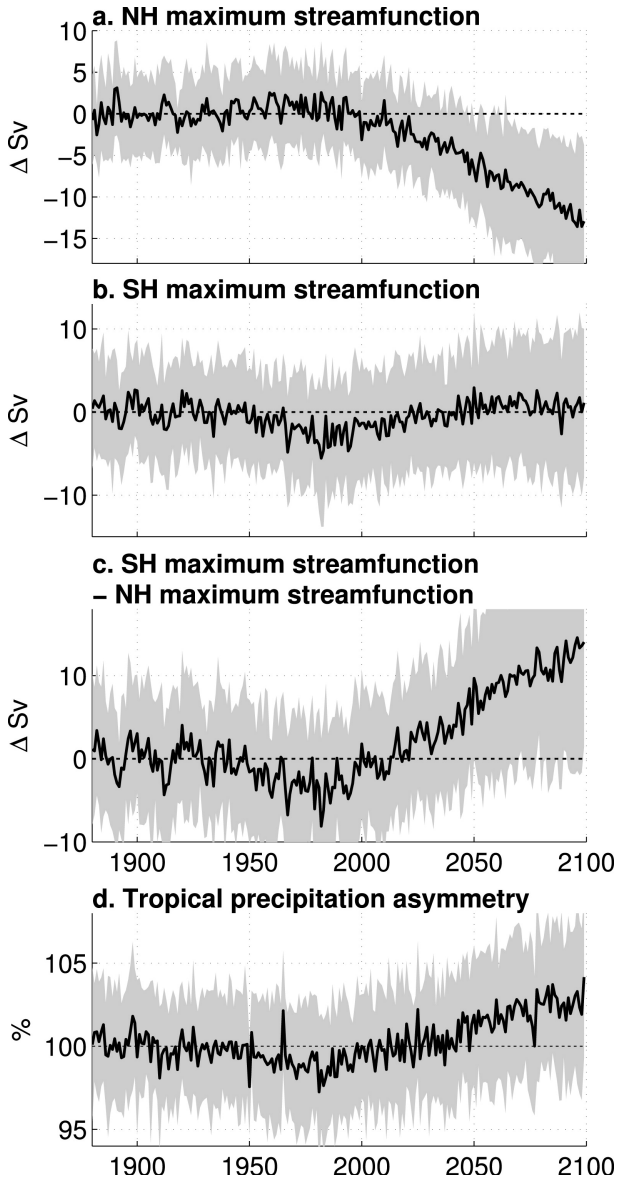

Figure 2.7. Mean meridional overturning mass streamfunction maximum anomalies for (a) NH, (b) SH, and (c) SH minus NH. (d) Tropical precipitation hemispheric asymmetry index [(0°–20°N) – (0°–20°S)]/(20°S–20°N) as a percentage of the 1891–1920 mean. The black line shows the ensemble mean and shading indicates ± one ensemble standard deviation of CMIP5 historical (1880–2004) and RCP8.5 (2005–99) simulations indicated in **Table 2.2**.

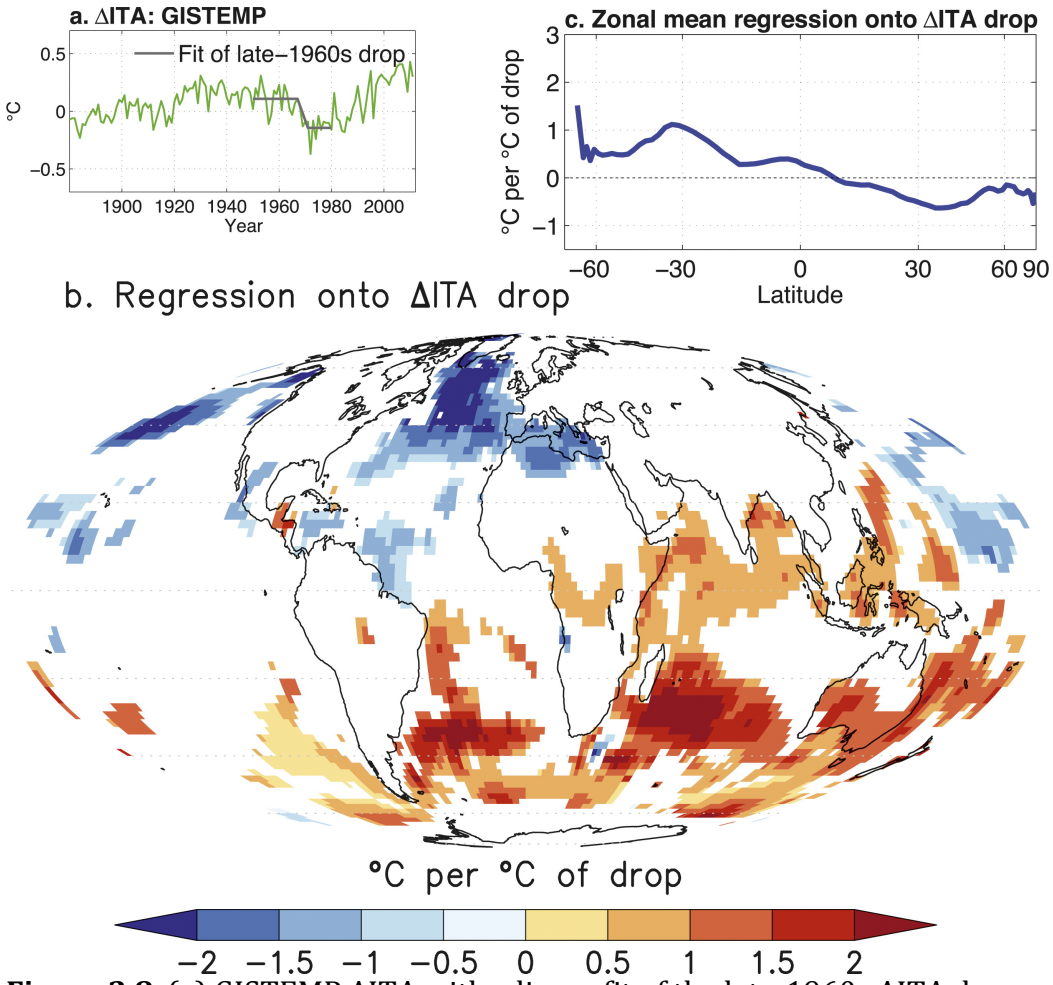

Figure 2.8. (a) GISTEMP ΔITA with a linear fit of the late-1960s ΔITA drop constructed by linearly interpolating between the means of 1950–67 and 1971–80, similar to the interhemispheric SST difference fit in Thompson et al. (2010). (b) Regression of GISTEMP temperatures onto the linear fit of late-1960s ΔITA drop (°C °C^{-1} of ΔITA drop), plotted where $p < 0.05$. (c) Regression of GISTEMP zonal-mean temperatures onto the linear fit of late-1960s drop (°C °C^{-1} of ΔITA drop). The *x* axis in (c) is linear in sine of latitude so that spacing corresponds to surface area.

3. Great Salinity Anomaly linked to interhemispheric SST shift around 1970

3.1. Introduction

The global north–south interhemispheric sea surface temperature (SST) difference is an important climate index that has profound impacts on tropical atmospheric circulation and rainfall (Chiang and Friedman 2012). One of the most visually striking features of the interhemispheric SST record is a north–south decrease around 1970 (Thompson et al. 2010), shown in the top 2 rows of **Figure 3.1**. This interhemispheric SST shift has been linked to abrupt changes in the tropical atmospheric overturning circulation (Baines and Folland 2007), and stark declines in monsoon rainfall over the Sahel, India, and north China (Liu and Chiang 2012).

The nature and cause of the shift remain unresolved. The shift has been hypothesized to be from a discrete internally-generated ocean event (Thompson et al. 2010). Alternatively, it has been described not as a shift but as a non-linear trend due to gradual cooling from sulfate aerosols (Wilcox, Highwood, and Dunstone 2013).

Compared with surface and atmospheric variables, the subsurface ocean changes associated with the interhemispheric SST shift have not been sufficiently examined. In this study, we investigate the corresponding changes in upper-ocean temperature, ocean heat content (OHC), and salinity. Our goal is to complement studies of the surface and paint a more comprehensive picture of the shift. Additionally, we revisit the interhemispheric SST time series in attempt to quantify the shift more formally.

The chapter proceeds as follows. Data and methods are outlined in **Section 3.2**. In **Section 3.3**, we identify the SST shift in updated datasets using a regime shift detection method. In **Section 3.4**, we examine changes in different upper-ocean fields associated with the shift. Finally, we discuss in **Section 3.5** how these features of the shift provide insight into its origins.

3.2. Data and methods

We examine hemispheric averages of the Met Office Hadley Center's SST dataset (HadSST3) (Kennedy et al. 2011a; Kennedy et al. 2011b) and the National Climatic Data Center's Extended Reconstructed SST product (ERSSTv3b) (T. M. Smith and Reynolds 2004; Vose et al. 2012). We also examine gridded HadSST3 and ERSSTv3b data. The median realization of HadSST3 is used. Annual means are calculated from the monthly SST data. For HadSST3, which is uninterpolated, we calculate the annual mean from the non-missing months; years without any monthly values are considered missing. We regrid the 2°×2° ERSSTv3b dataset to a 5°×5° grid by first splitting it into 1°×1° gridboxes and then box-averaging to 5°×5°.

We also examine several gridded upper-ocean datasets. We investigate single-level integrated products: annual mean 0-700m OHC from the National Oceanic Data Center (NODC) (Levitus et al. 2012) and the Japan Meteorological Agency (JMA) (Ishii and Kimoto

2009), and NODC 0-700m vertically-averaged pentadal salinity (Boyer et al. 2005). We express OHC in units of 10^9 J m^{-2}, and salinity on the practical salinity scale (PSS). Additionally, we investigate NODC annual mean temperature (Levitus et al. 2012) and pentadal salinity (Boyer et al. 2005) at 16 standard depth levels in the upper 700m of the ocean. The NODC data are available from 1955, and the JMA data from 1950. The salinity pentad year corresponds to its midpoint (e.g. 2011 for the 2009–2013 pentad). All the data are box-averaged from 1°×1° to 5°×5°.

The interhemispheric SST shift is formally identified using the regime shift detection algorithm described in Rodionov (2004) and Rodionov and Overland (2005), applied from 1900–2013. The algorithm sequentially applies a *t*-test to the difference between two adjacent segments of length *L*. A regime shift is identified when a point and the subsequent *L*-point mean differ from the previous *L*-point mean at significance level *p.* The regime shift index (RSI) is defined at this change point as the cumulative sum of the normalized deviations in the second segment from the minimum value that is significantly different from the first mean. The results shown use the parameters p=0.01 and cutoff length *L* of 10 years. Changing *L* or *p* or using annual instead of monthly data do not substantially change the RSI timing for the interhemispheric shift in either direction.

To examine the ocean patterns corresponding to the interhemispheric SST shift, we regress gridded datasets onto a linear fit of the shift, similar to Thompson et al. (2010). We construct the linear approximations of the interhemispheric SST by applying least-squares linear regression to obtain a best fit over the five-year interval from July 1967 to June 1972, chosen to encompass the start and end points identified by the forward and reverse RSI. Defined over this interval, the magnitude of the shift is 0.45°C for HadSST3 and 0.43°C for ERSSTv3b. The end values are extended 12 years backward and forward, from 1955 to 1984. This period was chosen to include all of the subsurface data, and to highlight the shift at a timescale between interannual variability and long-term trends. The fits are shown as the red lines in **Figure 3.1**.

We remove annual mean global average SST, 0-700m vertically-averaged temperature, and 0-700m OHC respectively prior to regressing in order to focus on hemispherically asymmetric changes. For the pentadal NODC salinity data, we regress onto a pentadal mean of the linear fit. For the spatial plots, we multiply the slopes by the magnitude of the linear fit so that they directly correspond to the change over the interhemispheric SST shift and are in the same units as the original data. Positive slopes correspond to cooling and freshening during the shift, and vice versa. Slopes are plotted where p<0.05, calculated using a two-tailed *t*-test. All maps (except HadSST3 in **Figure 3.2a**) are shown for the ERSSTv3b linear fit, as the HadSST3 fit is nearly identical.

Ocean basins are defined using boundaries from the World Ocean Atlas (Locarnini et al. 2010); our North Atlantic domain used for spatial correlation does not include the North Sea east of 0°E or the Mediterranean Sea. Spatial correlations are calculated with gridpoints weighted by the cosine of latitude, and after removing missing data. All data are expressed as anomalies from 1961–1990.

3.3. Regime shift identification and spatial SST structure of the shift

The bottom 2 rows of **Figure 3.1** show the results of the regime shift detection algorithm applied to the interhemispheric SST timeseries. We find that the regime shift detection algorithm identifies the shift around 1970 as the most pronounced change in the record. For both datasets, the largest magnitude RSI occurs during 1968 in the forward direction and 1971 in the reverse direction. This suggests that the 1970 shift was a discrete feature that both began and ended abruptly.

Figures 3.2a and **3.2b** show the SST changes associated with the interhemispheric shift, formed by regressing the annual gridded SST data onto the red linear fits in **Figure 3.1**. The resulting spatial structure features an interhemispheric dipole with the largest magnitudes in the extratropics. The most pronounced region of cooling is the subpolar North Atlantic north of 50°N, as noted in Thompson et al. (2010). We also observe that both datasets have a small region of warming in the western mid-latitude North Atlantic just offshore the U.S. east coast.

Focusing on the region of largest slope, **Figure 3.2c** shows the timeseries of subpolar North Atlantic minus global average SST. In both datasets, this region experiences a pronounced drop coincident with the interhemispheric SST shift.

3.4. Upper-ocean features of the SST shift

Figures 3.3a and **3.3b** show the spatial pattern of the changes in NODC and JMA 0-700m OHC associated with the interhemispheric SST shift. Compared with the broadly interhemispheric SST dipole, the spatial structure of the OHC changes is much more pronounced in the North Atlantic relative to the other basins. In both datasets, OHC decreases across the subpolar North Atlantic north of 50°N, extending southward along the west coast of Europe to the mid-latitude eastern North Atlantic. Additionally, OHC prominently increases in the western mid-latitude North Atlantic offshore the U.S. east coast between 35° 45°N, extending eastward to around 45°W. These two regions are outlined in the boxes on the maps.

The spatial pattern of the changes of 0-700m vertically-averaged salinity is shown in **Figure 3.3c**. It features a striking resemblance to the 0-700m OHC maps in the North Atlantic, and is highly spatially correlated (NODC OHC: r=0.66; JMA OHC: r=0.72). Coincident with decreased OHC, salinity decreases in the subpolar North Atlantic and to a lesser extent in the mid-latitude eastern North Atlantic. Likewise, salinity increases in the same region as OHC in the mid-latitude western North Atlantic offshore the U.S. east coast.

Figure 3.3d shows the timeseries of the differences between the subpolar and mid-latitude western North Atlantic regions for 0-700m OHC and vertically-averaged salinity. The differences in both OHC and salinity reach their maximum values just prior to the interhemispheric SST shift, drop sharply over the shift, and remain relatively stable in the following decades. These drops indicate a rapid accumulation of heat and salt in the western mid-latitude North Atlantic relative to the subpolar North Atlantic over the shift.

Next, we examine the vertical structure of the temperature and salinity changes in the western North Atlantic (75–40°W) corresponding to the interhemispheric SST shift.

The zonal mean slopes over this part of the basin are shown in **Figures 3.4a** and **3.4b**. For both temperature and salinity, the changes in the subpolar and western mid-latitude North Atlantic are not just surface features; they extend hundreds of meters throughout the upper-ocean. In particular, the warming and salting from 35–45°N are larger at depth than at the surface.

3.5. Discussion

Our findings of the global interhemispheric SST shift as a discrete event associated with coordinated upper-ocean heat and salinity changes in the North Atlantic present a more comprehensive picture of the shift than shown in previous studies, and have implications for the likely mechanisms of the shift. Though our results do not contradict prior studies showing broad-scale northern hemisphere cooling from aerosols during the mid-20th century (Rotstayn and Lohmann 2002; Friedman et al. 2013; Hwang, Frierson, and Kang 2013), we argue that aerosols alone cannot explain the temporal and spatial characteristics of the interhemispheric SST shift shown here. In terms of timing, the pronounced regime shift identification suggests additional factors besides aerosols, which had a more sustained timescale for northern hemisphere cooling. Likewise, the spatial features of warming and salting in the western North Atlantic are not indicative of a response to the negative radiative forcing from sulfate aerosols. These results are in agreement with the SST attribution of Terray (2012), which finds that aerosols do not explain the abrupt high latitude North Atlantic drop.

Rather, the upper-ocean salinity and OHC features of the interhemispheric SST shift support the hypothesis that it was related to the Great Salinity Anomaly (GSA), a rapid freshening of the subpolar North Atlantic beginning around 1968, as proposed by Dima and Lohmann (2010) and Thompson et al. (2010). The GSA is thought to have been generated by wind-driven freshwater export from the Arctic, likely caused by a sustained anomalous negative North Atlantic Oscillation in the mid-1960s (R. Zhang and Vallis 2006; Sundby and Drinkwater 2007). The freshening was strong enough to disrupt the formation of North Atlantic deepwater (Gelderloos, Straneo, and Katsman 2012). Consistent with the reduction in subpolar North Atlantic deepwater formation, our findings of the increase in salinity and temperature in the mid-latitude western North Atlantic indicate a reduction in northward ocean heat and salt transport. Together, these results support the suggestion of Dima and Lohmann (2010) that the GSA triggered the interhemispheric SST shift via a weakening of the North Atlantic thermohaline circulation (THC), used here as the northward flow of warm saline surface water and the southward flow of cold dense water at depth (Rahmstorf 2006; Stouffer et al. 2006).

The mechanistic linkage between the cooling and freshening in the subpolar North Atlantic and the interhemispheric SST remains to be described in detail. However, we note that the subpolar North Atlantic is capable of influencing hemispheric temperature via previously-described atmospheric teleconnections. High-latitude North Atlantic cooling can be rapidly mediated throughout the North Atlantic by the atmosphere (Chiang and Bitz 2005; Liu et al. in press), which could have caused the surface cooling in the parts of the western mid-latitude North Atlantic even where there was warming at depth. Moreover,

extratropical North Atlantic cooling has been shown to rapidly propagate to the other northern hemisphere ocean basins (R. Zhang, Delworth, and Held 2007; Lee and Hsu 2013).

We thus contend that the subpolar North Atlantic GSA was an important factor in the global interhemispheric SST shift around 1970. The results presented here suggest that better understanding the development of subpolar Atlantic GSAs is important for attributing and projecting shifts in interhemispheric SST.

3.6. Acknowledgments

HadSST3 data are from www.metoffice.gov.uk/hadobs/hadsst3/data/download.html. ERSSTv3b hemispheric averages are from ftp.ncdc.noaa.gov/pub/data/mlost/operational/products/ and gridded data are from www.esrl.noaa.gov/psd/data/gridded/data.noaa.ersst.html. NODC data are from www.nodc.noaa.gov/OC5/3M_HEAT_CONTENT. JMA OHC data are from www.data.kishou.go.jp/kaiyou/english/ohc/ohc_global_en.html. The regime shift code is from www.climatelogic.com. We acknowledge the NCAR Climate Data Guide for information about several datasets used in this study.

This work was supported by the National Science Foundation grants EAPSI-1311103 and AGS-1143329, the Taiwan National Science Council grant 102-2611-M-001-006, and the UC Berkeley Geography Department. We thank Tim Boyer for assistance with the NODC data, Yugarshi Mondal for insightful discussions, and Lisa Friedman for thoughtful suggestions.

3.7. Figures

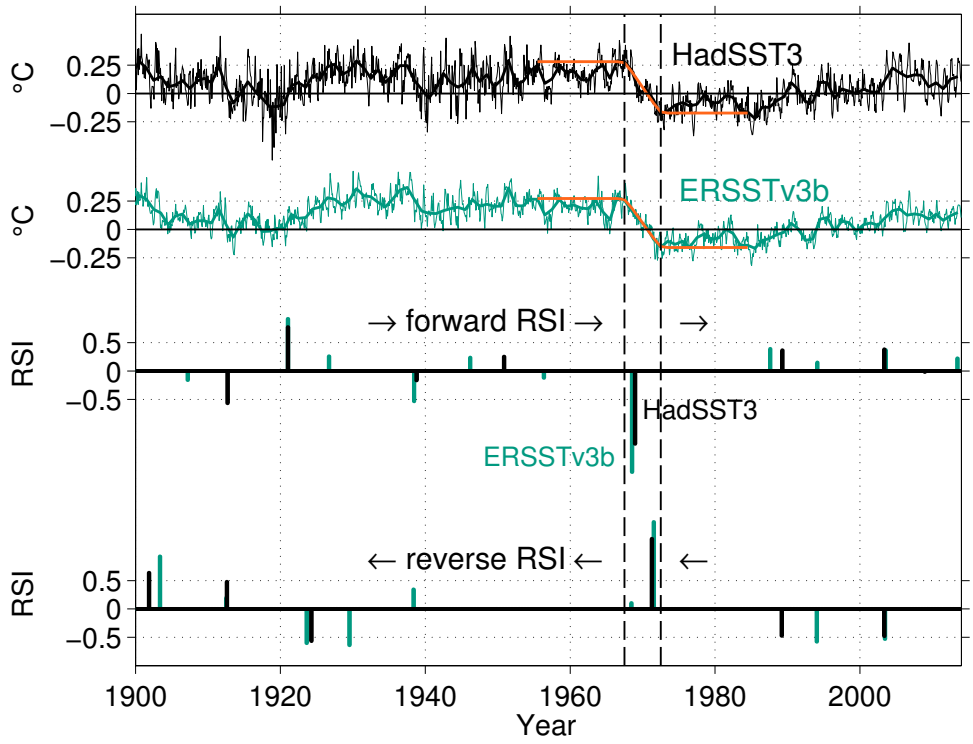

Figure 3.1. Top 2 rows: Monthly interhemispheric SST difference for HadSST3 (top row) and ERSSTv3b (second row, turquoise), in °C. The thin lines denote monthly and the thick lines denote annual means, and the red lines show the linear fit of the interhemispheric shift. Bottom 2 rows: regime shift index (RSI) for the monthly interhemispheric SST difference of HadSST3 (black) and ERSSTv3b (turquoise) in the forward direction (third row) and reverse direction (fourth row), in normalized units. The sign of the RSI corresponds to the sign of the shift in each direction. The dashed vertical lines indicate July 1967 and 1972.

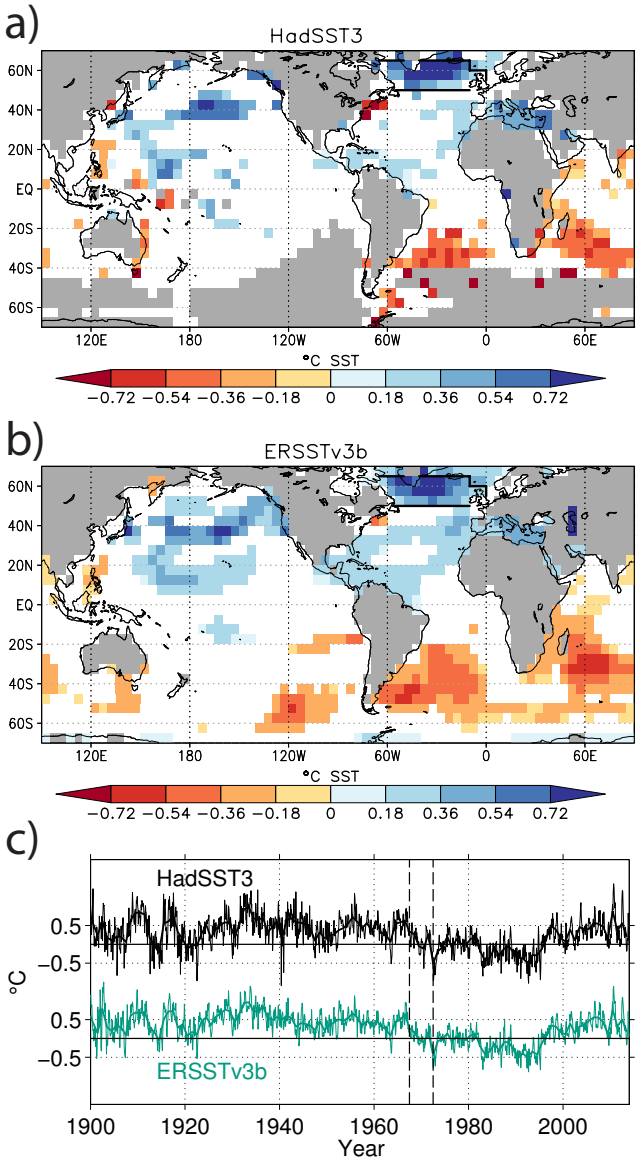

Figure 3.2. (a) and (b): Spatial maps of annual mean HadSST3 and ERSSTv3b changes associated with the linear fits of the interhemispheric SST shift, in °C. (c): Subpolar North Atlantic (boxed region) minus global average HadSST3 (top row, black) and ERSSTv3b (bottom row, turquoise), in °C. The thin lines denote monthly and the thick lines denote annual means. The dashed vertical lines indicate July 1967 and 1972.

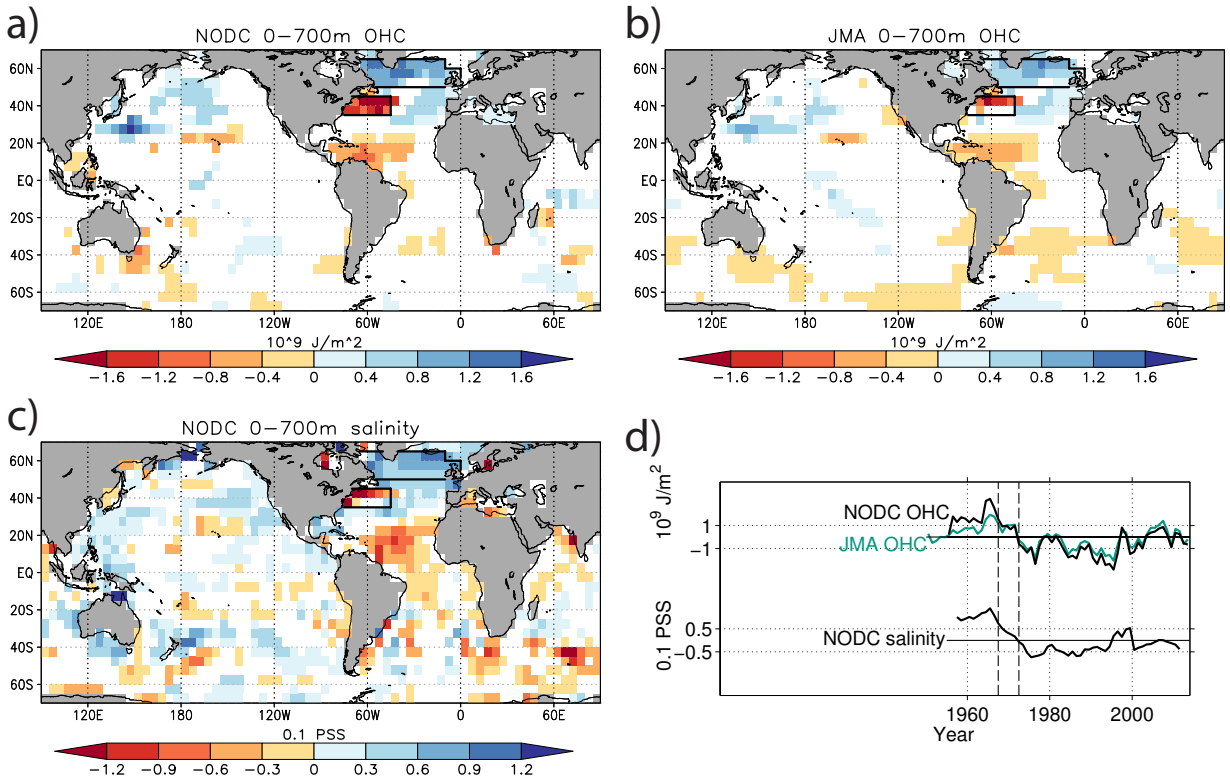

Figure 3.3. (a)–(c): Spatial maps of upper-ocean OHC and salinity changes associated with the linear fit of the interhemispheric SST shift. (a) NODC and (b) JMA annual mean 0-700m OHC, in 10^9 J m^{-2}. (c) NODC pentadal 0-700m vertically averaged salinity, in 0.1 PSS. Boxes outline the subpolar and the western mid-latitude North Atlantic regions. (d): Differences between the subpolar and the western mid-latitude North Atlantic regions for OHC and salinity. Top: annual mean NODC (black) and JMA (turquoise) 0-700m OHC, in 10^9 J m^{-2}. Bottom: pentadal 0-700m vertically-averaged NODC salinity, in 0.1 PSS. The dashed vertical lines indicate July 1967 and 1972.

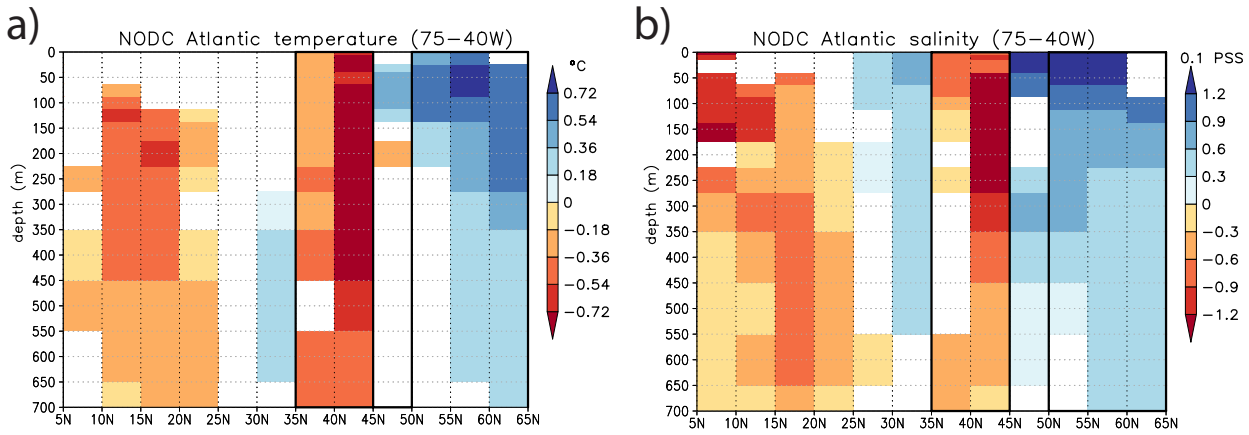

Figure 3.4. Vertical profiles of NODC western Atlantic (75–40°W) zonal mean temperature and salinity changes associated with the linear fit of the interhemispheric SST shift. (a) annual temperature, in °C. (b) pentadal salinity, in 0.1 PSS. Solid vertical lines outline the latitudes of the subpolar and the western mid-latitude North Atlantic regions.

4. Low-latitude hydrologic impacts of the interhemispheric temperature difference

4.1. Introduction

a. Motivation

This chapter examines the interhemispheric temperature difference as a potential climate index relevant to human livelihood. The focus is on water resources in the tropics, which are considered highly important climate impacts by the Intergovernmental Panel on Climate Change (Parry et al. 2007).

The history of studies into the impacts of the El Niño – Southern Oscillation (ENSO) can provide some parallels for exploring the impacts of the north–south temperature difference. Correlations between ENSO and rainfall were examined as part of the first studies into the phenomenon from the 1920s and 1930s; efforts to characterize the ENSO-precipitation impacts have continued, such as through composite analyses (Ropelewski and Halpert 1987; Ropelewski and Halpert 1989). Recent studies that have distinguished types of ENSO, which have different spatial SST patterns and rainfall impacts (Ashok and Yamagata 2009).

Likewise, the interhemispheric temperature difference has been identified as an important factor for low-latitude rainfall in studies extending back several decades. Folland et al. (1986) identified an interhemispheric SST dipole that was associated with the pronounced Sahel drought from the 1970s. Hastenrath and Heller (1977) and Nobre and Shukla (1996) explored the connection between droughts in northeast Brazil and the tropical Atlantic interhemispheric SST dipole. Studies have also linked interhemispheric contrasts with the Indian monsoon (Chung and Ramanathan 2006; Bollasina, Ming, and Ramaswamy 2011) and with global patterns of tropical rainfall (Wang et al. 2012; Sun et al. 2013).

Our aim in this chapter is two-fold. First, as a precursor to examining the hydrology impacts, we investigate and juxtapose two difference indices of interhemispheric temperature: the SST-only difference, and the combined SST + land surface temperature difference. Though these two indices have often been used interchangeably, the differences between them are important to clarify for use in impacts studies; this is analogous to exploring the different 'flavors' of ENSO. Second, we explore the statistical relationship of the interhemispheric temperature indices with low-latitude rainfall over land and flow of the largest rivers. We also conduct similar analysis using a dataset of the flow of the largest rivers in the tropics. Finally, we close by outlining some of the next steps in attributing the hydrologic impacts of the interhemispheric temperature difference.

b. Seasonal cycle

The seasonal cycle provides an analogue for the impacts of the interhemispheric temperature difference on tropical rainfall. **Figure 4.1** shows the 1981–2010 climatologies

of hemispheric temperature from NCEP/NCAR Reanalysis (Kalnay et al. 1996), and land rainfall from CPC Merged Analysis of Precipitation (CMAP) (P. Xie and Arkin 1997). Over the course of the year, the bands of tropical rainfall shift toward the warmer hemisphere. The strongest rainfall is found in the summer hemisphere in the Americas, Africa, and Southeast Asia / Maritime Continent. Though there is extensive longitudinal variation in seasonality (Mitchell and Wallace 1992; Hu, Li, and Liu 2007) and the impacts of longer-term variations below don't follow the same spatial pattern as the seasonal cycle, the north–south framework is a useful starting point for thinking about the rainfall response to the interhemispheric temperature difference.

4.2. Comparing interhemispheric temperature indices

a. Datasets and methods

We consider two variants of the north–south temperature difference that appear in the literature: the interhemispheric SST-only contrast, and the contrast of combined SST plus land surface air temperature. We compare the indices using hemispheric temperatures from the NOAA National Climate Data Center (NCDC). Two related datasets are examined. The SST hemispheric averages are based on the Extended Reconstructed SST product (ERSSTv3b) (T. M. Smith and Reynolds 2004). The combined land + SST averages are from the Merged Land-Ocean Surface Temperature Analysis (MLOST) (Vose et al. 2012). MLOST consists of the ERSSTv3b data combined with land surface air temperature from the Global Historical Climate Network (GHCN) database.

Temperature data are expressed as anomalies from 1961–1990. We calculate the annual mean from September–October for comparison with rainfall and river data (discussed later in the chapter). Data are smoothed using a 5-year running mean to focus on decadal variability, as in Hansen et al. (2010). Ordinary least-squares regression and Pearson's correlation are used for statistical calculations in the following sections (Wilks 2006). Significance is calculated considering one degree of freedom for every five years, following Biasutti et al. (2008).

b. Time series

One feature of the seasonal temperature climatologies in **Figure 4.1** is that the amplitude of the annual temperature cycle is larger in the northern hemisphere. Similarly, the amplitude of multidecadal variation has also been larger in the northern hemisphere. The individual hemispheric temperatures are plotted in **Figure 4.2** for both SST-only (**Figure 4.2a**) and combined land + SST (**Figure 4.2b**). The southern hemisphere timeseries of each index is very similar, as it mostly contains ocean. It features very steady warming over the period of record: a linear trend explains 93% of the variance of each of the southern hemisphere 5-year running means from 1901–2013. In contrast, the northern hemisphere has been much more variable: a linear trend only explains 77% of the SST and 78% of the combined land + SST running 5-year variance.

The hemispheric differences from both **Figure 4.2a** and **Figure 4.2b** are plotted in **Figure 4.3a**. The two indices are nearly identical until around 1980; in particular, both feature a pronounced drop around 1970, as discussed in **Chapter 3**. In the last 30 years,

however, the combined land+SST hemispheric difference has warmed around 0.15°C more than the SST difference. The interhemispheric SST difference has not completely recovered to its level before the shift, which explains much of the differences in the corresponding spatial patterns discussed in the next sub-section.

One question is the role of the El Niño / Southern Oscillation (ENSO) in the interhemispheric SST-only timeseries. We examine ENSO filtered ERSSTv3b data from Compo and Sardeshmukh (2010), in which the multivariate ENSO-related SST component is removed using dynamical eigenvectors. The north–south SST-only differences for the ERSSTv3b total, ENSO-unrelated, and ENSO-related components are shown in **Figure 4.3b**. Though the increase in the 1920s and the drop around 1970 are not as pronounced in the ENSO-removed version, the 5-year smoothed mean timeseries are very similar, indicating that ENSO does not have a large influence on the multidecadal behavior of the north–south SST difference.

c. Spatial patterns

We regress 5-year running mean 5°×5° gridded MLOST data onto the two indices, similar to Figure 9 in Wu et al. (2011). The regression maps are shown in **Figure 4.4**. The top panels **Figure 4.4a** and **Figure 4.4b** correspond to the entire record from 1901–2013, and the bottom panels **Figure 4.4c** and **Figure 4.4d** are for the years 1949–2013. The combined land + SST difference maps feature positive slopes in the landmasses of both the northern and southern hemispheres, with the largest ocean warming in the extratropical north Atlantic. Negative slopes are found mainly in the southern extratropics. There are also negative slopes in the east Pacific from 1949–2013, similar to that discussed in **Chapter 2.4**. The SST-only regression maps feature a similar Atlantic dipole and positive slopes in the north Pacific, but differ in that there are negative slopes over the continents, including much of North America and Eurasia.

The stark differences in slopes over the continents in **Figure 4.4** — when the 5-year indices in **Figure 4.3a** differ only in the amount of warming in the last 30 years — suggest that these regions have large amplitude trends and are mainly picking up the trend in global temperature. To emphasize the regions of strong relationship with the interhemispheric temperature difference, we plot the respective temperature correlation maps in **Figure 4.5**. Correlations are only plotted where the corresponding p-value < 0.10. For both interhemispheric temperature indices, the correlations over the continents are not very significant. Rather, the largest correlations are found in the northern north Atlantic and the extratropical southern hemisphere oceans, particularly in the full 1901–2013 record. These are the key SST regions of the interhemispheric shift around 1970, which is consistent with the shift being such dominant feature in the timeseries in **Figure 4.3a**.

4.3. Tropical hydrological impacts

a. Rainfall

In this section, we investigate the tropical rainfall changes corresponding to the interhemispheric temperature difference patterns described above. The interhemispheric

SST-only contrast has been considered to be the most relevant metric for tropical rainfall in several studies (C. Chung and Ramanathan 2007; S. Xie et al. 2010; Sun et al. 2013). However, the combined land and ocean hemispheric temperature contrast has also been emphasized (Wang et al. 2012).

We examine the 2.5°×2.5° gridded NOAA Precipitation Reconstruction over Land (PRECL) dataset (Chen et al. 2002), which is based on gauge data and extends from 1948. The long–term PRECL mean precipitation is shown in **Figure 4.6a**. Annual mean rainfall is defined from October through the following September, designated by the calendar year in which it ends. This contains the summer monsoon in both the northern and southern hemispheres, similar to the May–April monsoon from Wang et al. (2012). A five-year running mean is applied to these annual values. A note on terminology: we refer to zonal mean tropical rainfall as the tropical rainbands. We reserve the term Intertropical Convergence Zone (ITCZ) for the location of trade wind convergence, which is not necessarily co-located with the latitude of maximum rainfall (Zagar, Skok, and Tribbia 2011).

ENSO is a dominant factor for tropical land rainfall (Kevin E. Trenberth et al. 2014). Other than using a 5-year running mean, this introductory study does not explicitly attempt to remove the ENSO influence on rainfall, which is much more zonally asymmetric than SST (Chou and Lo 2007). A future question is to quantify the effects of ENSO on precipitation and river flow using a linear atmospheric bridge operator from Compo and Sardeshmukh (2010). This study also does not address the intriguing influence of the north–south SST difference on ENSO variance (Fang, Chiang, and Chang 2008).

Correlation maps of rainfall with the interhemispheric SST and combined land + SST differences are shown in **Figure 4.6b** and **Figure 4.6c**. In both, the most pronounced positive correlations are over the Sahel; there are also positive correlations in south and east Asia, southern equatorial Africa, and the Caribbean. Negative correlations are found in Australia, Madagascar, southwest Asia, northeast Brazil, and Mexico.

Two comparisons of **Figures 4.6b** and **Figure 4.6c** are shown in **Figure 4.7a** and **Figure 4.7b**. **Figure 4.7a** shows areas of correlation sign agreement between **Figure 4.6b** and **Figure 4.6c**: green where they are both positive, and orange where they are both negative. In most regions, the rainfall correlation is the same sign for each interhemispheric index. **Figure 4.7b** shows the difference in r^2, or variance explained, between the maps of **Figure 4.6b** and **Figure 4.6c**. The interhemispheric SST-only difference explains much more of the rainfall variance in the Sahel and northwest Africa more broadly. It also does better over central Australia, and southern South America. The combined land+SST difference explains more of the rainfall variance in northern Mexico, and in the extremely dry southwest Asia. The comparison over Asia is less consistent.

We plot the zonal mean rainfall correlation with the interhemispheric temperature indices in **Figure 4.8** for the global tropics and over different longitudinal regions: the Americas, Africa, and Asia + Australia. **Figure 4.8a** shows the correlations with the interhemispheric SST-only difference, and **Figure 4.8b** with the land + SST difference. The global zonal mean correlation with the SST-only difference features an interhemispheric dipole with positive values in the northern tropics and negative values in the southern

tropics, consistent with Sun et al. (2013). The global mean dipole is more pronounced than any of the three longitude zones plotted, but each of them does feature more positive correlations in the northern tropics than the southern tropics. The dipole is less pronounced for the combined land + SST difference, though correlation values are more positive in the northern than southern tropics globally and for the regions outside the Americas. Whether these dipoles actually indicate meridional shifts in the tropical rainbands or rather intensification of the mean annual cycle requires additional investigation of the different seasons.

b. River flow

River discharge is an important part of the water cycle and a critical resource in the human demand for freshwater. We investigate annual river discharge data from Dai et al. (2009). The data are from river gauge stations closest to the river mouth for the 925 largest rivers by volume. Data gaps are filled using data from other stations in the river system where possible; in some cases, the NCAR Community Land Model version 3 (Qian et al. 2006) was also used to fill in gaps. We investigate rivers whose mouth is between 35°S and 35°N and whose long-term flow is above 100 km^3, for a total of 23 rivers shown in **Figure 4.9**. The annual river discharge is measured from October–September, known as the water year (USGS 2014). In addition to the characteristics discussed for rainfall, the water year includes runoff from snowmelt, which is important in much of the northern hemisphere. The period of investigation is water years 1949–2004.

The correlations with the interhemispheric temperature difference are depicted in **Figure 4.10** and listed in **Table 4.1**. **Figure 4.10a** shows the correlation of 5-year smoothed river flow with the interhemispheric SST-only difference. The strongest correlation is for the Niger river (r=0.81), which drains the Sahel in west Africa; this is consistent with the high rainfall correlation of this region. The Indus river, which flows the Tibetan Plateau to the Arabian Sea, also is highly correlated (r=0.75). The Congo and Ogooué rivers of equatorial Africa and the Ganges of south Asia all have correlation values above 0.4. Positive correlations above r=0.2 are also found in major southeast and south Asian rivers: Irrawaddy, Chang Jiang, and Mekong. The Amazon is slightly negatively correlated, but two of its major tributaries – the Tapajos and Xingu – have positively correlations greater than 0.2.

The Mississippi river has the most negative correlation with the interhemispheric SST-only difference (r=-0.73). This is consistent with the negative flow correlations with the Atlantic Multidecadal Oscillation (AMO) (Enfield, Mestas-Nuñez, and Trimble 2001), which projects strongly onto the interhemispheric SST difference. Though the mouth of the Mississippi is just south of 30°N, most of its drainage basin is far to the north so this reflects mid-latitude dynamics. The Parana river in southeast South America is also strongly negatively correlated with the interhemispheric SST-only difference (r=-0.64). Another high value is the Tocantins river (r=-0.45); though its mouth is near the Amazon, its drainage basin is east-central Brazil including the western part of the Nordeste. The Uruguay river, which is part of the Parana river system in the La Plata basin, and the Magdalena river in Columbia are also both negatively correlated with the interhemispheric

SST-only difference (r=-0.39 and r=-0.38 respectively). The negative values in the La Plata basin

Figure 4.10b shows the correlation map for the combined land + SST interhemispheric difference, and **Figure 4.10c** shows the difference in variance explained between **Figure 4.10a** and **Figure 4.10b**. The correlation maps are generally similar. The largest correlations are similarly found for the Niger (r=0.75) and Mississippi (r=-0.55) rivers, albeit with smaller magnitudes. More rivers have better fits with the SST-only difference (16 out of 23 rivers). A notable exception is the Brahmaputra (r=0.33 for combined land + SST v. r=0.05 for SST). The Chang Jiang river is also better correlated with the combined land + SST difference (r=0.47 v. r=0.27).

4.4. Summary and future directions

a. Summary

This chapter examined the behavior of two indices of interhemispheric temperature: the north–south SST-only difference, and the combined land + SST difference. For both, the warming in the southern hemisphere has been much steadier since the early 20th century. Comparison of the two indices reveals that the inclusion of land results in more northern warming over the last few decades. The interhemispheric differences are most significantly correlated with surface temperatures in the extratropical north Atlantic and southern hemisphere oceans.

Both interhemispheric temperature indices are positively correlated with rainfall in the Sahel and tropical Africa, and south and southeast Asia; and negatively correlated with Australia, eastern South America, Mexico, and southwest Asia. The interhemispheric SST-only difference is much better correlated with the Sahel and tropical Africa, which largely accounts for the global zonal mean dipole correlation structure.

The striking correlation with Niger river flow underscores the sensitivity of the Sahel region to the interhemispheric temperature difference. Likewise, the high correlations in the south and east Asian river systems point to the importance of interhemispheric temperature for these basins, which support some of the densest populations in the world (Small and Cohen 2004). We also found that the rivers that drain the southern side of the Tibetan Plateau and receive moisture from the southwest monsoon – the Indus and Ganges – are better correlated with the interhemispheric SST difference compared with the rivers that drain farther to the east. The negative river flow correlations in southern and eastern South America suggest that this region also experiences impacts of the opposite sign.

b. Additional observational investigation

Further analysis may help distinguish the interhemispheric temperature signal from other factors affecting the hydrologic data. As mentioned earlier, investigation of seasonal rainfall may identify the mechanisms of the rainfall response, such as meridional shifts or modulations of the annual cycle. Other objective analyses using combined temperature and rainfall data may help remove the ENSO contribution. For river discharge, one question is

the role of snow and glacial meltwater for the rivers flowing from the Tibetan Plateau (Savoskul and Smakhtin 2013). Examination of the non-climatic factors in the individual river systems – such as diversions and land use change – should also allow for better attribution of the response to interhemispheric temperature.

c. Future hydrologic impacts of the interhemispheric temperature difference

Can the historical rainfall impacts discussed in this chapter provide guidance for the future hydrologic response to interhemispheric temperature change? Considering from **Chapter 2** that the projected increase in interhemispheric temperature increase is nearly monotonic with global mean temperature and the spatial variability among model rainfall projections is so large, it is difficult to distinguish the mean rainfall changes that are due to the interhemispheric temperature difference.

Rather, we suggest that the hydrologic patterns of this chapter will be most applicable for the impacts of multidecadal *variations* in the interhemispheric temperature difference that are based in the key variability regions from **Figure 4.5**: the extratropical North Atlantic and southern hemisphere oceans. For example, Drijfhout et al. (2013) found that models can produce spontaneous cooling events in the subpolar North Atlantic with similar features as the shift discussed in **Chapter 3**. We thus propose to investigate future simulations for such cooling events, and explore whether the associated low-latitude hydrologic changes resemble those in this chapter. River flow changes can be investigated by propagating the model precipitation and other output through a land surface model.

4.5. Acknowledgments

We appreciate the NCAR Climate Data Guide for providing information about several datasets used in this study.

NCEP temperature climatologies are from www.esrl.noaa.gov/psd/data/gridded/data.ncep.reanalysis.derived.surface.html. The CMAP monthly data are from iridl.ldeo.columbia.edu/SOURCES/.NOAA/.NCEP/.CPC/.Merged_Analysis/.monthly/.latest/.ver2/.prcp_est/.

The ERSSTv3b data are described at www.ncdc.noaa.gov/ersst/ and the MLOST data are described at www.ncdc.noaa.gov/ersst/merge.php. The NOAA NCDC hemispheric indices are from ftp.ncdc.noaa.gov/pub/data/mlost/operational/products/. The gridded MLOST data are from www.esrl.noaa.gov/psd/data/gridded/data.mlost.html. We appreciate Boyin Huang for additional information about the NOAA NCDC datasets.

The non-ENSO ERSSTv3b data was kindly provided by Gil Compo at ftp.cdc.noaa.gov/Public/gcompo/Removing_ENSO/1901_2010/noaa_ersst3/. The PRECL rainfall are from www.esrl.noaa.gov/psd/data/gridded/data.precl.html. The river flow data are from www.cgd.ucar.edu/cas/catalog/surface/dai-runoff/index.html, and we appreciate Aiguo Dai for providing helpful information about the dataset.

4.6 Figures and tables

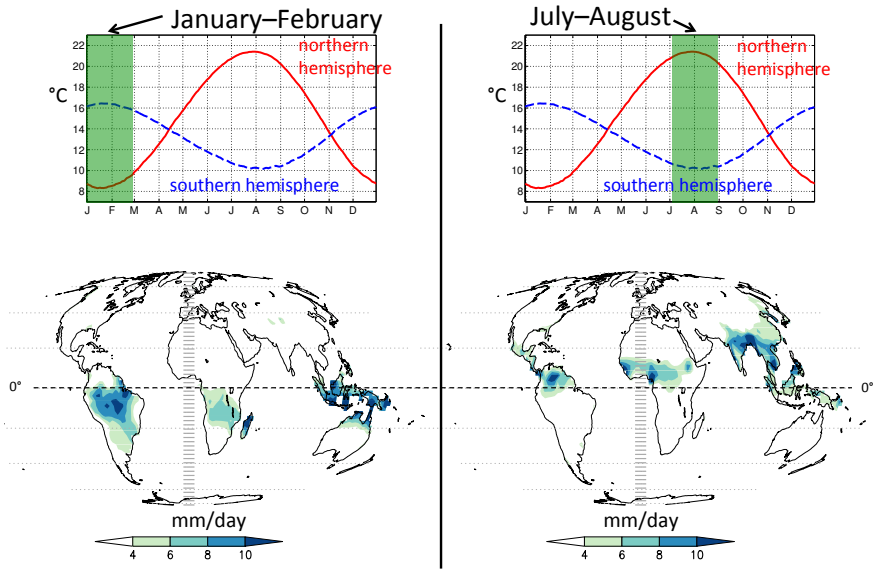

Figure 4.1. 1981–2010 climatologies. Top: NCEP average northern and southern hemisphere daily surface air temperature, in °C. Bottom: CMAP monthly rainfall over land for January–February (left) and July–August (right), in mm per day.

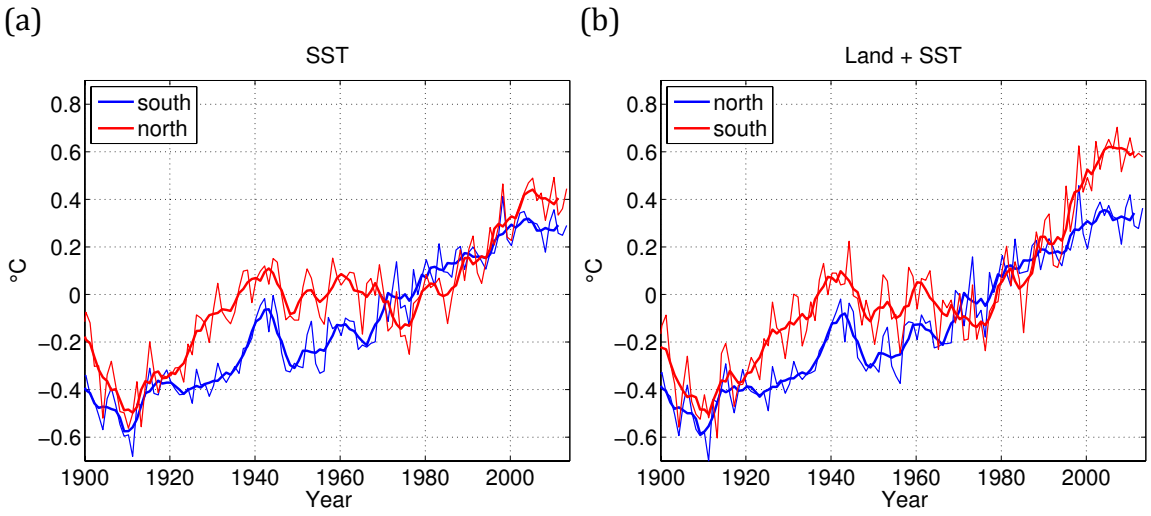

Figure 4.2. Northern (red) and southern (blue) hemispheric temperatures, in °C. (a) SST and (b) land + SST. Thin lines show annual (October–September) mean; thick lines show the 5-year running mean.

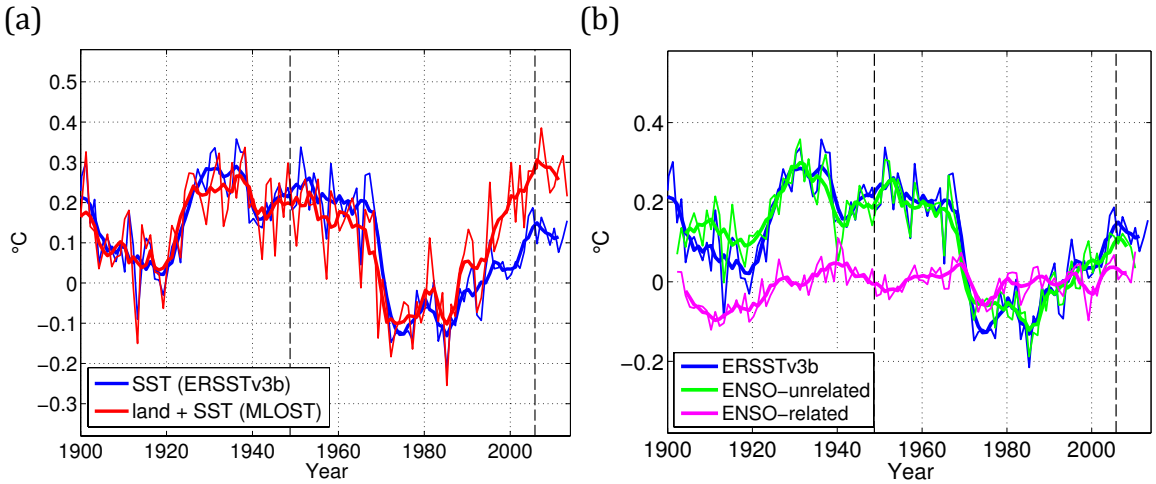

Figure 4.3. North–south temperature difference, in °C. (a) NOAA ERSSTv3b (blue) and MLOST (red). (b) NOAA ERSSTv3b (blue) and non-ENSO component of ERSSTv3b (green). Thin lines show annual (October–September) mean; thick lines show the 5-year running mean. Vertical lines mark October 1948 and 2005.

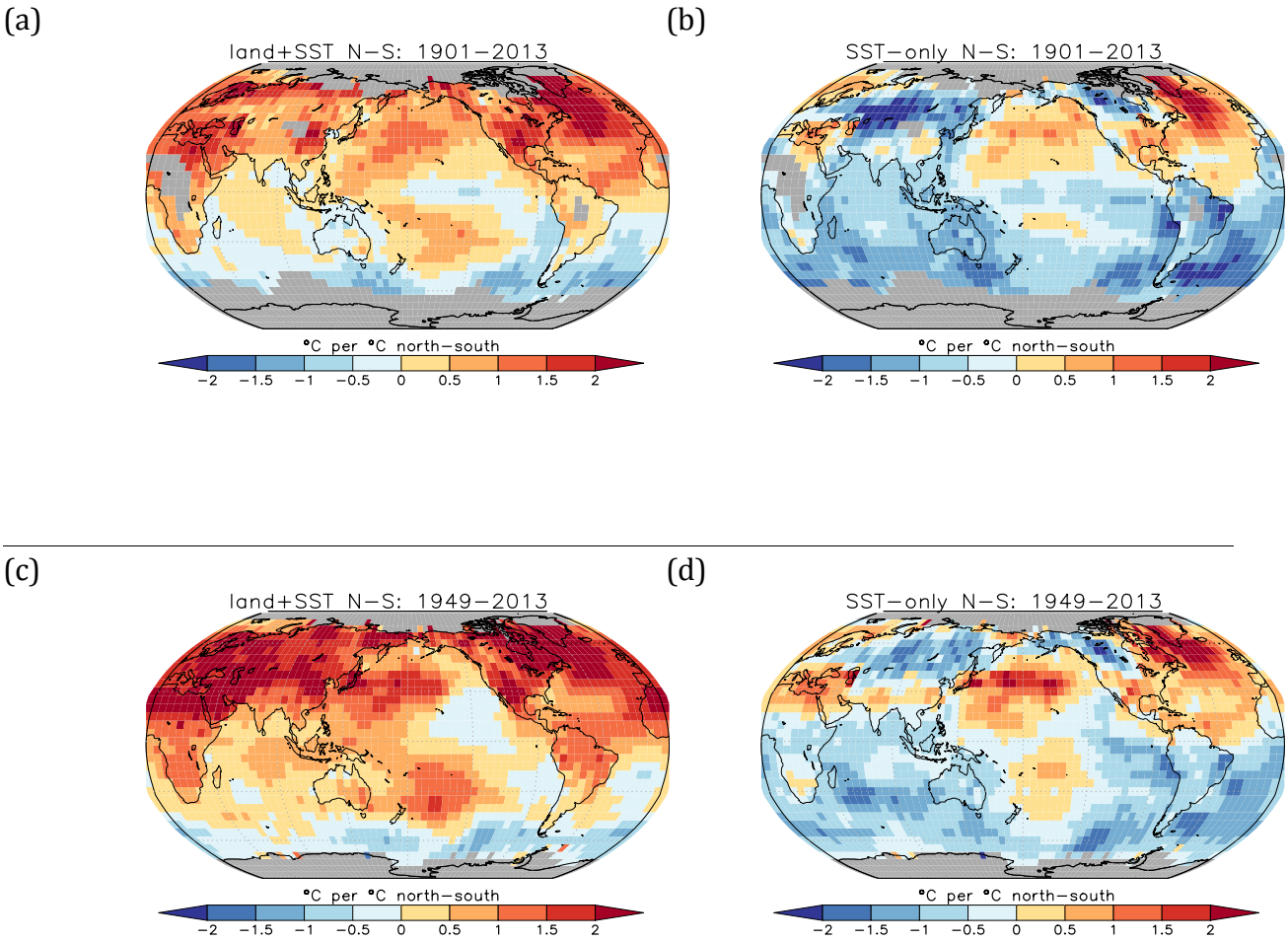

Figure 4.4. Regression maps of 5-year smoothed MLOST annual mean temperature onto indices of the north–south difference, in °C per °C north–south difference. (a) 1901–2013 land+SST, (b) 1901–2013 SST-only, (c) 1949–2013 land+SST, and (d) 1949–2013 SST-only. Missing data regions are shaded grey.

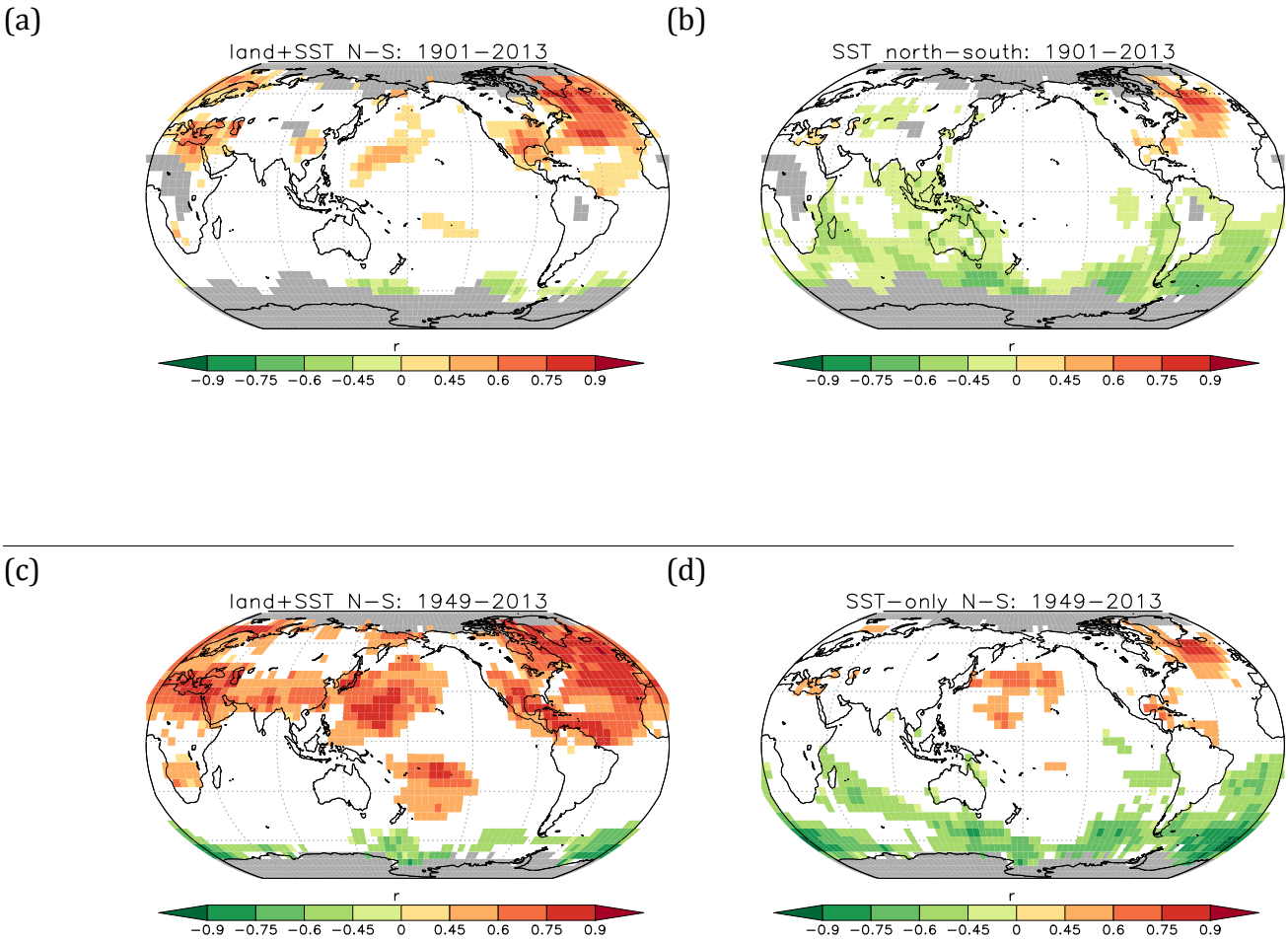

Figure 4.5. Correlation maps of 5-year smoothed MLOST annual mean temperature onto indices of the north–south difference, where $p<0.10$. (a) 1901–2013 land+SST, (b) 1901–2013 SST-only, (c) 1949–2013 land+SST, and (d) 1949–2013 SST-only. Missing data regions are shaded grey.

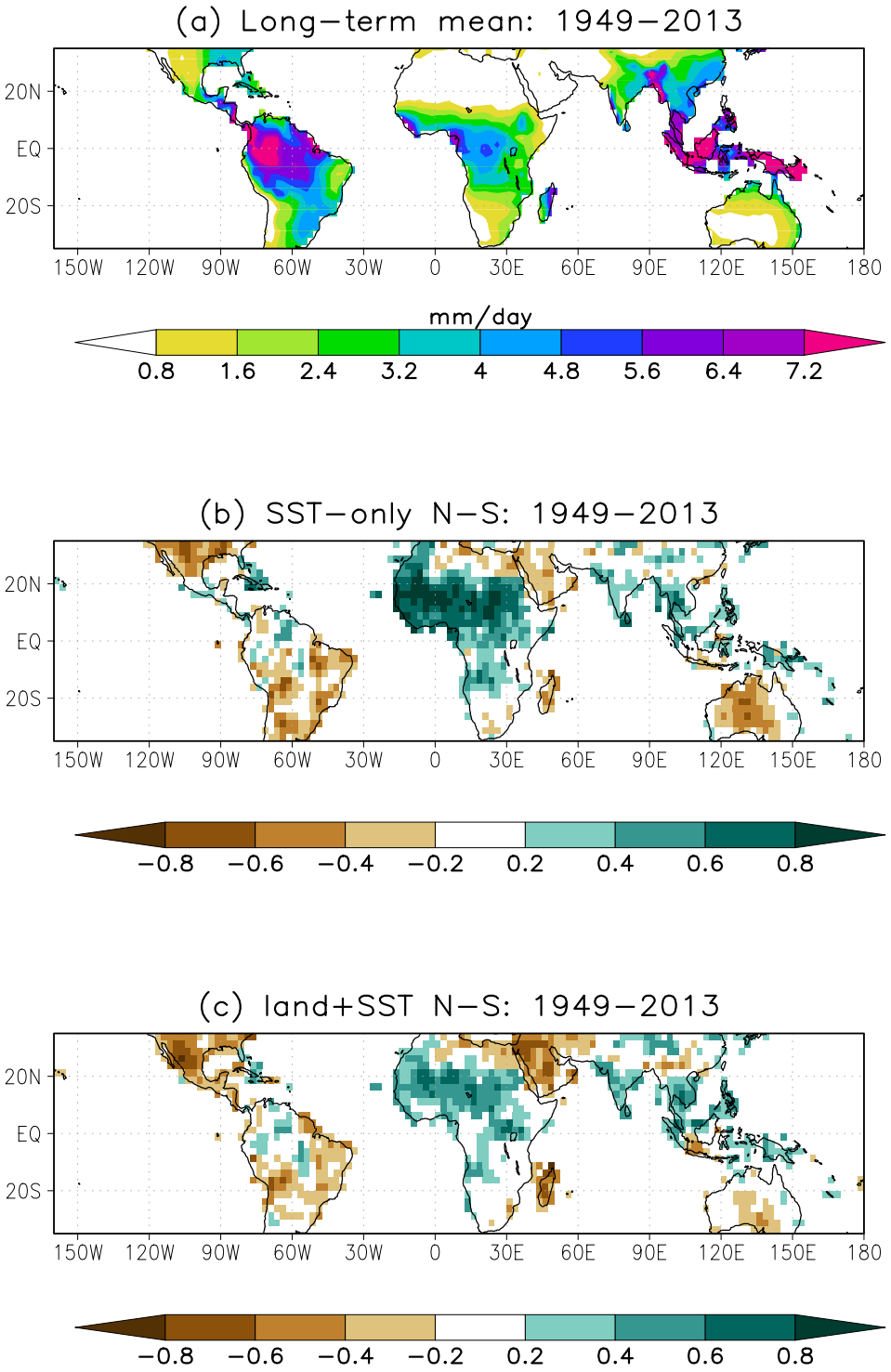

Figure 4.6. (a) PRECL 1949–2013 mean rainfall, in mm per day. (b) and (c): Correlation maps of 5-year smoothed PRECL annual mean rainfall with indices of the north–south difference: (b) SST-only, and (c) combined land + SST, from 1949–2013.

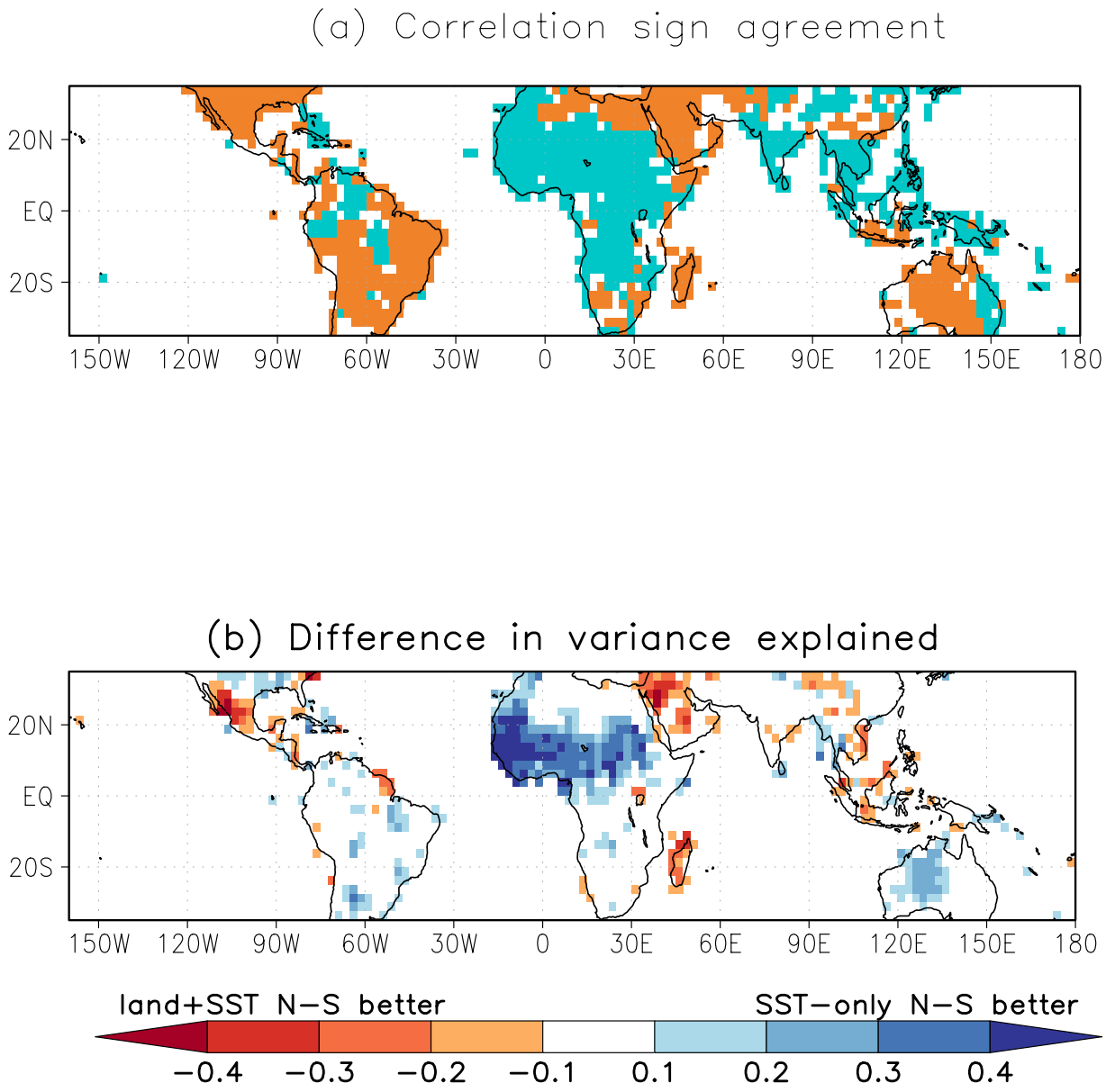

Figure 4.7. (a) Sign agreement between 5b and 5c: green shows where both slopes are positive, orange shows where both are negative. (b) Difference in variance explained between **Figure 4.6b** and **Figure 4.6c,** in r^2.

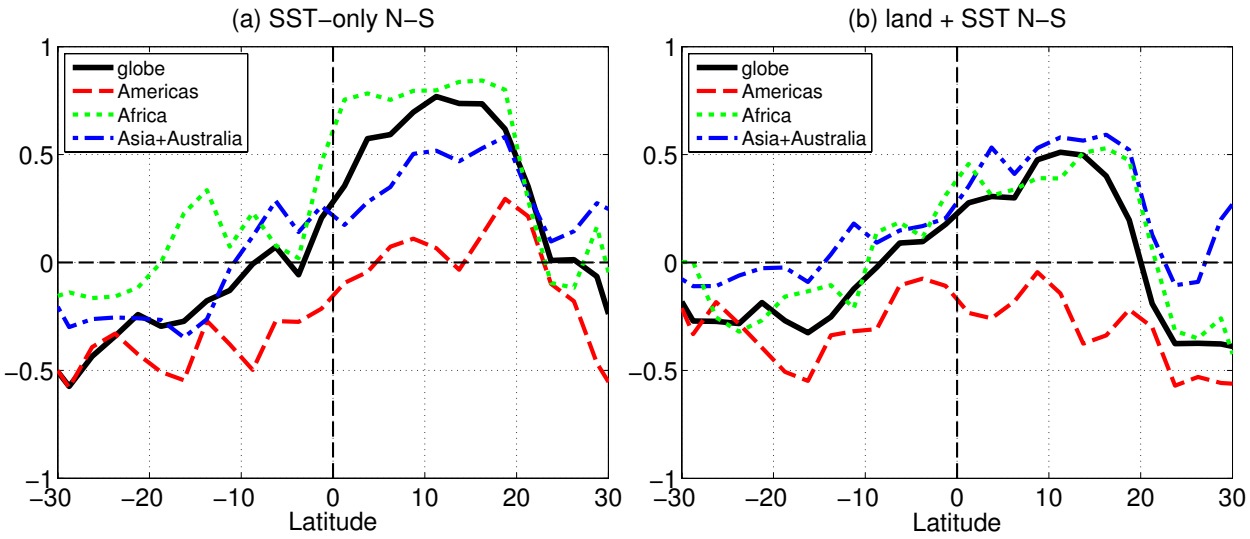

Figure 4.8. Correlation of zonal mean 5-year smoothed PRECL annual mean rainfall with indices of the north–south difference: (a) SST-only, and (b) combined land + SST, from 1949–2013. Results are shown for the global tropics and different longitudinal regions: the Americas (120°W–30°W), Africa (20°W–50°E), and Asia + Australia (60°E–160°E).

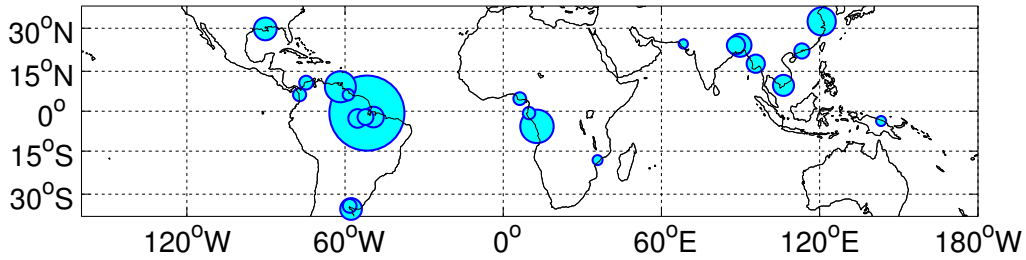

Figure 4.9. Rivers investigated in this study, plotted at their mouth. Marker size is proportional to long-term mean flow (km^3 per year) from Dai and Trenberth (2002). Rivers include the Amazon, Congo, Orinoco, Chang Jiang, Brahmaputra, Mississippi, Parana, Mekong, Tocantins, Tapajos, Ganges, Irrawaddy, Xingu, Xi Jiang, Magdalena, Uruguay, Atrato, Niger, Ogooué, Essequibo, Sepik, Zambezi, and Indus.

(a) SST-only N–S

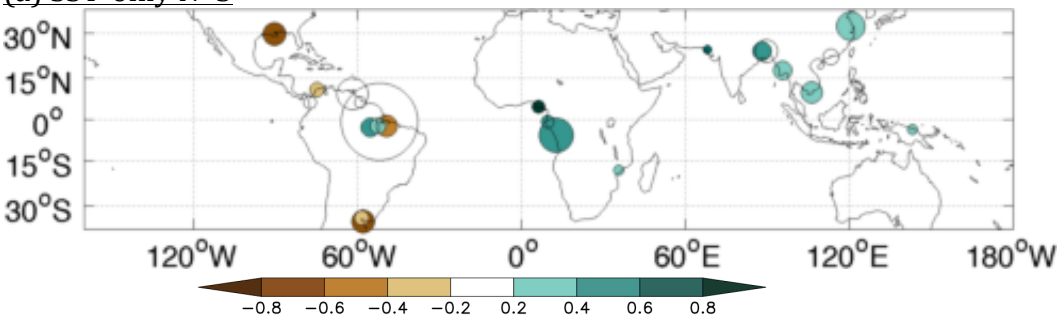

(b) Land + SST N–S

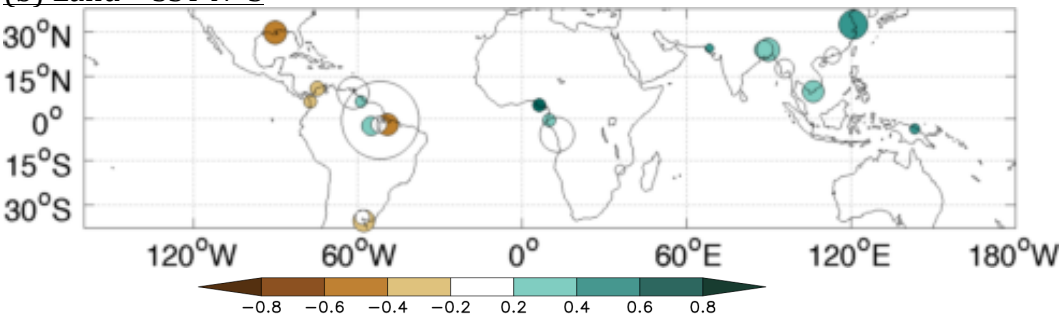

(c) Difference in variance explained between (a) and (b)

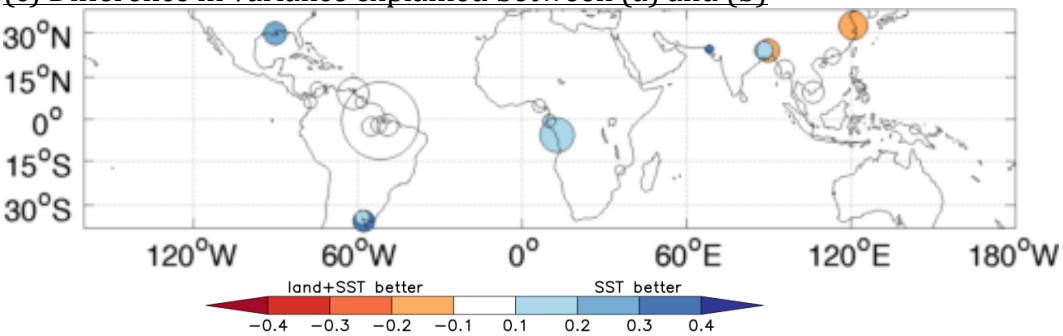

Figure 4.10. Correlation of 5-year smoothed annual river flow with the interhemispheric difference of (a) SST-only and (b) combined land + SST, from 1949–2004. (c) Difference in r^2 between a and b. Marker size is proportional to long-term mean flow as in **Figure 4.9.**

River	SST-only	land+SST
Amazon	-0.13	-0.05
Congo	0.45	0.12
Orinoco	-0.13	-0.01
Chang Jiang	0.27	0.47
Brahmaputra	0.05	0.33
Mississippi	**-0.73**	-0.55
Parana	**-0.64**	-0.25
Mekong	0.22	0.31
Tocantins	-0.43	-0.50
Tapajos	0.45	0.36
Ganges	0.43	0.24
Irrawaddy	0.32	0.11
Xingu	0.27	0.11
Xi Jiang	0.10	0.01
Magdalena	-0.38	-0.29
Uruguay	-0.39	-0.09
Atrato	0.05	-0.27
Niger	**0.81**	**0.75**
Ogooué	0.45	0.25
Essequibo	0.14	0.23
Sepik	0.35	0.43
Zambezi	0.29	-0.04
Indus	**0.75**	0.46

Table 4.1. Correlation of the 5-year smoothed annual river flow of the 23 largest low-latitude rivers with the interhemispheric difference of SST-only and combined land+SST, from 1949–2004. Correlations with $p < 0.05$ are highlighted.

5. Farmer strategies for dealing with climatic variability: a case study from the Mixteca Alta Region of Oaxaca, Mexico

This chapter is based on the following article, which is ordered slightly differently and includes additional material:

Rogé, Paul, Andrew R. Friedman, Marta Astier, and Miguel A. Altieri, 2014: "Farmer strategies for dealing with climatic variability: a case study from the Mixteca Alta Region of Oaxaca, Mexico." *Agroecology and Sustainable Food Systems*.
doi: 10.1080/21683565.2014.900842
©The Authors. Published by Taylor & Francis.

5.1. Introduction

Climate change is expected to disproportionately impact tropical regions where the majority of small farmers and pastoralists reside (Easterling et al. 2007). Small farmers that manage diversified and small-scale farms, that rely on family labor, and that produce both subsistence and commercial goods are a predominant mode of production in many regions of the world (Astier et al. 2012). One of the challenges for addressing twenty-first century climate change is that current climate models do not provide specific enough information for adaptation at small scales (Oreskes, Stainforth, and Smith 2010).

Effective adaptation to climate change requires location-specific understandings of climate variability (Gamble et al. 2010). This is especially true for small farmers, who often use local climate knowledge for decision-making. While climate may seem an unlikely candidate for management, small farmers are not limited to reacting to it (Wilken 1987, 224). Small farmers have developed innovative farming strategies for withstanding challenging climatic conditions (Miguel A. Altieri and Nicholls 2013). The recovery of traditional management practices from creative and motivated local stakeholders may in fact represent important strategies to prepare for climate change (Astier et al. 2011). Scientific and local knowledge must be bridged to contribute to the well-being of agricultural communities (Valdivia et al. 2010). Moreover, Roncoli (2006) recommends the use of ethnographic and participatory methods to move towards a climate vulnerability and adaptation paradigm led by farmers and institutions.

This chapter discusses participatory research in the Mixteca Alta Region of Oaxaca, Mexico that facilitated a process whereby farmers evaluated the ability of their agroecosystems to withstand the vagaries of climate. The proposed methodology documented small farmers' past strategies for dealing with climatic variability, developed local indicators to assess the ability of agroecosystems to withstand climatic variability, and placed the locally-derived indicator framework in the hands of farmers for evaluating the current state of their agroecosystems. Additionally, we put the farmers' description of climate history in conversation with regional climate records. This latter step of original quantitative climate analysis was not essential to identifying farmer adaptation strategies,

but rather may validate farmers' experiences to scholars, community organizers, and policy makers.

5.2. Study Area

The Mixteca Alta Region of Oaxaca, Mexico is both a political entity and a part of the larger geographical area predominated by the Mixtec people. We collaborated with three communities from the Nochixtlán District of the Mixteca Alta Region: San José Zaragoza (Zaragoza), El Rosario, and San Pedro Coxcaltepec Cántaros (Coxcaltepec; **Figure 5.1**). Due to its high elevation (much of it above 2000 meters), the Mixteca Alta is largely classified as a subtropical dry winter climate (*Cwb*) according to the Köppen-Geiger system, though it lies within the tropics (Kottek et al. 2006). Most precipitation occurs from June through September, with a mid-summer decrease known as the *canícula* (Magana, Amador, and Medina 1999). The highest average temperatures are in April and May, before the heaviest summer rains, and frosts are common from October through March at higher elevations. We show the monthly average temperature and rainfall from 2005–2010 for a 1°×1° region surrounding the communities (96.5–97.5°W, 17–18°N) in **Figure 5.2**.

Rainfed agriculture – particularly maize, beans, and wheat – is widely practiced in the Mixteca Alta (Altieri et al. 2006, 62; Velásquez 2002, 3–4). Two important rainfed cropping systems in the Mixteca Alta are cajete maize (*maíz de cajete*) and seasonal maize (*maíz de temporal*). The two maize systems differ significantly in their requirements for labor, technology, and social organization. Groups of farmers sow cajete maize at the end of the dry season between February and March, using a two-sided digging tool (*pico y coa*) to locate residual soil moisture. These sowing activities involve much of the community and require coordination throughout the winter months (Rivas Guevara, 2008, 146–158; García Barrios, Raúl, García Barrios, Luis, and Alvarez-Buylla 1991, 25–31). In contrast, families individually sow seasonal maize in furrows along with beans and squash at the beginning of the rainy season between May and July.

The Mixteca Alta is also marked by a legacy of severe soil erosion and desertification, a crisis of food production and poverty, and an aging demographic due to increasing out-migration by youth (Boege and Carranza 2009, 90–98). A group of farmers, with support from the international non-governmental organization (NGO) World Neighbors, organized in 1982 to address the environmental and social crises affecting the Mixteca Alta (Blauert, Jutta and Quintanar 2000, 34). This group's current manifestation, the farmer-led Center for Integral Rural Development of the Mixteca Alta (CEDICAM), continues to garner international recognition for promoting sustainable agriculture, appropriate technology, and gender equality through a farmer-to-farmer training network (Boege and Carranza 2009, 102–113). CEDICAM works to adapt the sustainable elements of traditional agriculture to modern conditions through "improved" indigenous technologies (Jesús León Santos, personal communication).

5.3. Methodology

Researchers and CEDICAM collaborated in participatory research for a period of three years, from 2009 to 2011, conducting a total of eight day-long workshops with

farmers in CEDICAM's farmer-to-farmer network. P.R. lived and worked alongside small farmers in the Mixteca Alta for a total of 20 months while conducting ethnographic studies, interviews, and agronomic field experiments. These experiences inform the research presented in this chapter.

Researchers and CEDICAM followed a co-investigation methodology similar to that described by Freire (1970, 125). Meetings between researchers and CEDICAM identified objectives and reflected on outcomes of farmer workshops (**Figure 5.3**). While farmer workshops primarily aimed to empower small farmers to conduct their own analysis in the vein of Freire (1970, 99), the workshops were also focus groups as described by Hennink (2007) and Wilkinson (1999), in that a series of qualitative research questions was embedded in the activities conducted by farmers. CEDICAM invited farmers in each community through their farmer-to-farmer training network. An average of 6 women and 7 men ranging from an estimated 18 to 70 years old attended each farmer workshop. However, participation varied greatly due to competing responsibilities in local governance positions and employment outside of their communities.

a. Farmer climate histories

In the first series of workshops, attended by 17 women and 23 men across the three communities, farmers discussed their adaptations to past climate challenges. Group discussions were an important strategy since participating communities maintain oral history traditions. From a focus group perspective, discussions between farmers obtained a more unified recollection of past experiences (Morgan and Krueger 1993). Farmers' climate narratives provided a basis for an investigation of the historical climate.

Researchers facilitated the workshops by recording farmers' narratives on a large sheet of paper. Key historical events in each community served as baseline references of a stratified timeline. The impacts and farmer adaptations to extreme climatic events – namely severe droughts, storms, and frosts – were layered upon this baseline. Researchers relied on the farmers' interpretations climatic extremes, since there are many possible interpretations of extreme events (Peralta-Hernandez, Balling, and Barba-Martinez 2009). We also asked farmers how they experienced and responded to long-term climate changes, and how their production systems changed over time, as did Geilfus (1998) and Ortiz-Ávila, Quiroz, and Camou (2007).

b. Climate record

For the climate, we examined a 1°×1° region encompassing the communities (96.5–97.5°W, 17–18°N). We investigated monthly-averaged data from a Mexican National Meteorological Service meteorological station in Nochixtlán and from high-resolution gridded datasets based on station data: temperature and rainfall from the Climatic Research Unit time series dataset (CRU-TS) version 3.21 (Harris et al. 2014); and rainfall from the Global Precipitation Climatology Center full data reanalysis (GPCC) version 6 (Schneider et al. 2014). The automatic station data were available from 2005 onward; we only used temperature since several months of rainfall appeared to be missing.

We investigated the 50-year climate record in the study region focusing on long-term secular changes to compare with farmer perceptions of climate. As the gridded products are at a much larger spatial scale compared to the farming communities and have lower temporal resolution compared to most extreme events, we did not expect individual local extreme events to be present in the data. Our workshop methodology may have primed respondents to associate climate changes with non-climate historical events in the communities. However, we believe that this is less likely to have affected the perceptions of a long-term signal. Since the workshop participants were from a wide age range, we examined both 50-year (1961–2010) and 25-year (1986–2010) trends. Trends were calculated using the Kendall-Theil robust slope to reduce the influence of outliers, and we evaluated significance using a two-tailed Mann–Kendall test with a cutoff of $\alpha=0.05$ (Helsel and Hirsch 2002). We characterized El Niño / Southern Oscillation (ENSO) events using the Multivariate ENSO Index (Wolter and Timlin 2011).

c. Local agroecosystem practices

A second series of workshops, attended by a total of 17 women and 36 men across the three communities, asked farmers to describe the biophysical attributes of their production systems that enable or limit productivity given the climatic variability described in the previous workshop series. We refer to these biophysical attributes as indicators. The use of indicators in participatory research with farmers is well established in Latin America (Astier et al. 2011; Pulido and Bocco 2003).

The identification of local indicators followed a similar study of cacao agroforestry systems in Costa Rica and Nicaragua conducted by Altieri (2010). Field visits to three agroecosystems in each community stimulated a conversation between researchers and participating farmers about the most important indicators. It also became evident through these discussions that some of the indicators described conditions beyond the scale of one farmer's fields (*Landscape*), while others were related to conditions directly influenced by farmers' actions on the field-scale (*Farmer Management*) or to conditions of soil quality at the field scale that for some indicators were indirectly related to farmers' intervention in the system (*Soil Quality*).

Farmers described conditions for each indicator within a three-tiered ordinal scale of marginal, acceptable, and optimal that were respectively linked to red, yellow, and green colors. Describing conditions of indicators with stop-light colors has been developed in Latin America as a simple methodology for farmers to evaluate their agroecosystems (Altieri 2010; Cammaert et al. 2007). However, farmers participating in this case study did not intuitively associate indicator conditions with colors since many had limited interaction with stop lights in their day-to-day lives. For the agroecosystem assessment phase described below, researchers paired colors with facial iconography: sad for marginal, normal for acceptable, and happy for optimal. While facial iconography was effective at improving communication between researchers and farmers during the workshops, for the purpose of this chapter we make reference to the scales of marginal, acceptable, and optimal.

Researchers and CEDICAM subsequently refined the indicators described by farmers into a set of 14 indicators. Repetitive indicators across communities were combined, as were those indicators that distinguished between dry and wet years. For example, while wheat was described as more resistant to drought than to excess soil moisture, most varieties of maize were sensitive to both drought and excess soil moisture. Therefore, we described wheat as more resistant to climatic variability than maize.

In the third series of workshops, three women farmers in Zaragoza and three groups of five predominantly women farmers in El Rosario independently evaluated four production systems in their communities using the set of 14 indicators. Researchers pooled the agroecosystem evaluations within each community by assigning numerical scores of 0 for marginal, 1 for acceptable, and 2 for optimal. Farmers analyzed outcomes by drawing bar plots of the pooled scores for their community. Farmers were prompted to analyze the results of their evaluations as a group by the following questions: How to obtain more happy faces (i.e. the optimal condition) in the *Landscape, Farmer Management*, and *Soil Quality* categories? How to maintain the happy faces (i.e. optimal condition) that you already have in the *Landscape, Farmer Management*, and *Soil Quality* categories?

5.4. Results

a. Farmer climate histories

Climate histories dated back to the 1970s in Zaragoza, to 1969 in El Rosario, and to the 1930s for one individual in Coxcaltepec. Farmers reported that climate changes in recent decades – namely later rains and more drought – have made growing conditions less favorable for traditional forms of agriculture. Across the three communities, participants reported a shift towards a later onset of the rainy season. Zaragoza participants recalled the onset of rainfall before the 1990s between February and March while since approximately 1990 rainfall began from May to July. In El Rosario rainfall began from May to June during the 1970s, whereas they began between June and July starting in the 1990s. Farmers in Coxcaltepec observed a progressive shift beginning in the 1970s in the onset of rainfall from May towards July. These shifts were associated with historically important dates in the communities: the years electricity arrived in Zaragoza and Coxcaltepec and the year El Rosario's main road was built.

Increased storm intensities were particularly noted in the last decade by the three communities. Extreme climatic events described by farmers in the three communities were remembered for their impacts on agroecosystems. Zaragoza experienced a near complete crop failure in 2006 due to frost, as well as suppressed yields in 2009 due to high rainfall in June followed by an unusually dry mid-summer drought. El Rosario farmers recalled a catastrophic drought in 1996 that killed crops, trees, and palms alike.

Farmers identified multiple instances of agroecosystem change that in some cases were associated with climate. Particular mention was made by farmers of detrimental climate changes during the beginning of the rainy season when many crops are sown. Sowing dates for temporal maize had shifted from May to June in Zaragoza since the 1990s, and from between May to June 16 to between June and July 14 in El Rosario. Coxcaltepec

and El Rosario participants noted that later sowing dates place temporal maize and beans at greater risk to frost damage in September and October.

In addition to shifting sowing dates, participants in El Rosario and Coxcaltepec largely abandoned cajete maize. While at one time approximately half of arable lands were cultivated to cajete maize, today the practice is greatly reduced in the three communities. One reason cited by farmers was greater heat (*calor*), consisting of both extended dry seasons as well as more frequent droughts (*sequía*) during the rainy season. We note that this is similar to the findings of Sánchez-Cortés and Chavero (2011), who describe that changes in the agroecosystems of Zoque farmers in the Mexican State of Chiapas was provoked by less rain and increased temperature.

Farmers associated greater heat during the dry season with elevated post-harvest losses in Zaragoza and El Rosario due to the increased prevalence of grain weevils and moths. According to farmers, post-harvest pest damage is exacerbated by state-subsidized construction materials of cement, cinder block, and corrugated metal introduced since the 1980s that elevate indoor temperatures compared to traditional building materials of adobe, palm, reeds, and oak. Temperature is an important environmental factor in the degree of post-harvest grain damage, which is why cooling techniques are well established in the classic approach of insect pest control (McFarlane 1988).

Farmer observations would suggest that they do not necessarily respond to specific cases of climatic extremes, but rather their long-term management strategies buffer agroecosystems from climatic shocks. During a series of dry years from 2004 to 2009, cajete maize and wheat were most resistant while temporal maize and beans failed. Farmers attributed this to cajete maize suffering less damage from excessive rainfall and frost at the end of the rainy season since it is harvested earlier than temporal maize.

b. Climate record

Figure 5.4 shows the annual mean CRU–TS temperature anomalies from 1961–1990 over the study region. The 25-year and 50-year trends both show statistically significant warming (0.16 and 0.18°C per decade). This is consistent with our finding of regional-scale warming over south–central Mexico (15–20°N, 95–100°W) in the Climatic Research Unit variance-adjusted land surface temperature record (CRUTEM4) version 4.2.0.0 (Jones et al. 2012), which is not shown. The influence of ENSO is also apparent on interannual timescales, with anomalously high temperatures associated with the strong El Niño events of 1982–1983 and 2009.

For an estimate of rainfall intensity, we divided total annual rainfall by the count of days with rainfall from CRU–TS to obtain an average of the rainfall amount per rain day. **Figure 5.5** shows this estimate of annual mean rainfall intensity. There are increasing trends over both 1961–2010 and 1986–2010, though neither is statistically significant. The increase has been larger in recent years; the 1986–2010 trend is over three times as large as the 1961–2010 trend (0.03 cm/ rain day and 0.10 cm/ rain day per decade), and three of the four most intense years were in the 2001–2010 decade. There is also an association with the ENSO activity: the very intense rain years of 1983 and 2010 were each in the

second year of a strong El Niño. 2010 also transitioned quickly into a strong La Niña (Ruiz-Barradas 2011).

It is difficult to directly assess the length and timing of the rainfall season both because we did not examine daily rainfall data, and there is not a strict threshold for the onset of the local rainy season. For a sense of changes in rainfall seasonality, we examined the time series of early season rainfall (April–June), late season rainfall (July–September), and the difference between these two seasons, shown in **Figure 5.6**. The early and late rainfall seasons have different associations with ENSO. July–September had dramatic spikes in rainfall in 1983, 1998, and 2010 - each the second year of a strong El Niño (as mentioned above, 2010 also transitioned into a strong La Niña. These years had low April–June rainfall, resulting in a very large seasonal difference. 1969 had a similar rainfall pattern, but does not appear to have been a strong El Niño.

The 1961–2010 and 1986–2010 trends are slightly positive for both April–June (0.39 and 0.78 cm per decade) and July–September (1.68 and 4.43 cm per decade). Since the July–September trend is larger, the difference also has a positive trend over both 1961–2010 (0.98 cm per decade) and 1986–2010 (2.43 cm per decade). None of the trends is statistically significant. Similar results were found in the GPCC dataset (not shown).

Though the data do not directly support a later spring rainfall onset, the increasing difference between the late and early season may account for the perception of a shift to later rainfall, as found in a recent study of farmer climate perceptions in the Caribbean (Gamble et al. 2010). Alternatively, the rains may indeed be arriving later on the order of days or weeks, which would not be recorded in the monthly data we analyzed. Another caveat is that we did not investigate changes in the variability of rainfall, which could relate to the frequency of droughts that was identified by some farmers.

c. Local agroecosystem practices

Beyond climate, farmers reported that crises of labor and soil fertility also contributed to the shift from cajete maize to temporal maize. Participants in the three communities noted a decrease in rural labor and an increase in labor-saving agricultural technologies. Farmers reported that the massive out-migration of youth from Coxcaltepec contributed to the abandonment of cajete maize in favor of labor-saving crops such as temporal maize. Farmers associated reduced rural labor with declines in animal husbandry since the 1980s. The majority of oxen used for plowing fields were sold by Coxcaltepec farmers with the introduction of tractor technology in 2009. Consequently, farmers substituted traditional soil fertility management based on animal manures with purchased synthetic fertilizers in Zaragoza since 1998 and in Coxcaltepec since the 1990s. Maize yields increased initially by the change in soil fertility management. However, soils were negatively affected over time and productivity eventually declined. Zaragoza farmers began experimenting with green manures and composts in 2002 to reduce the costs of synthetic fertilizers and to improve soil quality. An initial reduction in yields was followed by increases in subsequent years. Research from Mixteca Alta (Edinger 1996; García-Barrio and García-Barrios 1990) and elsewhere in Mexico (Eakin 2000; Eakin 2006) support the

observation by farmers that decisions for managing their agroecosystems are influenced by larger economic and technological forces.

The conditions of *Optimal, Acceptable*, and *Marginal* for the 14 indicators were described per category of *Landscape*, *Farmer Management*, and *Soil Quality*. We highlight below several indicator conditions to demonstrate how they are grounded in farmers' local knowledge for dealing with climatic variability.

At the level of the community, Zaragoza farmers observed that vegetated borders and perennial vegetation with multiple uses mitigate exposure to extreme climatic events. Similarly, Coxcaltepec farmers' recognized that heterogeneous and forested landscapes provide ecosystem services, including protecting fields, bringing rain, retaining groundwater, accumulating soil organic matter, and controlling insect pests. In addition, some tree species may compete with crops for resources or negatively affect crops if their leaves give heat (*calor*), such as juniper and pine, in contrast to the cool leaves of oak, manzanita, and madrone. El Rosario participants described how ditches along the upslope of contour bunds capture soil and water, and how a slight slope to contour bunds avoids flooding and breaching during heavy rainfall events.

Indicators of farmer management at the field-scale included the importance of crop genetic and species diversity for stabilizing overall yields given the variation in crop performance from year to year. While farmers described maize as generally more vulnerable to climatic extremes than wheat, cajete maize was described as more resistant than temporal maize. The apparent contradiction between farmers' prior narratives of abandoning cajete maize and subsequent ranking of cajete maize as more resistant than temporal maize will be discussed later in this chapter. The indicator of *Soil Amendments* were derived from farmer testimonies that synthetic fertilizer only improves crop yields with favorable rainfall; in drought years, synthetic fertilizer is ineffective and may even burn crops. Coxcaltepec participants recommended substituting synthetic fertilizers with various locally-derived soil amendments, including animal manures, worm castings, forest humus, and human urine.

Soil quality was also described by farmers to affect the impact of climatic variability on agroecosystems. The three communities associated soil moisture retention with soil texture and depth. Although soil color was also mentioned as an indicator, it was difficult to use due to apparent contradictions of color classifications across communities. Generally, clayey soils were described as the most productive in drought years, but also difficult to work in wet years. In contrast, farmers described sandy soils as the easiest to work in wet years but also the least productive. Deep soils, measured by farmers as the depth that the Egyptian plow enters the soil, are considered by farmers to be the most productive soils in both wet and dry years.

Farmers in the three communities described how contour bunds improve water infiltration, recharge aquifers, retain water in dry years, and facilitate drainage of fields in wet years. Vegetated borders and windbreaks, as told by farmers, protect maize from windthrow. Farmers noted the role that CEDICAM plays in training communities to conserve soils using appropriate technologies, such as the Apparatus A (Léon-Santos 2007, 14–21). Additionally, farmers noted the importance of governmental support for

conservation practices, like the funding Zaragoza's municipality received from government sources to build contour bunds in 2009.

5.5. Discussion and conclusions

This research described farmers' interpretations of climate and identified local strategies for dealing with climatic variability. The workshops highlighted the depth of farmers' knowledge for dealing with climatic variability. The basis of small farmer agroecosystem management in traditional ecological knowledge is well documented in Mesoamerica (Toledo and Barrera-Bassols 2008; Pulido and Bocco 2003; Wilken 1987). Participatory methods based on qualitative evaluations in combination with local farming knowledge of the Mixteca Alta produced a set of best agricultural practices for the region. While the detailed strategies outlined by farmers may be highly site specific, the participatory methodologies used with small farmers in this study can easily be adapted and applied in other regions of the world.

The active participation of the CEDICAM network in all aspects of this research validated local ways of knowing and prioritized farmer interventions. We observed that the pre-Hispanic practices for regulating soil erosion described by Rivas Guevara (2008, 124–144) inspire modern efforts by CEDICAM to reduce soil loss and crop damage from extreme climatic events. The methodology that we proposed and implemented in this research may be scaled up through farmer networks and applied in different regions to motivate local preparation, adaptation, and mitigation strategies.

It is noteworthy that farmers' analysis of their situation mirror general policy recommendations for climate change adaptation and mitigation. Farmers' criteria for evaluating landscape features, agricultural practices, and soil attributes overlap with many of the indicators of agricultural resilience proposed by Cabell and Oelofse (2012), including ecological self regulation, connectedness, and spatial and temporal heterogeneity. Moreover, farmers' ideas for transforming their agroecosystems correspond to climate adaptation and mitigation strategies recommended by the Intergovernmental Panel on Climate Change (IPCC), notably increasing reforestation, increasing soil carbon retention, composting, decreasing emissions from manure and petroleum-based fertilizers, and reducing fossil fuel dependency in agriculture (Smith, P. et al. 2007).

Farmers in the Mixteca Alta described long-term modifications to their agroecosystems that represent important strategies for adjusting to changes in mean climatic conditions. Oral histories of farmers document significant changes in farming practices over the past generation. Farmers responded to changes in rainfall patterns by shifting sowing dates, sowing different crops, and selecting crop varieties that succeeded given environmental disturbances. Farmers guide their cropping decisions based on rainfall patterns in a given year, which has led to progressively later sowing of rainfed crops and the selection of more precocious crop varieties.

In this region that experiences climatic variability, maximizing yields does not appear to matter as much to farmers as stabilizing fluctuations in yields over time. Such stabilizing practices identified from the workshops included soil management to increase soil organic matter, agricultural diversification, and landscape complexity. This perspective

may offer space to broaden the lens of appropriate mitigation and adaptation strategies to a changing climate. It is particularly important to consider local strategies and multiple agroecosystem objectives for greater responsiveness to climate change and social need.

Dealing with challenges posed by climatic variability involves much more than a set of farming practices. The apparent contradiction of farmers abandoning cajete maize – one of the drought resistant crops identified by farmers – requires further investigation. Farmer narratives and climate records point to changes in agricultural environments of the Mixteca Alta that may favor temporal maize over cajete maize despite cajete's resistance to drought events. Though maize cajete is more resistant to drought events, it requires cooler temperatures and moist soils during the dry season. We speculate that the warming and intensity trends have caused a drying of the mean state of soils, so that planting temporal maize is more favorable. Just as important may be reductions in available rural labor for maintaining traditional practices associated with the production systems like cajete maize. Farmers expressed concerns that labor-saving technologies were negatively affecting their production systems, but considered that many labor-intensive traditional technologies are today impractical.

An unanticipated outcome of the workshops were calls by participating farmers in Zaragoza and El Rosario for greater community mobilization. Farmers recognized that improving landscape-scale indicators would require community-level education and collective action. Before evaluating their agroecosystems, farmers expressed sentiments typified by one participant in El Rosario: "the rains come differently every year. When there is no rain, there is nothing we can do." After conducting their assessments, farmers recognized how their management strategies influence their ability to cope with climatic variability. Again in El Rosario, a farmer asked the group "we know what we need to do now, but how will we make it happen?" The farmers agreed to organize working groups to take action. We interpret this as a process of moving from inevitability, to empowerment, and finally action.

5.6. Author Contributions

P.R. and A.R.F. jointly conceived the study. P.R. designed the research, and A.R.F. contributed the climate-related questions. P.R. and M. Astier conducted the workshops, P.R. analyzed the workshop data, and A.R.F. analyzed the climate data. P.R. and A.R.F. wrote the manuscript, and M. Astier and M. Altieri provided feedback and improvement.

5.7. Acknowledgments

Köppen-Geiger climate classification data are from koeppen-geiger.vu-wien.ac.at/present.htm. CRU-TS data are from badc.nerc.ac.uk/view/badc.nerc.ac.uk__ATOM__dataent_1256223773328276. GPCC rainfall data are from ftp://ftp.dwd.de/pub/data/gpcc/html/fulldata_v6_doi_download.html. Multivariate ENSO Index data are from www.esrl.noaa.gov/psd/enso/mei/table.html. Thanks to Jeff Burkey for providing the Kendall-Theil slope script, *ktaub.m*, from the Matlab file exchange.

We wish to express our gratitude to the farmers at CEDICAM, in particular Abelino Célis, Anastasia Velasco López, Eleazar García Jiménez, Estela Rosendo Palacios and Jesús León Santos. Thanks to the student interns Aida Carmen Ríos Colín, Jessica Parra-Fitch, Leslie López, Luis Suárez, Maya Stanton, Michelle Roses, Natalia García-Pasmanick, Silvia Victoria Ruiz Narváez, Soledad Loreily Soto Sarmiento, Víctor Bautista Vásquez, and Xochitl Victoria Juárez Martinez. For guidance and collaboration, thanks to Gabriel Córdova Gámez, Jutta Blauert, Nathan Sayre, John Chiang, Ben Orlove, Teddy Allen, Shoshana Perrey, and Tamara Ortiz-Ávila. We thank Alejandro González Serratos and Emmanuel Álvarez Ramírez for providing station data. Financial support for this project was provided by Garcia Robles-Fulbright, UC MEXUS, and CONACYT.

5.8. Figures

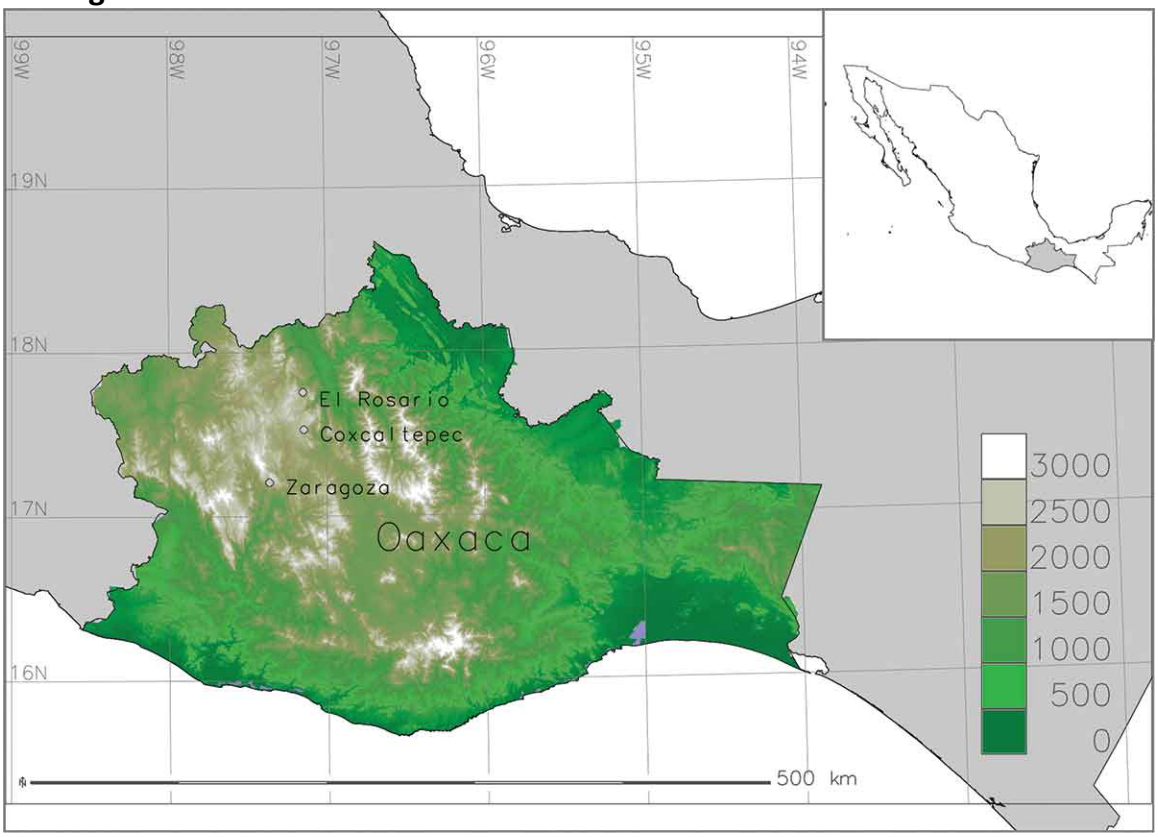

Figure 5.1. Location of the communities from the Mixteca Alta region of Oaxaca, Mexico that participated in this case study: San José Zaragoza (Zaragoza), El Rosario, and San Pedro Coxcaltepec Cántaros (Coxcaltepec). Elevation is shown in meters.

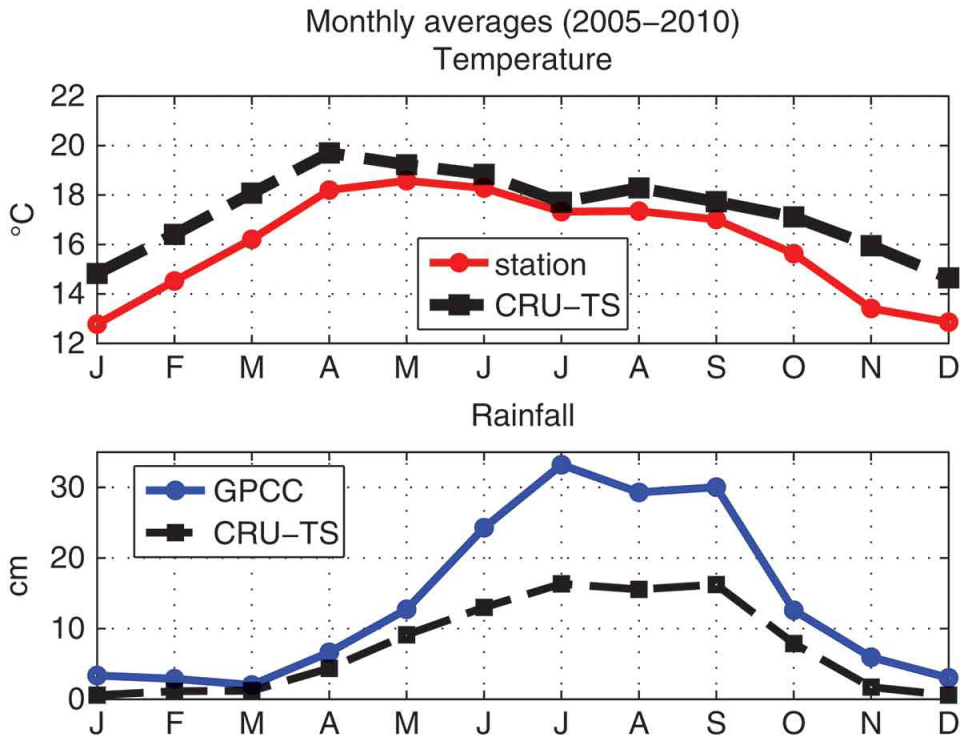

Figure 5.2. 2005–2010 monthly averages based on data from the Nochixtlán meteorological station (17°26' N, 97°15' W, 2040 m) and gridded averages over 96.5–97.5°W, 17–18°N. Top: Temperature (°C) based on data from the Nochixtlán meteorological station (red solid) and CRU–TS (black dashed). Bottom: Rainfall (cm) based on data from GPCC (blue solid) and CRU–TS (black dashed).

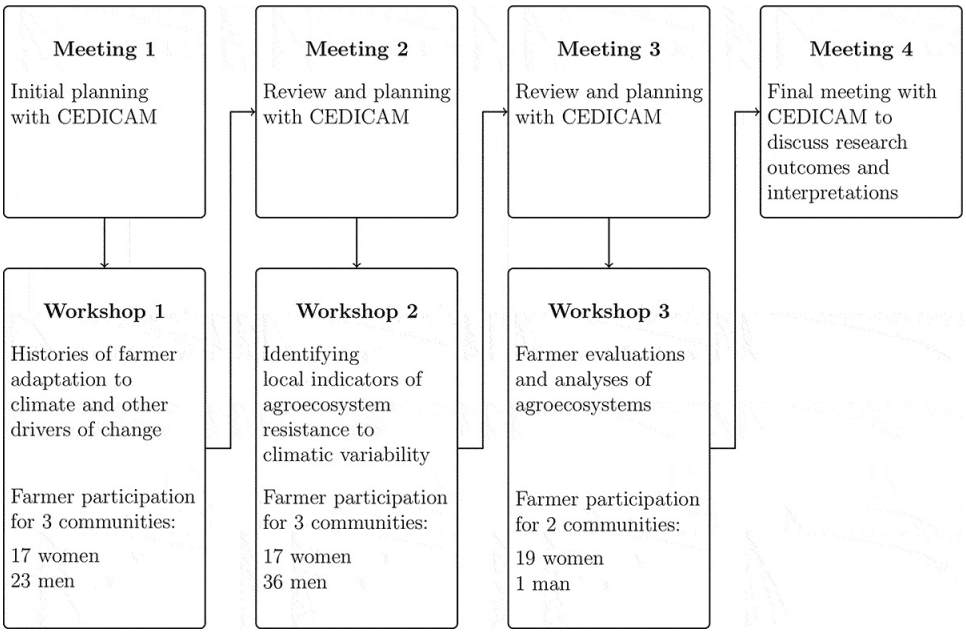

Figure 5.3. Outline of the flow of co-investigation with the farmer-led Center for Integral Rural Development of the Mixteca Alta (CEDICAM) and researchers. The co-investigation process jointly defined objectives, refined methodologies, organized community members for workshops, and interpreted results. A constant emphasis was also placed on validating farmer perceptions throughout the research process. The number of communities and participating farmers during each phase of workshops is also displayed.

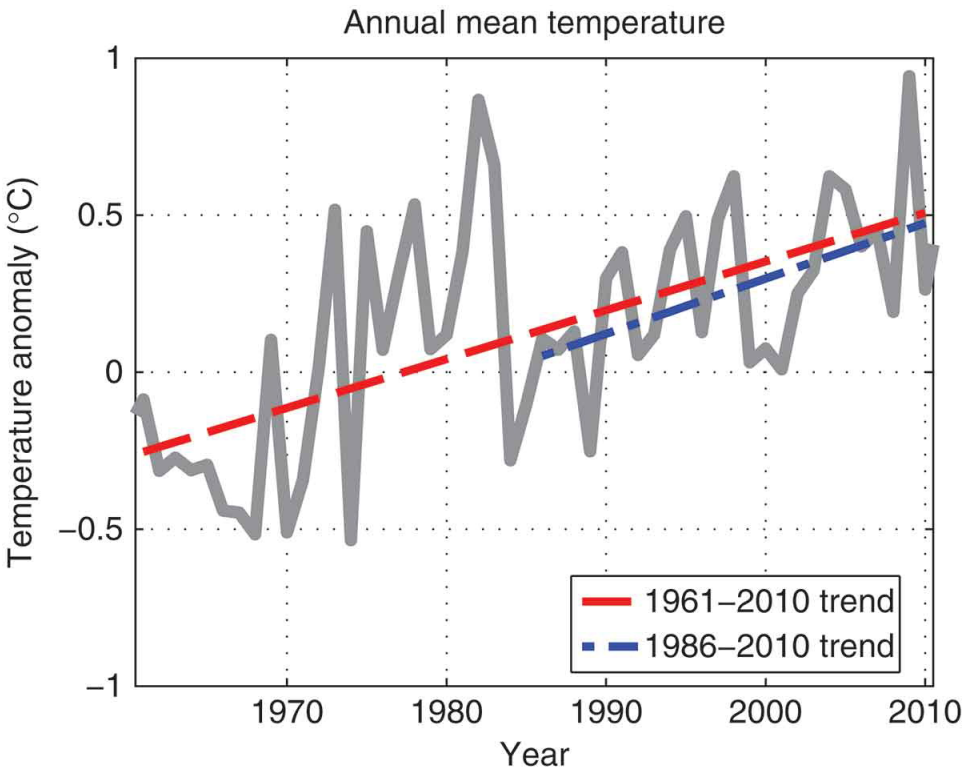

Figure 5.4. Annual mean temperature anomalies (°C; solid grey) over 96.5–97.5°W, 17–18°N based on data from CRU–TS. The dashed lines show the 1961–2010 (red) and 1986–2010 (blue) trend lines. Anomalies are calculated from 1961–1990.

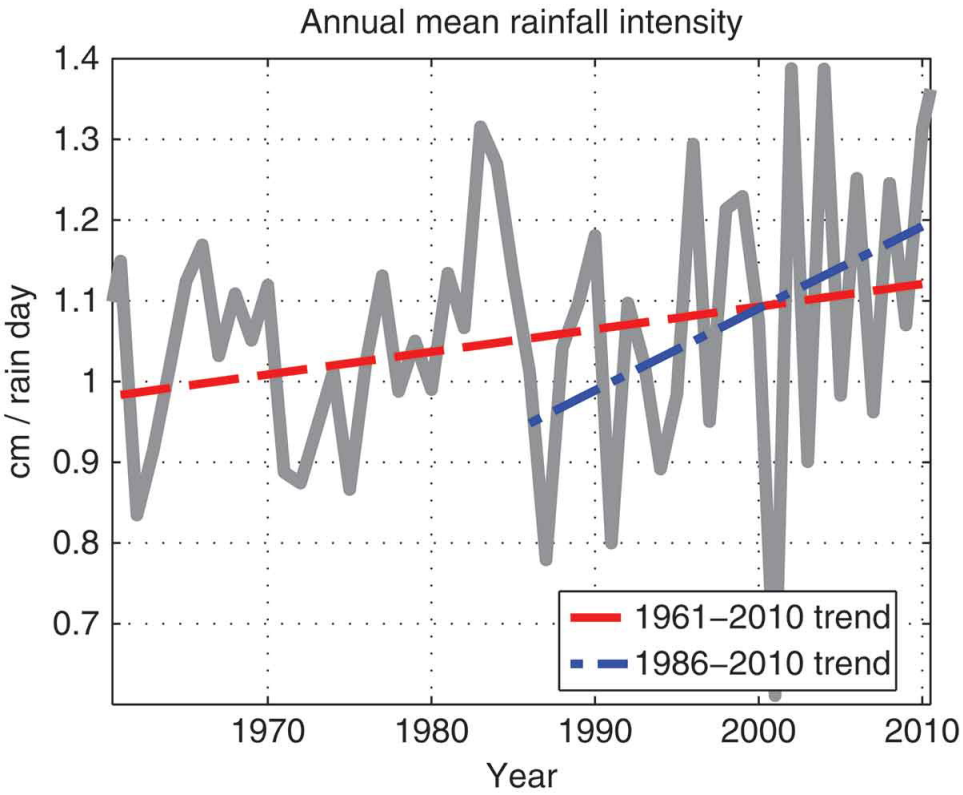

Figure 5.5. Annual mean rainfall intensity (cm per rain day; solid grey) over 96.5–97.5°W, 17–18°N based on data from CRU–TS. The dashed lines show the 1961–2010 (red) and 1986–2010 (blue) trend lines.

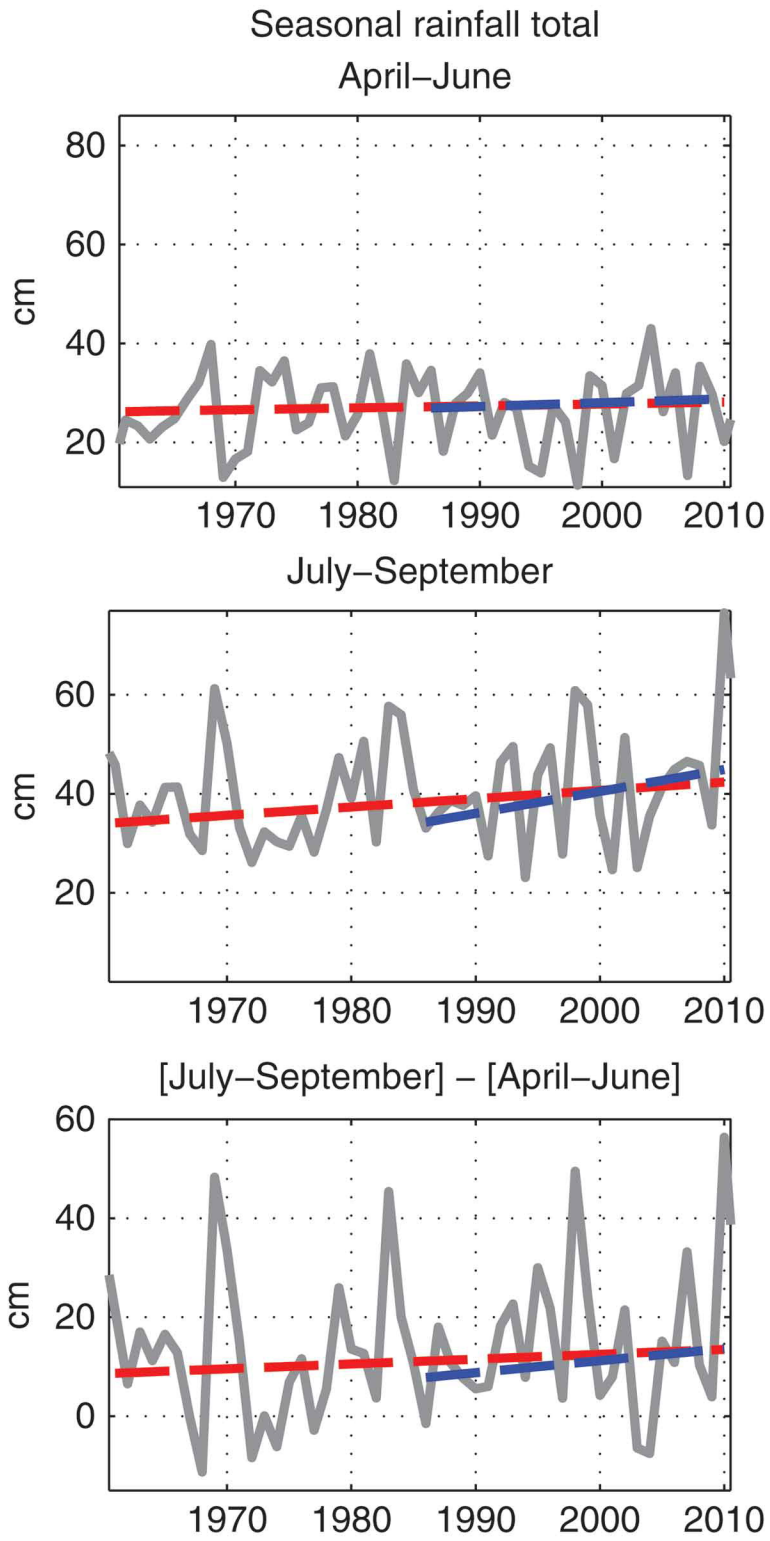

Figure 5.6. Seasonal rainfall totals (cm; solid grey) over 96.5–97.5°W, 17–18°N for April–June (top), July–September (middle), and the seasonal difference (bottom) based on data from CRU–TS. The dashed lines show the 1961–2010 (red) and 1986–2010 (blue) trend lines.

Bibliography

Altieri, M. A. 2010. "Determinando La Capacidad de Adaptación Y Resiliencia de Los Sistemas Agroforestales (SAF) Con Cacao Frente Al Cambio Climático". Inter-American Development Bank (BID-FMAM).

Altieri, M. A., S.A. Fonseca, J.J. Caballero, and J.J. Hernández. 2006. "Manejo Del Agua Y Restauración Productiva En La Región Indígena Mixteca de Puebla Y Oaxaca". México D.F.: CEDEC México: Banco Internacional de Reconstrucción y Fomento / El Banco Mundial.

Altieri, Miguel A., and Clara I. Nicholls. 2013. "The Adaptation and Mitigation Potential of Traditional Agriculture in a Changing Climate." *Climatic Change*, September, 1–13. doi:10.1007/s10584-013-0909-y.

Ashok, Karumuri, and Toshio Yamagata. 2009. "Climate Change: The El Niño with a Difference." *Nature* 461 (7263): 481–84. doi:10.1038/461481a.

Astier, Marta, Luis Garcia-Barrios, Yankuic Galvan-Miyoshi, Carlos E. Gonzalez-Esquivel, and Omar R. Masera. 2012. "Assessing the Sustainability of Small Farmer Natural Resource Management Systems. A Critical Analysis of the MESMIS Program (1995-2010)." *Ecology and Society* 17 (3): 25. doi:10.5751/ES-04910-170325.

Astier, Marta, Erika N. Speelman, Santiago Lopez-Ridaura, Omar R. Masera, and Carlos E. Gonzalez-Esquivel. 2011. "Sustainability Indicators, Alternative Strategies and Trade-Offs in Peasant Agroecosystems: Analysing 15 Case Studies from Latin America." *International Journal of Agricultural Sustainability* 9 (3): 409–22. doi:10.1080/14735903.2011.583481.

Baines, PG, and CK Folland. 2007. "Evidence for a Rapid Global Climate Shift across the Late 1960s." *Journal of Climate* 20 (12): 2721–44. doi:10.1175/JCLI4177.1.

Bekryaev, Roman V., Igor V. Polyakov, and Vladimir A. Alexeev. 2010. "Role of Polar Amplification in Long-Term Surface Air Temperature Variations and Modern Arctic Warming." *Journal of Climate* 23 (14): 3888–3906. doi:10.1175/2010JCLI3297.1.

Biasutti, M., I. M. Held, A. H. Sobel, and A. Giannini. 2008. "SST Forcings and Sahel Rainfall Variability in Simulations of the Twentieth and Twenty-First Centuries." *Journal of Climate* 21 (14): 3471–86.

Blauert, Jutta, and Eduardo Quintanar. 2000. "Seeking Local Indicators: Participatory Stakeholder Evaluation of Farmer-to-Farmer Projects, Mexico." In *Learning from Change: Issues and Experiences in Participatory Monitoring and Evaluation*. Ottowa: IDRC Books.

Boege, Eckart, and Tzinnia Carranza. 2009. "La agricultura sostenible campesino-indígena frente a la Mixteca Alta: La experiencia del Centro de Desarrollo Integral Campesino de la Mixteca Hita Nuni, AC (Cedicam)." In *Agricultura Sostenible Campesino-Indígena, Soberanía Alimentaria y Equidad de Género*, 87–138. México D.F.: PIDAASSA.

Bollasina, Massimo A., Yi Ming, and V. Ramaswamy. 2011. "Anthropogenic Aerosols and the Weakening of the South Asian Summer Monsoon." *Science* 334 (6055): 502–5. doi:10.1126/science.1204994.

Boyer, Timothy P., S. Levitus, J. I. Antonov, R. A. Locarnini, and H. E. Garcia. 2005. "Linear Trends in Salinity for the World Ocean, 1955–1998." *Geophysical Research Letters* 32 (1): L01604. doi:10.1029/2004GL021791.

Braganza, K., D. J. Karoly, A. C. Hirst, P. Stott, R. J. Stouffer, and S. F. B. Tett. 2004. "Simple Indices of Global Climate Variability and Change Part II: Attribution of Climate Change during the Twentieth Century." *Climate Dynamics* 22 (8): 823–38. doi:10.1007/s00382-004-0413-1.

Cabell, Joshua F., and Myles Oelofse. 2012. "An Indicator Framework for Assessing Agroecosystem Resilience." *Ecology and Society* 17 (1). doi:10.5751/ES-04666-170118. http://www.ecologyandsociety.org/vol17/iss1/art18/.

Cammaert, C., M. T. Palacios, H. Arango, and Z. Calle. 2007. "Mi Finca Biodiversa: Herramienta Didáctica Para La Planificación de La Biodiversidad En Finca". Bogotá, Colombia: Instituto Alexander von Humboldt.

Chang, C-Y., J. C. H. Chiang, M. F. Wehner, A. R. Friedman, and R. Ruedy. 2011. "Sulfate Aerosol Control of Tropical Atlantic Climate over the Twentieth Century." *Journal of Climate*, May, 110301125651015. doi:10.1175/2010JCLI4065.1.

Chen, MY, PP Xie, JE Janowiak, and PA Arkin. 2002. "Global Land Precipitation: A 50-Yr Monthly Analysis Based on Gauge Observations." *Journal of Hydrometeorology* 3 (3): 249–66.

Chiang, John C H, and Celia M Bitz. 2005. "Influence of High Latitude Ice Cover on the Marine Intertropical Convergence Zone." *Climate Dynamics* 25 (5): 477–96. doi:10.1007/s00382-005-0040-5.

Chiang, John C.H. 2009. "The Tropics in Paleoclimate." *Annual Review of Earth and Planetary Sciences* 37 (1): 263–97. doi:10.1146/annurev.earth.031208.100217.

Chiang, John C.H., and Andrew R. Friedman. 2012. "Extratropical Cooling, Interhemispheric Thermal Gradients, and Tropical Climate Change." *Annual Review of Earth and Planetary Sciences* 40 (1): 383–412. doi:10.1146/annurev-earth-042711-105545.

Chou, C, and MH Lo. 2007. "Asymmetric Responses of Tropical Precipitation during ENSO." *Journal of Climate* 20 (14): 3411–33. doi:10.1175/JCLI4197.1.

Chou, C, JY Tu, and PH Tan. 2007. "Asymmetry of Tropical Precipitation Change under Global Warming." *Geophysical Research Letters* 34 (17). doi:10.1029/2007GL030327.

Chung, C. E., and V. Ramanathan. 2006. "Weakening of North Indian SST Gradients and the Monsoon Rainfall in India and the Sahel." *Journal of Climate* 19 (10): 2036–45. doi:10.1175/JCLI3820.1.

Chung, CE, and V Ramanathan. 2007. "Relationship between Trends in Land Precipitation and Tropical SST Gradient." *Geophysical Research Letters* 34 (16). doi:10.1029/2007GL030491.

Compo, Gilbert P., and Prashant D. Sardeshmukh. 2010. "Removing ENSO-Related Variations from the Climate Record." *Journal of Climate* 23 (8): 1957–78. doi:10.1175/2009JCLI2735.1.

Dai, A., and K. E. Trenberth. 2002. "Estimates of Freshwater Discharge from Continents: Latitudinal and Seasonal Variations." *Journal of Hydrometeorology* 3 (6): 660–87. doi:10.1175/1525-7541(2002)003<0660:EOFDFC>2.0.CO;2.

Dai, Aiguo, Taotao Qian, Kevin E. Trenberth, and John D. Milliman. 2009. "Changes in Continental Freshwater Discharge from 1948 to 2004." *Journal of Climate* 22 (10): 2773–92. doi:10.1175/2008JCLI2592.1.

Dickson, Robert R., Jens Meincke, Svend-Aage Malmberg, and Arthur J. Lee. 1988. "The 'Great Salinity Anomaly' in the Northern North Atlantic 1968–1982." *Progress in Oceanography* 20 (2): 103–51.
Dima, Mihai, and Gerrit Lohmann. 2010. "Evidence for Two Distinct Modes of Large-Scale Ocean Circulation Changes over the Last Century." *Journal of Climate* 23 (January): 5–16. doi:10.1175/2009JCLI2867.1.
Drijfhout, Sybren, Emily Gleeson, Henk A. Dijkstra, and Valerie Livina. 2013. "Spontaneous Abrupt Climate Change due to an Atmospheric Blocking–sea-Ice–ocean Feedback in an Unforced Climate Model Simulation." *Proceedings of the National Academy of Sciences* 110 (49): 19713–18. doi:10.1073/pnas.1304912110.
Drost, Frank, and David Karoly. 2012. "Evaluating Global Climate Responses to Different Forcings Using Simple Indices." *Geophysical Research Letters* 39 (16): L16701. doi:10.1029/2012GL052667.
Drost, Frank, David Karoly, and Karl Braganza. 2012. "Communicating Global Climate Change Using Simple Indices: An Update." *Climate Dynamics* 39 (3-4): 989–99. doi:10.1007/s00382-011-1227-6.
Eakin, Hallie. 2000. "Smallholder Maize Production and Climatic Risk: A Case Study from Mexico." *Climatic Change* 45 (1): 19–36. doi:10.1023/A:1005628631627.
———. 2006. *Weathering Risk in Rural Mexico: Climatic, Institutional, and Economic Change*. University of Arizona Press.
Easterling, W., P. Aggarwal, P. Batima, K. Brander, J. Bruinsma, L. Erda, M. Howden, F. Tubiello, J. Antle, and W. Baethgen. 2007. "Food, Fibre, and Forest Products." In *Climate Change 2007: Impacts, Adaptation, and Vulnerability. Contribution of Working Group II to the Fourth Assessment Report of the Intergovernmental Panel on Climate Change*. Cambridge University Press. http://ipcc-wg2.gov/AR4/SOD/Ch05.pdf.
Edinger, Steven T. 1996. *The Road from Mixtepec: A Southern Mexican Town and the United States Economy*. Fresno, Calif: Asociación Cívica Benito Juárez.
Enfield, David B., Alberto M. Mestas-Nuñez, and Paul J. Trimble. 2001. "The Atlantic Multidecadal Oscillation and Its Relation to Rainfall and River Flows in the Continental U.S." *Geophysical Research Letters* 28 (10): PAGES 2077–2080.
Fang, Y, JCH Chiang, and P Chang. 2008. "Variation of Mean Sea Surface Temperature and Modulation of El Nino-Southern Oscillation Variance during the Past 150 Years." *Geophysical Research Letters* 35 (14). doi:10.1029/2008GL033761.
Flohn, H. 1981. "A Hemispheric Circulation Asymmetry during Late Tertiar." *International Journal of Earth Sciences* 70 (2): 725–36.
Folland, CK, TN Palmer, and DE Parker. 1986. "Sahel Rainfall And Worldwide Sea Temperatures, 1901-85." *Nature* 320 (6063): 602–7.
Freire, Paolo. 1970. *Pedagogy of the Oppressed*. New York: Herder and Herder.
Friedman, Andrew R., Yen-Ting Hwang, John C. H. Chiang, and Dargan M. W. Frierson. 2013. "Interhemispheric Temperature Asymmetry over the Twentieth Century and in Future Projections." *Journal of Climate* 26 (15): 5419–33. doi:10.1175/JCLI-D-12-00525.1.
Frierson, Dargan M. W., and Yen-Ting Hwang. 2012. "Extratropical Influence on ITCZ Shifts in Slab Ocean Simulations of Global Warming." *Journal of Climate* 25 (2): 720–33. doi:10.1175/JCLI-D-11-00116.1.

Gamble, Douglas W., Donovan Campbell, Theodore L. Allen, David Barker, Scott Curtis, Duncan McGregor, and Jeff Popke. 2010. "Climate Change, Drought, and Jamaican Agriculture: Local Knowledge and the Climate Record." *Annals of the Association of American Geographers* 100 (4): 880. doi:10.1080/00045608.2010.497122.

García Barrios, Raúl, García Barrios, Luis, and Elena Alvarez-Buylla. 1991. "Lagunas: Deterioro Ambiental Y Tecnológico En El Campo Semiproletarizado". México, D.F.: Colegio de México, Programa sobre Ciencia, Tecnología y Desarrollo.

García-Barrio, Raúl, and Luis García-Barrios. 1990. "Environmental and Technological Degradation in Peasant Agriculture: A Consequence of Development in Mexico." *World Development* 18 (11): 1569–85. doi:10.1016/0305-750X(90)90044-X.

Geilfus, Frans. 1998. *80 Herramientas Para El Desarrollo Participativo: Diagnóstico, Planificación, Monitoreo, Evaluación*. El Salvador: IICA.

Gelderloos, Renske, Fiammetta Straneo, and Caroline A. Katsman. 2012. "Mechanisms behind the Temporary Shutdown of Deep Convection in the Labrador Sea: Lessons from the Great Salinity Anomaly Years 1968–71." *Journal of Climate* 25 (19): 6743–55. doi:10.1175/JCLI-D-11-00549.1.

Hansen, J., R. Ruedy, M. Sato, and K. Lo. 2010. "Global Surface Temperature Change." *Reviews of Geophysics* 48 (December): 29 PP. doi:201010.1029/2010RG000345.

Hansen, James W., Andrew Challinor, Amor Ines, Tim Wheeler, and Vincent Moron. 2006. "Translating Climate Forecasts into Agricultural Terms: Advances and Challenges." *Climate Research* 33 (1): 27–41. doi:10.3354/cr033027.

Harris, I., P.d. Jones, T.J. Osborn, and D.h. Lister. 2014. "Updated High-Resolution Grids of Monthly Climatic Observations – the CRU TS3.10 Dataset." *International Journal of Climatology* 34 (March): 623–42. doi:10.1002/joc.3711.

Hartmann, Dennis L. 1994. *Global Physical Climatology*. San Diego: Academic Press.

Hastenrath, Stefan, and Leon Heller. 1977. "Dynamics of Climatic Hazards in Northeast Brazil." *Quarterly Journal of the Royal Meteorological Society* 103 (435): 77–92. doi:10.1002/qj.49710343505.

Hegerl, G. C., F. W. Zwiers, P. Braconnot, N. P. Gillett, Y. Luo, J. A. Marengo, N. Nicholls, J. E. Penner, and P. A. Stott. 2007. "Understanding and Attributing Climate Change." In *Climate Change 2007: The Physical Science Basis. Contribution of Working Group I to the Fourth Assessment Report of the Intergovernmental Panel on Climate Change, 2007*, 663–745. Cambridge University Press.

Held, IM, and BJ Soden. 2006. "Robust Responses of the Hydrological Cycle to Global Warming." *Journal of Climate* 19 (21): 5686–99.

Held, Isaac. 2012. "Estimating TCR from Recent Warming." *Isaac Held's Blog*. http://www.gfdl.noaa.gov/blog/isaac-held/2012/04/30/27-estimating-tcr-from-recent-warming/.

Helsel, D.R., and R.M. Hirsch. 2002. *Statistical Methods in Water Resources*. U.S. Geological Survey.

Hennink, Monique M. 2007. *International Focus Group Research: A Handbook for the Health and Social Sciences*. Cambridge: Cambridge University Press.

Hu, YY, DW Li, and JP Liu. 2007. "Abrupt Seasonal Variation of the ITCZ and the Hadley Circulation." *Geophysical Research Letters* 34 (18). doi:10.1029/2007GL030950.

Hwang, Yen-Ting, Dargan M. W. Frierson, and Sarah M. Kang. 2013. "Anthropogenic Sulfate Aerosol and the Southward Shift of Tropical Precipitation in the Late 20th Century." *Geophysical Research Letters* 40 (11): 2845–50. doi:10.1002/grl.50502.

Hwang, Yen-Ting, Dargan M. W. Frierson, and Jennifer E. Kay. 2011. "Coupling between Arctic Feedbacks and Changes in Poleward Energy Transport." *Geophysical Research Letters* 38 (September): 5 PP. doi:201110.1029/2011GL048546.

Ishii, Masayoshi, and Masahide Kimoto. 2009. "Reevaluation of Historical Ocean Heat Content Variations with Time-Varying XBT and MBT Depth Bias Corrections." *Journal of Oceanography* 65 (3): 287–99. doi:10.1007/s10872-009-0027-7.

Jones, P. D., D. H. Lister, T. J. Osborn, C. Harpham, M. Salmon, and C. P. Morice. 2012. "Hemispheric and Large-Scale Land-Surface Air Temperature Variations: An Extensive Revision and an Update to 2010." *Journal of Geophysical Research* 117 (March): 29 PP. doi:201210.1029/2011JD017139.

Kalnay, E, M Kanamitsu, R Kistler, W Collins, D Deaven, L Gandin, M Iredell, et al. 1996. "The NCEP/NCAR 40-Year Reanalysis Project." *Bulletin of the American Meteorological Society* 77 (3): 437–71.

Kang, S. M. 2009. "The Response of Tropical Precipitation to Extratropical Thermal Forcing". Princeton.

Kang, SM, DMW Frierson, and IM Held. 2009. "The Tropical Response to Extratropical Thermal Forcing in an Idealized GCM: The Importance of Radiative Feedbacks and Convective Parameterization." *Journal of the Atmospheric Sciences* 66 (9): 2812–27. doi:10.1175/2009JAS2924.1.

Karoly, D. J., and K. Braganza. 2001. "Identifying Global Climate Change Using Simple Indices." *Geophysical Research Letters* 28 (11): 2205–8. doi:10.1029/2000GL011925.

Kaufmann, R. K., and D. I. Stern. 1997. "Evidence for Human Influence on Climate from Hemispheric Temperature Relations." *Nature* 388 (6637): 39–44. doi:10.1038/40332.

Kennedy, J. J., N. A. Rayner, R. O. Smith, D. E. Parker, and M. Saunby. 2011a. "Reassessing Biases and Other Uncertainties in Sea Surface Temperature Observations Measured in Situ since 1850: 2. Biases and Homogenization." *Journal of Geophysical Research* 116 (July): 22 PP. doi:201110.1029/2010JD015220.

———. 2011b. "Reassessing Biases and Other Uncertainties in Sea Surface Temperature Observations Measured in Situ since 1850: 1. Measurement and Sampling Uncertainties." *Journal of Geophysical Research* 116 (July): 13 PP. doi:201110.1029/2010JD015218.

Kiehl, J. T., and B. P. Briegleb. 1993. "The Relative Roles Of Sulfate Aerosols And Greenhouse Gases In Climate Forcing." *Science* 260 (5106): 311–14.

Kottek, Markus, Jürgen Grieser, Christoph Beck, Bruno Rudolf, and Franz Rubel. 2006. "World Map of the Köppen-Geiger Climate Classification Updated." *Meteorologische Zeitschrift* 15 (3): 259–63. doi:10.1127/0941-2948/2006/0130.

Lambert, F. Hugo, and John C. H. Chiang. 2007. "Control of Land-Ocean Temperature Contrast by Ocean Heat Uptake." *Geophysical Research Letters* 34 (13). doi:10.1029/2007GL029755.

Lee, Ming-Ying, and Huang-Hsiung Hsu. 2013. “Identification of the Eurasian-North Pacific Multidecadal Oscillation and Its Relationship to the AMO.” *Journal of Climate*, June, 130628134828003. doi:10.1175/JCLI-D-13-00041.1.

Léon-Santos, Jesús. 2007. “Programa Escuela Campesina: Primera Parte: Acciones Que Contribuyen a La Restauración de Suelos Y El Mejoramiento Del Medio Ambiente”. Nochixtlán, Mexico: CEDICAM.

Levitus, S., J. I. Antonov, T. P. Boyer, O. K. Baranova, H. E. Garcia, R. A. Locarnini, A. V. Mishonov, et al. 2012. “World Ocean Heat Content and Thermosteric Sea Level Change (0–2000 M), 1955–2010.” *Geophysical Research Letters* 39 (10). doi:10.1029/2012GL051106.

Lindzen, RS, and S Nigam. 1987. “On the Role of Sea-Surface Temperature-Gradients in Forcing Low-Level Winds and Convergence in the Tropics.” *Journal of the Atmospheric Sciences* 44 (17): 2418–36.

Liu, Y., and J. C. H. Chiang. 2012. “Coordinated Abrupt Weakening of the Eurasian and North African Monsoons in the 1960s and Links to Extratropical North Atlantic Cooling.” *Journal of Climate* 25 (10): 3532–48. doi:10.1175/JCLI-D-11-00219.1.

Liu, Y., J. C. H. Chiang, C. Chou, and C. M. Patricola. in press. “Atmospheric Teleconnection Mechanisms of Extratropical North Atlantic SST Influence on Sahel Rainfall.” *Climate Dynamics*

Locarnini, R. A., A. V. Mishonov, J. I. Antonov, T. P. Boyer, H. E. Garcia, O. K. Baranova, M. M. Zweng, and D. R. Johnson. 2010. “World Ocean Atlas 2009, Volume 1: Temperature. S. Levitus, Ed.” In Vol. 1. NOAA Atlas NESDIS 68. Washington, D.C: U.S. Government Printing Office.

Ma, Jian, and Shang-Ping Xie. 2013. “Regional Patterns of Sea Surface Temperature Change: A Source of Uncertainty in Future Projections of Precipitation and Atmospheric Circulation*.” *Journal of Climate* 26 (8): 2482–2501. doi:10.1175/JCLI-D-12-00283.1.

Magana, V, JA Amador, and S Medina. 1999. “The Midsummer Drought over Mexico and Central America.” *Journal of Climate* 12 (6): 1577–88.

Manabe, S., R. J. Stouffer, M. J. Spelman, and K. Bryan. 1991. “Transient Responses of a Coupled Ocean–Atmosphere Model to Gradual Changes of Atmospheric CO2. Part I. Annual Mean Response.” *Journal of Climate* 4 (8): 785–818. doi:10.1175/1520-0442(1991)004<0785:TROACO>2.0.CO;2.

Mantsis, DF, and AC Clement. 2009. “Simulated Variability in the Mean Atmospheric Meridional Circulation over the 20th Century.” *Geophysical Research Letters* 36 (March). doi:10.1029/2008GL036741.

Marcott, Shaun A., Jeremy D. Shakun, Peter U. Clark, and Alan C. Mix. 2013. “A Reconstruction of Regional and Global Temperature for the Past 11,300 Years.” *Science* 339 (6124): 1198–1201. doi:10.1126/science.1228026.

McFarlane, J.A. 1988. “Pest Management Strategies for Prostephanus Truncatus (Horn) (Coleoptera; Bostrichidae) as a Pest of Stored Maize Grain: Present Status and Prospects.” *Tropical Pest Management* 34 (2): 121–32. doi:10.1080/09670878809371226.

Meehl, GA, C Covey, T Delworth, M Latif, B McAvaney, JFB Mitchell, RJ Stouffer, and KE Taylor. 2007. “The WCRP CMIP3 Multimodel Dataset - A New Era in Climate Change

Research." *Bulletin of the American Meteorological Society* 88 (9): 1383–94. doi:10.1175/BAMS-88-9-1383.
Mitchell, TP, and JM Wallace. 1992. "The Annual Cycle In Equatorial Convection and Sea-Surface Temperature." *Journal of Climate* 5 (10): 1140–56.
Morgan, David L., and R. A. Krueger. 1993. "When to Use Focus Groups and Why." In *Successful Focus Groups: Advancing the State of the Art*, 3–19. Newbury Park, CA: SAGE Publications.
Morice, Colin P., John J. Kennedy, Nick A. Rayner, and Phil D. Jones. 2012. "Quantifying Uncertainties in Global and Regional Temperature Change Using an Ensemble of Observational Estimates: The HadCRUT4 Data Set." *Journal of Geophysical Research* 117 (April): 22 PP. doi:201210.1029/2011JD017187.
Nobre, P, and J Shukla. 1996. "Variations of Sea Surface Temperature, Wind Stress, and Rainfall over the Tropical Atlantic and South America." *Journal of Climate* 9 (10): 2464–79.
Oreskes, Naomi, David A. Stainforth, and Leonard A. Smith. 2010. "Adaptation to Global Warming: Do Climate Models Tell Us What We Need to Know?" *Philosophy of Science* 77 (5): 1012–28.
Ortiz-Ávila, T., R. A. Quiroz, and T. Camou. 2007. "Manual Para El Técnico Comunitario En Evaluación de Sustentabilidad de Agroecosistemas Campesinos". Mexico: GIRA.
Parry, M., O. Canziani, J. Palutikof, P. Linden, and C. Hanson. 2007. "Cross-Chapter Case Study." *Climate Change 2007: Impacts, Adaptation and Vulnerability Contribution of Working Group II to the Fourth Assessment Report of the Intergovernmental Panel on Climate Change*.
Peralta-Hernandez, AR, RC Balling, and LR Barba-Martinez. 2009. "Comparative Analysis of Indices of Extreme Rainfall Events: Variations and Trends from Southern Mexico." *Atmosfera* 22 (2): 219–28.
Polvani, Lorenzo M., Michael Previdi, and Clara Deser. 2011. "Large Cancellation, due to Ozone Recovery, of Future Southern Hemisphere Atmospheric Circulation Trends." *Geophysical Research Letters* 38 (4): L04707. doi:10.1029/2011GL046712.
Pulido, Juan S., and Gerardo Bocco. 2003. "The Traditional Farming System of a Mexican Indigenous Community: The Case of Nuevo San Juan Parangaricutiro, Michoacán, Mexico." *Geoderma* 111 (3–4). Ethnopedology: 249–65. doi:10.1016/S0016-7061(02)00267-7.
Qian, Taotao, Aiguo Dai, Kevin E. Trenberth, and Keith W. Oleson. 2006. "Simulation of Global Land Surface Conditions from 1948 to 2004. Part I: Forcing Data and Evaluations." *Journal of Hydrometeorology* 7 (5): 953–75. doi:10.1175/JHM540.1.
Rahmstorf, Stefan. 2006. "Thermohaline Ocean Circulation." *Encyclopedia of Quaternary Sciences*. Elsevier. http://pik-potsdam.de/~stefan/Publications/Book_chapters/rahmstorf_eqs_2006.pdf.
Rayner, N. A., D. E. Parker, E. B. Horton, C. K. Folland, L. V. Alexander, D. P. Rowell, E. C. Kent, and A. Kaplan. 2003. "Global Analyses of Sea Surface Temperature, Sea Ice, and Night Marine Air Temperature since the Late Nineteenth Century." *Journal of Geophysical Research* 108 (July): 29 PP. doi:200310.1029/2002JD002670.
Rivas Guevara, M. 2008. "Caracterización del manejo de suelo y uso del agua de lluvia en la Mixteca Alta: jollas y maíces de cajete estudio de caso: San Miguel Tulancingo, Oaxaca". Ph.D. Dissertation, Montecillo, Mexico: Colegio de Postgraduados.

Rodionov, Sergei N. 2004. “A Sequential Algorithm for Testing Climate Regime Shifts.” *Geophysical Research Letters* 31 (9). doi:10.1029/2004GL019448.
Rodionov, Sergei, and James E. Overland. 2005. “Application of a Sequential Regime Shift Detection Method to the Bering Sea Ecosystem.” *ICES Journal of Marine Science: Journal Du Conseil* 62 (3): 328–32. doi:10.1016/j.icesjms.2005.01.013.
Roncoli, C. 2006. “Ethnographic and Participatory Approaches to Research on Farmers’ Responses to Climate Predictions.” *Climate Research* 33 (1): 81–99.
Ropelewski, C. F., and M. S. Halpert. 1987. “Global and Regional Scale Precipitation Patterns Associated with the El Niño/Southern Oscillation.” *Monthly Weather Review* 115 (8): 1606–26. doi:10.1175/1520-0493(1987)115<1606:GARSPP>2.0.CO;2.
———. 1989. “Precipitation Patterns Associated with the High Index Phase of the Southern Oscillation.” *Journal of Climate* 2 (3): 268–84. doi:10.1175/1520-0442(1989)002<0268:PPAWTH>2.0.CO;2.
Rotstayn, LD, and U Lohmann. 2002. “Tropical Rainfall Trends and the Indirect Aerosol Effect.” *Journal of Climate* 15 (15): 2103–16.
Ruiz-Barradas, Alfredo. 2011. “Inundaciones 2010: Lluvias Extremas En Veracruz Y Su Relación Con La Variabilidad Natural Del Clima (Floods in 2010: Extreme Rainfall in Veracruz and Its Relationship with Natural Climate Variability).” In *Inundaciones 2010 En El Estado de Veracruz (Floods in 2010 in the State of Veracruz, Mexico)*. Universidad Veracruzana.
Sánchez-Cortés, Maria Silvia, and Elena Lazos Chavero. 2011. “Indigenous Perception of Changes in Climate Variability and Its Relationship with Agriculture in a Zoque Community of Chiapas, Mexico.” *Climatic Change* 107 (3-4): 363–89. doi:10.1007/s10584-010-9972-9.
Santer, B. D., K. E. Taylor, T. M. L. Wigley, T. C. Johns, P. D. Jones, D. J. Karoly, J. F. B. Mitchell, et al. 1996. “A Search for Human Influences on the Thermal Structure of the Atmosphere.” *Nature* 382 (6586): 39–46. doi:10.1038/382039a0.
Savoskul, Oxana S., and Vladimir Smakhtin. 2013. “Glacier Systems and Seasonal Snow Cover in Six Major Asian River Basins: Hydrological Role under Changing Climate”. 150. Colombo, Sri Lanka: i International Water Management Institute.
Schneider, Udo, Andreas Becker, Peter Finger, Anja Meyer-Christoffer, Markus Ziese, and Bruno Rudolf. 2014. “GPCC’s New Land Surface Precipitation Climatology Based on Quality-Controlled in Situ Data and Its Role in Quantifying the Global Water Cycle.” *Theoretical and Applied Climatology* 115 (1-2): 15–40. doi:10.1007/s00704-013-0860-x.
Seager, Richard, and Naomi Naik. 2012. “A Mechanisms-Based Approach to Detecting Recent Anthropogenic Hydroclimate Change.” *Journal of Climate* 25 (1): 236–61. doi:10.1175/JCLI-D-11-00056.1.
Serreze, Mark C., and Roger G. Barry. 2011. “Processes and Impacts of Arctic Amplification: A Research Synthesis.” *Global and Planetary Change* 77 (1–2): 85–96. doi:10.1016/j.gloplacha.2011.03.004.
Shindell, D, and G Faluvegi. 2009. “Climate Response to Regional Radiative Forcing during the Twentieth Century.” *Nature Geoscience* 2 (4): 294–300. doi:10.1038/NGEO473.
Small, C., and J. E. Cohen. 2004. “Continental Physiography, Climate, and the Global Distribution of Human Population 1.” *Current Anthropology* 45 (2): 269–77.

Smith, Thomas M., and Richard W. Reynolds. 2004. "Improved Extended Reconstruction of SST (1854–1997)." *Journal of Climate* 17 (12): 2466–77. doi:10.1175/1520-0442(2004)017<2466:IEROS>2.0.CO;2.
Smith, TM, RW Reynolds, TC Peterson, and J Lawrimore. 2008. "Improvements to NOAA's Historical Merged Land-Ocean Surface Temperature Analysis (1880-2006)." *Journal of Climate* 21 (10): 2283–96. doi:10.1175/2007JCLI2100.1.
Smith, P., D. Martino, Z. Cai, D. Gwary, H. Janzen, P. Kumar, B. McCarl, et al. 2007. "Agriculture." In *Climate Change 2007: Mitigation. Contribution of Working Group III to the Fourth Assessment Report of the Intergovernmental Panel on Climate Change*. Cambridge, United Kingdom and New York, NY, USA: Cambridge University Press.
Stouffer, RJ, S Manabe, and K Bryan. 1989. "Interhemispheric Asymmetry In Climate Response To A Gradual Increase Of Atmospheric CO2." *Nature* 342 (6250): 660–62.
Stouffer, RJ, J Yin, JM Gregory, KW Dixon, MJ Spelman, W Hurlin, AJ Weaver, et al. 2006. "Investigating the Causes of the Response of the Thermohaline Circulation to Past and Future Climate Changes." *Journal of Climate* 19 (8): 1365–87.
Sun, Cheng, Jianping Li, Fei-Fei Jin, and Ruiqiang Ding. 2013. "Sea Surface Temperature Inter-Hemispheric Dipole and Its Relation to Tropical Precipitation." *Environmental Research Letters* 8 (4): 044006. doi:10.1088/1748-9326/8/4/044006.
Sundby, Svein, and Kenneth Drinkwater. 2007. "On the Mechanisms behind Salinity Anomaly Signals of the Northern North Atlantic." *Progress in Oceanography* 73 (2): 190–202. doi:10.1016/j.pocean.2007.02.002.
Taylor, Karl E., Ronald J. Stouffer, and Gerald A. Meehl. 2012. "An Overview of CMIP5 and the Experiment Design." *Bulletin of the American Meteorological Society* 93 (4): 485–98. doi:10.1175/BAMS-D-11-00094.1.
Terray, Laurent. 2012. "Evidence for Multiple Drivers of North Atlantic Multi-Decadal Climate Variability." *Geophysical Research Letters* 39 (October). doi:10.1029/2012GL053046.
Thompson, David W. J., John M. Wallace, Phil D. Jones, and John J. Kennedy. 2009. "Identifying Signatures of Natural Climate Variability in Time Series of Global-Mean Surface Temperature: Methodology and Insights." *Journal of Climate* 22 (22): 6120–41. doi:10.1175/2009JCLI3089.1.
Thompson, David W. J., John M. Wallace, John J. Kennedy, and Phil D. Jones. 2010. "An Abrupt Drop in Northern Hemisphere Sea Surface Temperature around 1970." *Nature* 467 (7314): 444–47. doi:10.1038/nature09394.
Toggweiler, J. R., and David W. Lea. 2010. "Temperature Differences between the Hemispheres and Ice Age Climate Variability." *Paleoceanography* 25 (June). doi:10.1029/2009PA001758.
Toledo, Víctor M., and Narciso Barrera-Bassols. 2008. *La memoria biocultural: la importancia ecológica de las sabidurías tradicionales*. Icaria Editorial.
Trenberth, K. E., P. D. Jones, P. Ambenje, R. Bojariu, D. Easterling, A. Klein Tank, D. Parker, F. Rahimzadeh, J. A. Renwick, and M. Rusticucci. 2007. "Observations: Atmospheric Surface and Climate Change." In *Climate Change 2007: The Physical Science Basis*, 235–336.
Trenberth, Kevin E., Aiguo Dai, Gerard van der Schrier, Philip D. Jones, Jonathan Barichivich, Keith R. Briffa, and Justin Sheffield. 2014. "Global Warming and Changes in Drought." *Nature Climate Change* 4 (1): 17–22. doi:10.1038/nclimate2067.

USGS. 2014. “Explanations for the National Water Conditions.” *Explanations for the National Water Conditions*. Accessed March 18. http://water.usgs.gov/nwc/explain_data.html.

Valdivia, Corinne, Anji Seth, Jere L. Gilles, Magali García, Elizabeth Jiménez, Jorge Cusicanqui, Fredy Navia, and Edwin Yucra. 2010. “Adapting to Climate Change in Andean Ecosystems: Landscapes, Capitals, and Perceptions Shaping Rural Livelihood Strategies and Linking Knowledge Systems.” *Annals of the Association of American Geographers* 100 (4): 818. doi:10.1080/00045608.2010.500198.

Vecchi, Gabriel A., and Brian J. Soden. 2007. “Global Warming and the Weakening of the Tropical Circulation.” *Journal of Climate* 20 (17): 4316–40.

Vecchi, Gabriel A., Brian J. Soden, Andrew T. Wittenberg, Isaac M. Held, Ants Leetmaa, and Matthew J. Harrison. 2006. “Weakening of Tropical Pacific Atmospheric Circulation due to Anthropogenic Forcing.” *Nature* 441 (7089): 73–76. doi:10.1038/nature04744.

Velásquez, J. C. 2002. “Sustainable Improvement of Agricultural Production Systems in the Mixteca Region of Mexico.” *NRG Paper*, 02–01.

Vose, Russell S., Derek Arndt, Viva F. Banzon, David R. Easterling, Byron Gleason, Boyin Huang, Ed Kearns, et al. 2012. “NOAA’s Merged Land–Ocean Surface Temperature Analysis.” *Bulletin of the American Meteorological Society* 93 (11): 1677–85. doi:10.1175/BAMS-D-11-00241.1.

Vuuren, Detlef P. van, Jae Edmonds, Mikiko Kainuma, Keywan Riahi, Allison Thomson, Kathy Hibbard, George C. Hurtt, et al. 2011. “The Representative Concentration Pathways: An Overview.” *Climatic Change* 109 (1-2): 5–31. doi:10.1007/s10584-011-0148-z.

Wang, Bin, Jian Liu, Hyung-Jin Kim, Peter J. Webster, and So-Young Yim. 2012. “Recent Change of the Global Monsoon Precipitation (1979-2008).” *Climate Dynamics* 39 (5): 1123–35. doi:10.1007/s00382-011-1266-z.

Webster, P. J. 2005. “The Elementary Hadley Circulation.” In *The Hadley Circulation: Present, Past and Future.*, 21:9–60. Advances in Global Change Research. Kluwer Academic Publishers: the Netherlands.

Wilcox, L. J., E. J. Highwood, and N. J. Dunstone. 2013. “The Influence of Anthropogenic Aerosol on Multi-Decadal Variations of Historical Global Climate.” *Environmental Research Letters* 8 (2): 024033. doi:10.1088/1748-9326/8/2/024033.

Wilken, Gene C. 1987. *Good Farmers: Traditional Agriculture and Resource Management in Mexico and Central America*. Berkeley: University of California Press.

Wilkinson, S. 1999. “How Useful Are Focus Groups in Feminist Research?” In *Developing Focus Group Research: Politics, Theory, and Practice*, 64–78. London, Thousand Oaks: SAGE Publications.

Wilks, Daniel S. 2006. *Statistical Methods in the Atmospheric Sciences*. 2nd ed. Burlington, MA: Academic Press.

Wolter, Klaus, and Michael S. Timlin. 2011. “El Niño/Southern Oscillation Behaviour since 1871 as Diagnosed in an Extended Multivariate ENSO Index.” *International Journal of Climatology* 31 (7): 1074–87. doi:10.1002/joc.2336.

Wu, Zhaohua, Norden E. Huang, John M. Wallace, Brian V. Smoliak, and Xianyao Chen. 2011. “On the Time-Varying Trend in Global-Mean Surface Temperature.” *Climate Dynamics* 37 (3-4): 759–73. doi:10.1007/s00382-011-1128-8.

Xie, P., and P. A. Arkin. 1997. “Global Precipitation: A 17-Year Monthly Analysis Based on Gauge Observations, Satellite Estimates, and Numerical Model Outputs.” *Bulletin of the American Meteorological Society* 78 (11): 2539–58.

Xie, SP, C Deser, GA Vecchi, J Ma, HY Teng, and AT Wittenberg. 2010. “Global Warming Pattern Formation: Sea Surface Temperature and Rainfall.” *Journal of Climate* 23 (4): 966–86. doi:10.1175/2009JCLI3329.1.

Xu, Yangyang, and Veerabhadran Ramanathan. 2012. “Latitudinally Asymmetric Response of Global Surface Temperature: Implications for Regional Climate Change.” *Geophysical Research Letters* 39 (13). doi:10.1029/2012GL052116.

Yoshimori, M, and AJ Broccoli. 2008. “Equilibrium Response of an Atmosphere-Mixed Layer Ocean Model to Different Radiative Forcing Agents: Global and Zonal Mean Response.” *Journal of Climate* 21 (17): 4399–4423. doi:10.1175/2008JCLI2172.1.

Zagar, N, G. Skok, and J. Tribbia. 2011. “Climatology of the ITCZ Derived from ERA Interim Reanalyses.” *Journal of Geophysical Research - Atmospheres*.

Zelinka, Mark D., and Dennis L. Hartmann. 2012. “Climate Feedbacks and Their Implications for Poleward Energy Flux Changes in a Warming Climate.” *Journal of Climate* 25 (2): 608–24. doi:10.1175/JCLI-D-11-00096.1.

Zhang, Minghua, and Hua Song. 2006. “Evidence of Deceleration of Atmospheric Vertical Overturning Circulation over the Tropical Pacific.” *Geophysical Research Letters* 33 (12): L12701. doi:10.1029/2006GL025942.

Zhang, R, TL Delworth, and IM Held. 2007. “Can the Atlantic Ocean Drive the Observed Multidecadal Variability in Northern Hemisphere Mean Temperature?” *Geophysical Research Letters* 34 (2). doi:10.1029/2006GL028683.

Zhang, R., and G. K. Vallis. 2006. “Impact of Great Salinity Anomalies on the Low-Frequency Variability of the North Atlantic Climate.” *Journal of Climate* 19 (3): 470–82. doi:10.1175/JCLI3623.1.